Modeling the Intersegmental Coordination of Heart Motor Neurons in the Medicinal Leech

A Thesis
Presented to
The Academic Faculty

by

Paul Anthony García

In Partial Fulfillment
of the Requirements for the Degree
Doctor of Philosophy

Department of Biomedical Engineering
Georgia Institute of Technology

July 2004

Modeling the Intersegmental Coordination of Heart Motor Neurons in the Medicinal Leech

Approved by:

Professor Robert J. Butera, Committee Chair

Professor Raymond Dingledine (Pharmacology Department, Emory University)

Professor Ronald L. Calabrese, Adviser

Professor Lena Ting

Professor Robert H. Lee

Professor Nael McCarty (School of Biology)

Date Approved: 12 July 2004

To all of my teachers,

ACKNOWLEDGEMENTS

I am grateful to my committee members for their advice and guidance, especially my research advisor Ron Calabrese, PhD. Ron is a scientist of the highest integrity, and is a gifted teacher. I have enjoyed working alongside all of the members of the Calabrese Lab. My research project built upon previous studies by Brian Norris, PhD, and Angela Wenning, PhD, I thank them for their scientific insight. I thank the MD/PhD Program at Emory University for giving me this opportunity to achieve my career goals. I also acknowledge funding from the National Institutes of Health. My loving family has been a large source of support for me.

TABLE OF CONTENTS

LIST OF TABLES

LIST OF FIGURES

SUMMARY

We constructed a model of the coordination of segmental heart motor neurons driving blood circulation in leeches. The heart motor neuron models were conductance-based; conductances of voltage-gated and synaptic currents were adjusted to match the firing pattern of heart motor neurons from the living system. Each motor neuron receives a specific pattern of inhibitory input from rhythmic premotor heart interneurons and translates this spatiotemporal pattern into the fictive heartbeat motor pattern. The temporal pattern of synaptic input to the model was derived from extracellularly recorded spikes of the premotor heart interneurons [41]. We focused on determining the components necessary to produce side-to-side asymmetry in the motor pattern: motor neurons on one side fire nearly in synchrony (synchronous coordination), while on the other they fire in a rear-to-front progression (peristaltic coordination). The model reproduces the general trends in phasing and was used to investigate the effective contribution of several synaptic and cellular properties of the motor neurons. The spatial and temporal pattern of premotor synaptic input, the electrical coupling between the segmental motor neurons, intra-burst, short-term synaptic plasticity of the synaptic inputs, and the axonal conduction delays all were integrated with the intrinsic membrane properties to influence intersegmental phasing.

CHAPTER I

GENERAL INTRODUCTION

Rhythmic behaviors such as locomotion, respiration, feeding and in some animals, heartbeat, are controlled by oscillatory neuronal networks that in isolated nervous systems without sensory feedback can produce a pattern of activity similar to that observed in more intact preparations. The quantitative analysis of these central pattern generator (CPG) circuits has elucidated many aspects of how rhythmic activity is accomplished by organized sets of neurons [9, 34]. In isolated nervous system preparations lacking sensory input, the pattern generator produces a fictive motor pattern in the motor neurons that closely mimics the motor pattern observed in intact or semi-intact preparations [11, 57]. The leech heartbeat is no exception; the fictive motor pattern continues in the absence of sensory information, and closely matches the constriction pattern measured in semi-intact preparations [54, 55, 60].

1.1 Previous Models of Rhythmic Pattern Generating Circuits

Wavelike rhythmic behaviors are characterized by a temporal phase lag in the activation of muscles. Examples of this type of behavior are present in the leech heartbeat system [53, 54, 55, 59, 60], swimming in the leech [5], lamprey [19], and tadpole [48] and the beating of crayfish swimmerets [37] . A number of experimental and mathematical studies have investigated the origin of phase lag in nervous systems of these animals. For example, in leech [16] and lamprey [26, 12, 18, 50] swimming and the beating of crayfish swimmerets [51, 52] the underlying neuronal network has been represented mathematically as a chain of oscillators with nearest-neighbor coupling.

Although, the production of the rhythm of the leech heartbeat shares many qualities with these other motor patterns that rely on CPGs for timing [21, 8], the intersegmental coordination of the motor neurons in the leech heartbeat is unique compared to these other systems because segmental oscillators do not exist in every coordinated segment [53, 54, 55, 6, 22, 25, 36, 35] and because temporal phase lag is not constant for each coordinated segment [59, 60].

We chose to incorporate experimentally measured values for cellular and synaptic properties in our model of the intersegmental coordination of leech heart motor neurons, by using a conductance-based model. These types of models have been used to study several CPG systems, such as lamprey swimming [28], the gastric and pyloric rhythms of crustaceans [31, 56, 45, 24], and the timing network of the leech heartbeat [42, 38, 22, 20, 25]. Certainly previous models of the heartbeat CPG network of the medicinal leech, *Hirudo medicinalis*, have enhanced our general understanding of coordination in the nervous system [42, 38, 22, 20, 25]. This success inspired us to construct this first-generation model of the motor neurons which lie between the CPG network and the hearts of this organism (Figure 1). This work is our first attempt at characterizing the contribution of the motor neuron's intrinsic properties and synaptic inputs from the CPG in the production of the coordinated motor pattern through the use of a conductance-based model of heart motor neurons.

1.2 The Role of Heart Motor Neurons in Circulation of Blood through the Leech

Figure 1 shows a diagram of the nervous system of the leech and its relation to the circulatory system. The blood flow in the circulatory system of the medicinal leech is asymmetric. Two lateral heart tubes run the length of the organism and each contracts with a specific rhythm in order to circulate the blood. While one of these muscular heart tube constricts segment-by-segment in a rear-to-front peristaltic wave,

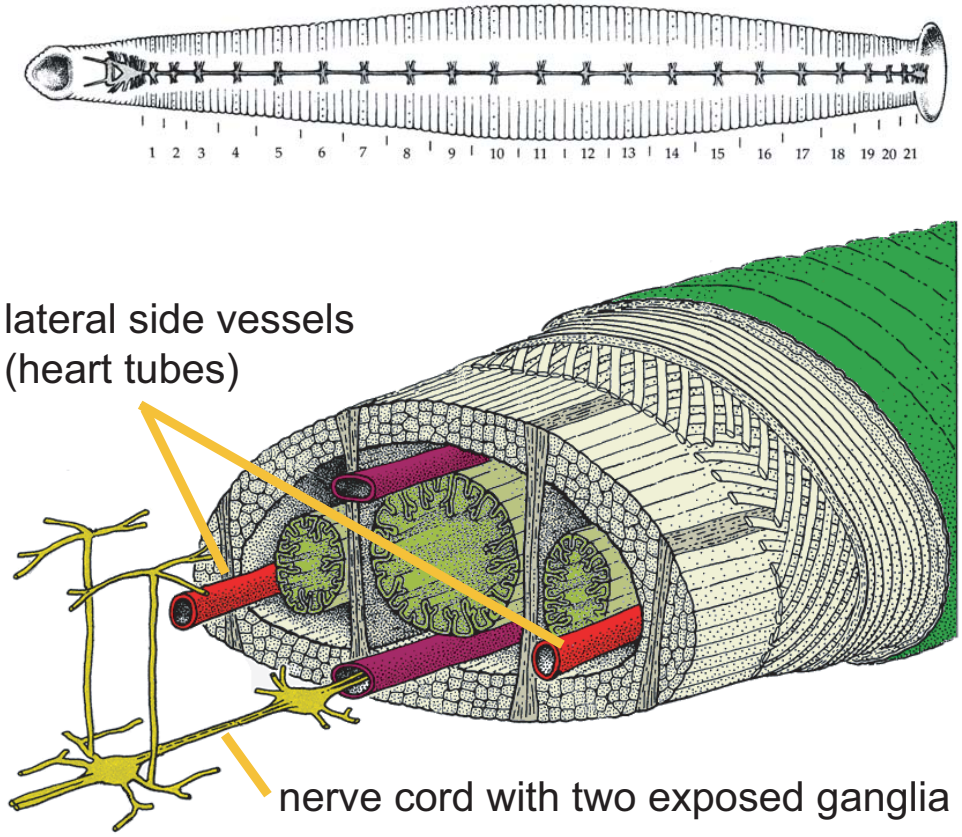

Figure 1: The nervous system of the leech, *Hirudo medicinalis*, and its relation to the circulatory system. A. The central nervous system of the leech consists of 21 segmental ganglia, a head ganglion, and a tail ganglion. The heart motor neurons reside as bilateral pairs in ganglia 3 to 18. B. The nerve cord resides ventrally inside a blood sinus. The axons of each motor neuron exit the nerve cord and innervate that segmental section of the heart tube on the same side. Rhythmic heart motor neuron activity controls the rhythmic constriction of the heart tubes that circulate the blood in this animal. Figure adapted from [40].

the tube on the other side constricts nearly synchronously along all of the segments of the animal. After about 20-40 heartbeat cycles the two heart tubes switch states. Each segmental ganglion from midbody segment 3 to 18 contains a bilateral pair of electrically coupled heart motor neurons which send projections that innervate that segmental section of heart tube on the same side. The activity of these heart (HE) motor neurons control the contractions of the heart tubes [59, 53, 32, 33, 7]. These motor neurons, and the integration of their chemical synaptic input with their input via the electrical junctions [44] are the focus of our model of the intersegmental coordination in leech heart motor neurons.

Figure 2 shows the simultaneous activity of three heart motor neurons on the same side (left, L) of the organism as they switch from peristaltic to synchronous coordination . The activity was recorded extracellularly from nerves that contained the axons of the heart motor neurons designated by heart nerve numbers [60]. The switch is usually completed in one or two heartbeat cycles; it is always complete and always simultaneous on the two sides [17, 54, 55, 6, 60]. Through the combination of several unilateral and bilateral experiments, the relationship of the timing of the motor neuron bursts can be represented as averages in a phase diagram. Figure 3 shows the phase diagram for the heart motor neuron activity across all segments. Examining the production of this phase relationship among the heart motor neurons is the primary goal of our modeling efforts.

The pattern of activity in the motor neurons is driven by a corresponding pattern of interneuronal CPG activity, which is also asymmetric [58, 54, 55, 6]. The CPG network consists of bilateral pairs of heart interneurons (HN) in the first seven segmental ganglia of the leech. A circuit diagram of the interconnections among the CPG network is shown in Figure 4. The interneurons from ganglia (G) 3, 4, 6, and 7 are "premotor", they make inhibitory synaptic connections onto the motor neurons. Evidence of this inhibition and the connection relationship of these premotor cells to

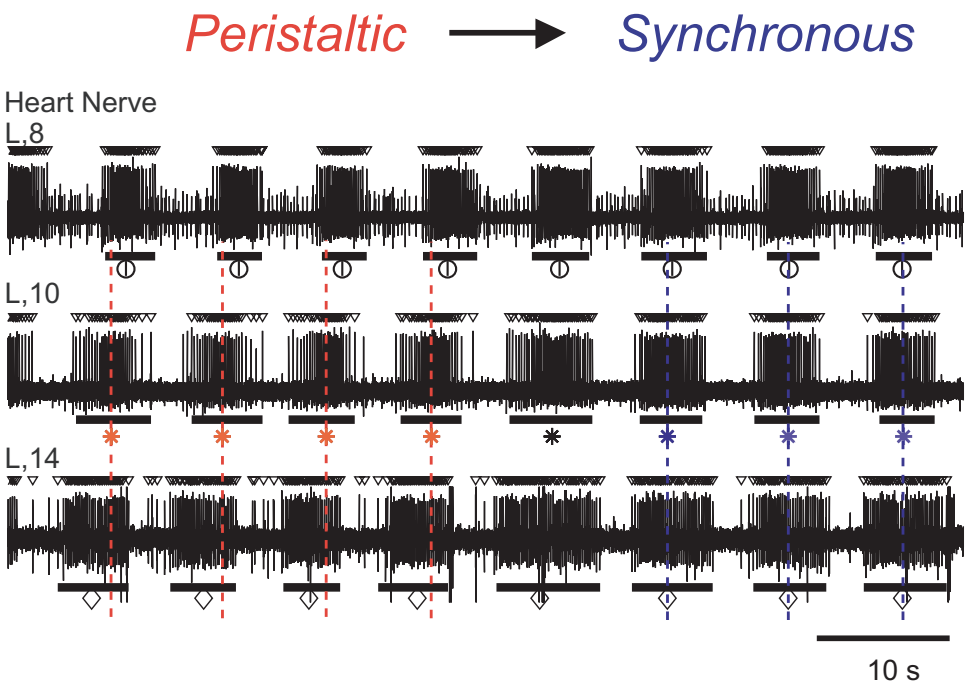

Figure 2: Heart motor neuron activity recorded from the heart nerves in the living system. Simultaneous extracellular recordings from the left side of the leech illustrate the two coordination modes. Initially, the motor pattern is in the peristaltic coordination mode (red) with bursts of action potentials first appearing in segment 14, followed by segments 10 and 8. Dashed lines mark the position of the median spike in our phase reference segment 10 (asterisk). The median spike of other segments are denoted by different symbols above each burst. In the synchronous coordination (blue), heart motor neurons in segments 8, 10, and 14 fire nearly simultaneously. Mean cycle period of this record was 8.4 s. Figure adapted from [60].

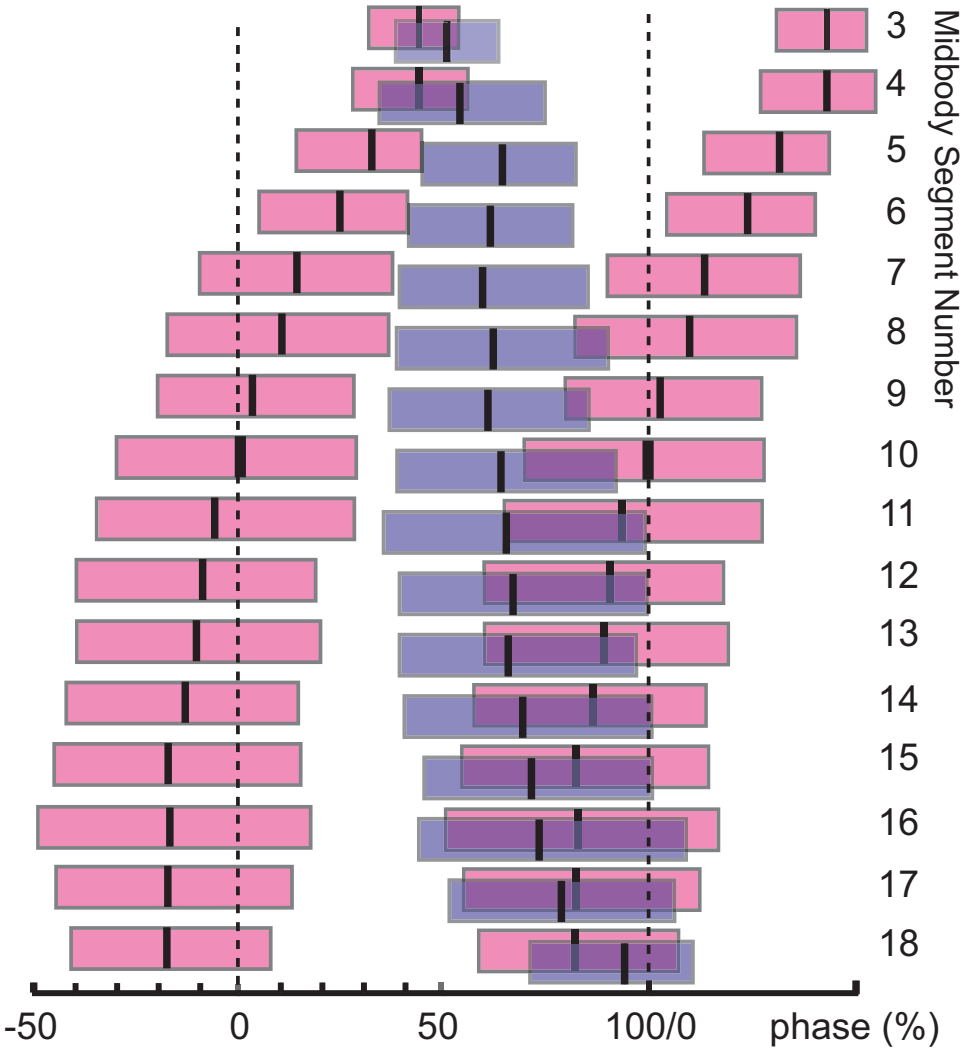

Figure 3: Bilateral phase diagram illustrating intersegmental coordination of heart motor neurons in the living system. Normalized duty cycles are displayed as box plots. Each box represents the average duty cycle of heart motor neuron bursts from combining several bilateral and unilateral recordings, similar to Figure 2. The beginning of each burst is represented by the left edge of each box and the end of each burst by the right edge of each box. Error bars were removed for clarity. Peristaltic bursts are shown in red and synchronous in blue. The phase reference in segment 10 (peristaltic) was assigned zero phase. Note that the heart motor neuron bursts come together in phase in the front and rear segments. Figure adapted from [60].

the motor neurons are shown in Figure 5 [41]. Of the premotor inputs, only the front premotor cells (HN(3) and HN(4) interneurons) are involved in pacing the network activity. The HN(5) interneurons are involved in the switching of coordination modes [17, 55, 6]. The rear premotor cells (HN(6) and HN(7) interneurons), although not directly involved in rhythmogenesis, function to shape the motor pattern especially in the posterior segments (see Figure 7).

As shown by Figure 6, both peristaltic and synchronous coordination modes are reflected in the firing pattern of the premotor inputs to the heart motor neurons [54, 55, 6, 58]. Obviously, the temporal pattern of action potential firing in the inputs plays an important role in the production of the motor neuron phase relationships. However, the translation of the phasing of the premotor interneurons in each coordination mode (Figure 6) to the phasing of the motor neurons 3 is not obvious.

Recent experiments have revealed a spatial pattern of synaptic weights at the interneuron - motor neuron synapse in the heartbeat system of the leech [41]. Figure 7 illustrates this spatial pattern of connection strength for the G3, G4, G6, and G7 premotor interneurons. These results were obtained by measuring the average post-synaptic current precisely timed by each premotor input. A typical simultaneous recording of two premotor interneurons (the HN(3) and the HN(6) interneurons) and their post-synaptic target, the G10 motor neuron is presented at the bottom of Figure 7. The spatial pattern of synaptic input strengths to the heart motor neurons in Figure 7 includes only the connection strengths of the identified premotor interneurons. An additional bilateral input to the motor neurons is known to exist; yet their cell bodies are yet to be identified [6, 54, 55]. These additional inputs are designated HN(X) interneurons and estimates of their contribution to motor neuron phasing were included in the thesis research. The details of the HN(X) interneurons and how their synaptic contribution was integrated into the model are described in Chapter 2. Other synaptic inputs may also exist for rear motor neurons; these have

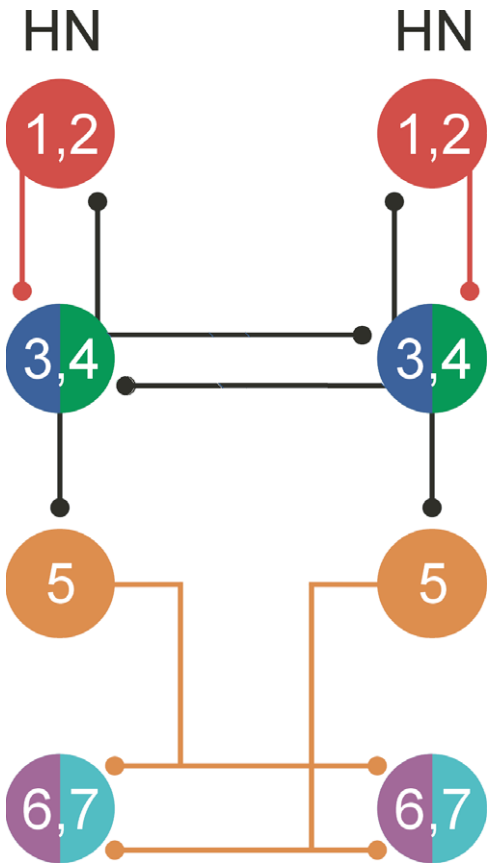

Figure 4: Wiring diagram for the central pattern generator (CPG) of the leech heartbeat. The CPG network controls the timing and coordination of the heart motor neurons. It consists of 7 bilateral pairs of heart interneurons that reside in segments 1 to 7. Neuron cell bodies are represented as circles, and all synaptic connections in the diagram are inhibitory. For simplicity, ipsilateral cells with equivalent wiring are combined (as one cell) and the ganglia numbers are separated with a comma (e.g. 3, 4). The oscillations of the CPG originate from the activity of the neuronal networks in the third and fourth ganglia [21]. The premotor cells are the heart interneurons in ganglia 3 (blue), 4 (green), 6 (magenta), and 7 (cyan); these provide synaptic inhibition to the heart motor neurons. The CPG network drives the motor neurons and the motor neurons drive the hearts (see text). Figure from [58].

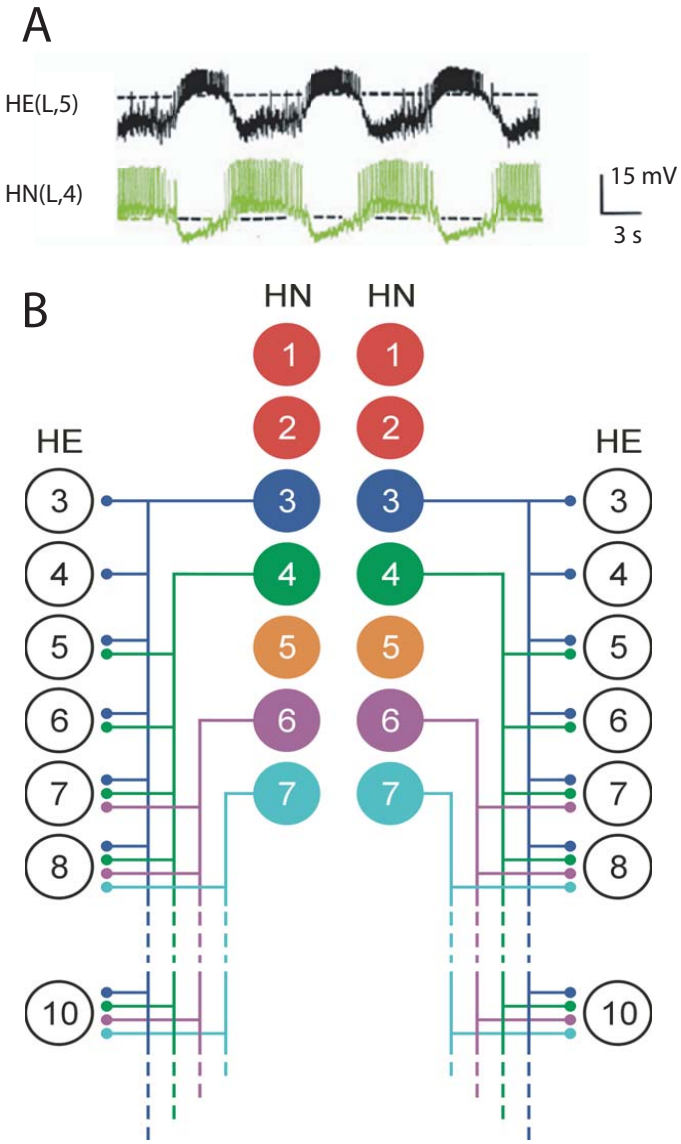

Figure 5: The synaptic connections from premotor heart interneurons to heart motor neurons are inhibitory. A. Simultaneous ipsilateral intracellular recordings reveal that the heart interneuron in ganglion 4 (HN(L,4)) inhibits the heart motor neuron in ganglion 5 (HE(L,5)) on the same side and "sculpts out" the burst activity of the motor neuron. [49, 6] B. Inhibitory synapses between the interneuronal CPG network and the motor neurons (see also Figure 7). Neuron cell bodies are represented as circles, and all synaptic connections are inhibitory. The color legend is the same as Figure 4.

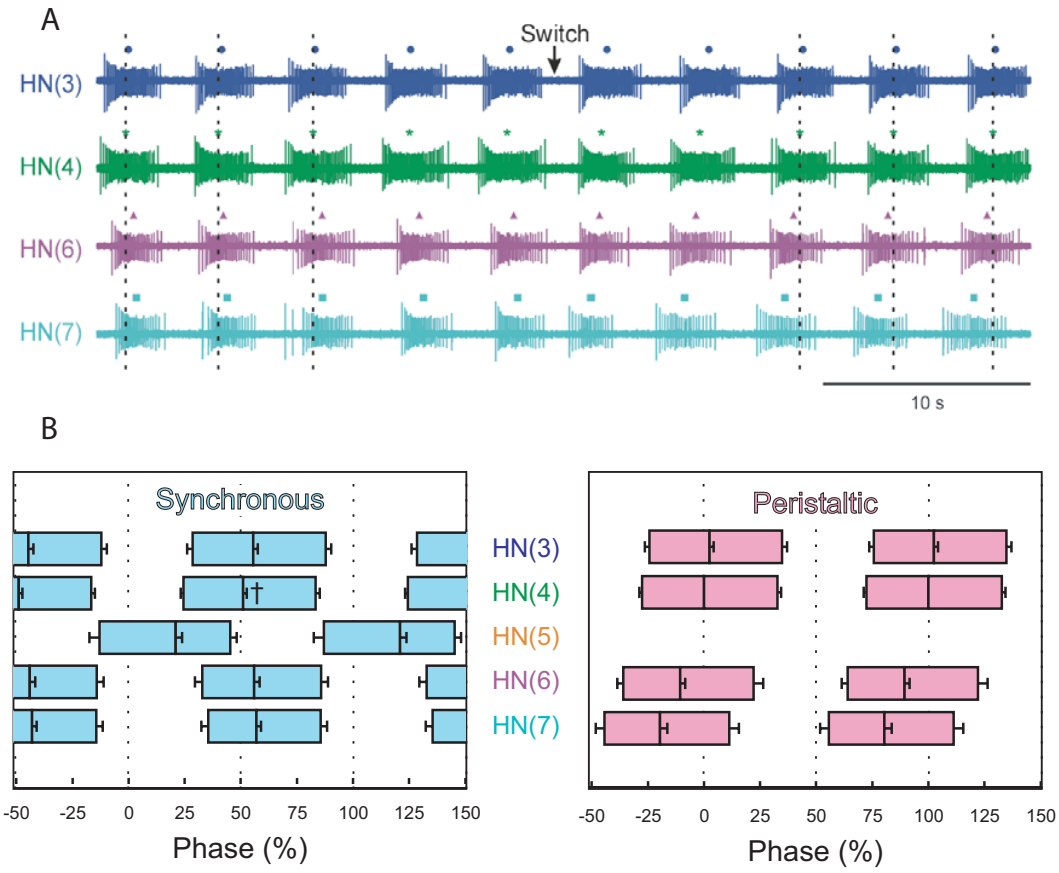

Figure 6: Synchronous and peristaltic coordination modes are represented in the activity of premotor heart interneurons. A. Simultaneous ipsilateral extracellular recordings from the premotor interneurons of the CPG network during a switch from synchronous to peristaltic coordination mode. Initially, the bursts of action potentials fire nearly synchronously and after the switch the bursts of the rear premotor cells (HN(6) and HN(7)) precede the front premotor cells (HN(3) and HN(4)) in time. The color designations are the same as in Figure 4. The input into our model of intersegmental coordination consisted of spike time data from recordings such as these (see Chapter 2). B. Like Figure 3 the normalized duty cycle and average phase differences are represented as box plots. The phase reference is the median spike of the G4 interneuron. Error bars denote standard deviation. Figure adapted from [58].

not been well studied and are not included in the model.

Chapter 2 describes the model construction including the electrical coupling and synaptic properties such as short-term intra-burst synaptic plasticity and delays due to axonal conduction that play a role in shaping the phase relationship of the motor neurons. Chapter 3 describes how the coordinated burst activity by the motor neurons is shaped by the interaction of inhibitory synaptic input and electrical coupling with intrinsic properties in the model. Chapter 4 examines the intersegmental coordination produced by the model and the results of experimentation with the model. Chapter 5 is an introduction to a more abstract model of intersegmental coordination that could be used to study general theories of different neurophysiological mechanisms on phasing. Finally, a discussion of this work is presented in Chapter 6.

The purpose of this thesis is to determine how the output of a central pattern generating (CPG) network coordinates segmental motor neurons into bilaterally asymmetric patterns of rhythmic activity. We explore this through the use of a conductance-based model that incorporates the most recent experimental results of both the presynaptic input from premotor cells and the relationship of the bursts of the actual motor neurons. We present this model in its canonical form and determine the critical parameters for generation of intersegmental phase differences among the motor neurons through an investigation of the synaptic and cellular properties. We examine the synaptic connectivity and weight pattern as it relates to intersegmental coordination. We further show through the use of a more abstract form of the model the balance between the electrical and chemical input and how it influences phase progression.

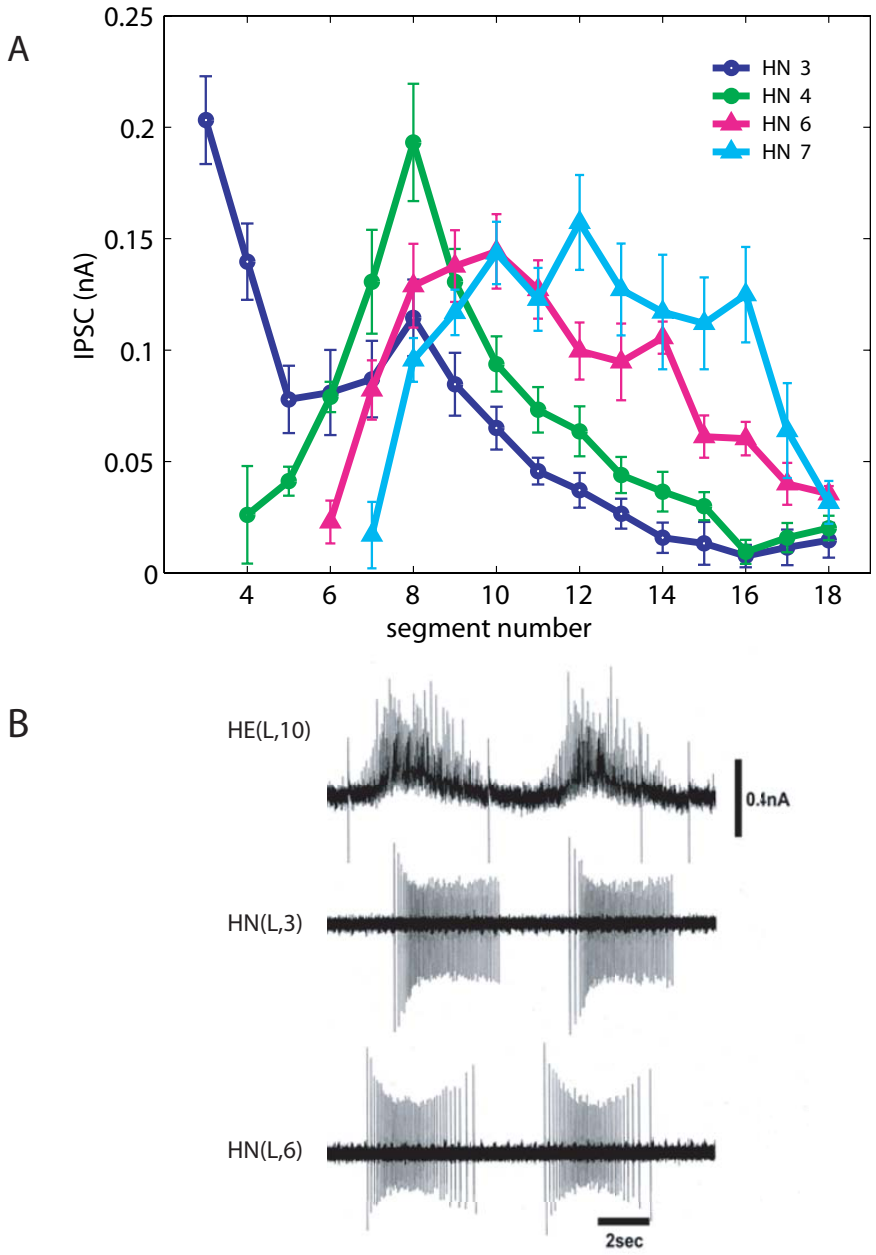

Figure 7: A specific pattern of synaptic weights exists at premotor - motor neuron synapses. A. Each premotor interneuron has a specific synaptic contribution to each motor neuron on that side [41]. B. Typical simultaneous recording of two premotor interneurons (the HN(3) and the HN(6) interneurons) and their post-synaptic target, the G10 motor neuron. The measured results for A were obtained by averaging the post-synaptic current in the post-synaptic cell timed by the spike data recorded extracelllularly in the premotor cells [41].

CHAPTER II

MODEL CONSTRUCTION

This chapter describes the *de novo* construction of the model of intersegmental coordination in the heart motor neurons of the medicinal leech. As this is the first examination of the motor neuron involvement in the heartbeat system in model form, a thorough description of the model construction is necessary. Here, the different features of the model are introduced and the mathematical equations used to describe the behavior of the system are presented. Results of our canonical model and variations of this model are described in subsequent chapters.

2.1 Nomenclature

Segmental ganglia are numbered according to Kristan *et al* [27]. Segment 1 is assigned to the first noncephalic ganglion of the ventral nerve cord. The remaining segmental ganglia of the midbody are numbered consecutively up to 21, which is just anterior to the tail brain. We often designate cells by their ganglion number; and we use G1 to describe the ganglion in segment 1, G2 for the ganglion in segment 2, and so on. first, second, and third ganglion, respectively. Heart interneurons from a particular ganglion are often abbreviated as either G# interneurons or HN(#) interneurons, where # is the segment number. Heart motor neurons are often abbreviated as G# motor neurons or HE(#) motor neurons. The premotor heart interneuron that is yet to be identified is designated as the HN(X) interneuron. When describing the phasing of neurons we often refer to the maximal longitudinal phase difference or simply the maximal phase difference. This value is calculated as the phase difference between the neuron whose average phase is most leading and the neuron whose average phase

is most lagging with respect to the phase reference. For motor neuron phasing the phase reference is usually the ipsilateral G10 motor neuron.

2.2 General Modeling Methods

The model was implemented using GENESIS (GEneral NEural Simulation System) software [4]. Each of the 32 heart motor neurons (16 bilateral pairs) were modeled as single compartment neurons with intrinsic currents, synaptic currents, and currents for the electrical junctions linking bilateral segmental pairs. Thirteen bursts of inhibitory synaptic input data gathered from the living system were presented to the model motor neurons during the simulation. Synaptic input onto the model motor neurons is inhibitory [49] and arises from ipsilateral heart interneurons. These premotor cells exist as four identified bilateral pairs of premotor heart interneurons (in HN(3), HN(4), HN(6), and HN(7)) and one unidentified bilateral pair (designated HN(X)) [53, 54, 55, 6]. Side-to-side timing was imposed by offsetting one coordination mode in order to produce 50% phase difference between the pair of heart interneurons in the fourth ganglion. The simulation ran for 60 s with a time step of 0.0001 s, and the middle ten bursts of the motor neurons were used in analysis. The intrinsic currents of the heart motor neurons are not well-characterized. We adapted a subset of the currents from the model of the heartbeat CPG for our heart motor neuron model [22]. Figure 8A is a schematic description of our model of intersegmental coordination of heart motor neurons. The **temporal pattern** is the arrangement of premotor spike times within a burst and within a series of bursts. It is derived from recordings made in the living system. The **spatial pattern** is the specific weight of each premotor cell onto each ipsilateral motor neuron. Experimentally measured values from premotor cells from the G3, G4, G6, and G7 ganglia were used in the model of motor neurons [41]. The estimation of the synaptic weights of the unidentified premotor cell are described in a later section of this chapter.

A cellular model of the bilateral pair of electrically coupled motor neurons in one ganglion forms the fundamental unit of our model of intersegmental coordination. Although we often present the analyzed results of the model experiments separately for each coordination mode; both peristaltic and synchronous inputs were simultaneously presented to the pair of coupled model motor neurons. A wiring diagram illustrates this simultaneous presentation of inputs in Figure 8B for two arbitrary segments in our model. Each segmental pair of model motor neurons received inhibitory synaptic input with a specific spatial pattern and a specific temporal pattern. The spatial pattern differed in each section by the relative values of maximal inhibitory synaptic conductance. The different values of synaptic weight are represented in Figure 8B as different sizes of presynaptic terminals. The absence of a presynaptic terminal symbolizes a connection not known to exist in the living system; in the model the maximal conductance of these null connections was set to zero.

2.3 Modeling Intrinsic Cellular Properties

The current balance equation for the membrane potential (V) of each individual model heart motor neuron is:

$$C\frac{dV}{dt} = -(I_{Na} + I_P + I_{KA} + I_{K1} + I_{K2} + I_{leak} + I_{coup} + I_{SynTotal}) \qquad (1)$$

where t is time, C is total membrane capacitance, I_{leak} is the leak current, I_{coup} is the junctional current for the electrical coupling, and $I_{SynTotal}$ is the sum of the synaptic currents for the inhibitory chemical synapses. Each motor neuron contained five voltage-dependent ionic currents: a fast Na+ current (I_{Na}), a persistent Na+ current (I_P), a fast transient K+ current (I_{KA}), an inactivating delayed rectifier K+ current (I_{K1}), and a non-inactivating delayed rectifier K+ current (I_{K2}). The maximal conductances of the currents were set empirically to match the general activity of heart motor neurons recorded intracellularly in the living system (see Chapter 3). The specific membrane resistance was 1.1 Ωm^2, the specific membrane capacitance was

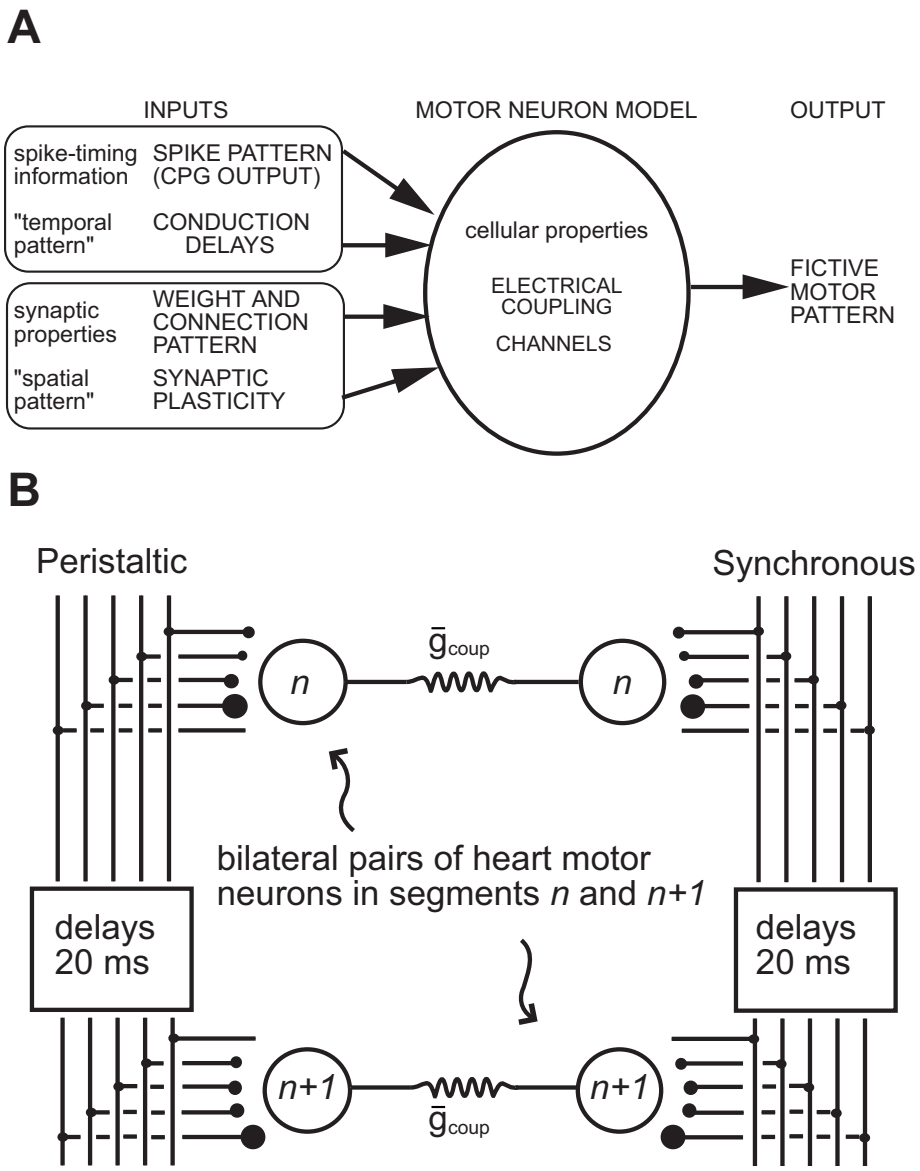

Figure 8: Description of the model of intersegmental coordination. A. Thematic description of the model. B. Schematic of model construction. Two bilateral motor neurons in each segment were modeled as single compartment neurons with membrane voltage determined from the integration of changes in ionic currents. These currents were modeled as Hodgkin-Huxley style ion channels [23]. Appropriately timed synaptic inputs from one of the two coordination states were "played-back" onto these motor neurons. The specific synaptic weights are represented by different sized circles and they were based on experimental studies. If that motor neuron was not known to have a synaptic connection by a particular premotor cell that synaptic weight was set to zero (indicated by the absence of a circle). The only connections between motor neurons are the electrical synapses within each segment (maximal conductance is indicated by $\overline{g}_{coup}$).

0.05 Fm^{-2}. The axial resistance was not applicable because the single compartment neuron was modeled as an isopotential cylinder with length and diameter equal to 60 μm. With these cell proportions the input resistance of each model motor neuron was 97 $M\Omega$ which falls within the range measured in the living system [43].

2.4 The Temporal and Spatial Patterns of Premotor Inputs

Sixty seconds of extracellular recording from the G3, G4, G6, and G7 premotor interneurons in synchronous and peristaltic coordination modes formed the basis of the temporal pattern of synaptic inputs into the model motor neurons. The period of the data set used for playback in our canonical model was 4.3 s. The average period for the living system varies from 4.0 – 8.5 s (average 5.8 s) [41]. Figure 9 shows a raster plot of the spike times used in the model. Because extracellular recordings of the spike times were not available for the HN(X) interneuron, its spatial and temporal patterns had to be estimated in our model (see Section 2.5).

Norris *et al* [41] demonstrated experimentally that the post-synaptic responses in motor neurons had different average sizes depending on the given motor neuron and on which premotor cell initiated that synaptic inhibition. In Chapter 1, Figure 7A showed the measured values for the weight of each of the identified premotor inputs. Some modifications to the experimentally-derived spatial pattern were necessary. In the two most posterior heart motor neurons the contribution from the G6 and G7 interneurons was increased. The maximal conductance of these inputs was increased to two times the calculated value in the pair of G17 motor neurons and three times the calculated value in the G18 motor neurons (see Section 2.6). Without these increases the intervals between the bursts of the G17 and G18 motor neurons were difficult to distinguish and designations for the beginning and end of a burst would have been arbitrary. Figure 10A illustrates the relative contribution of the premotor inputs onto

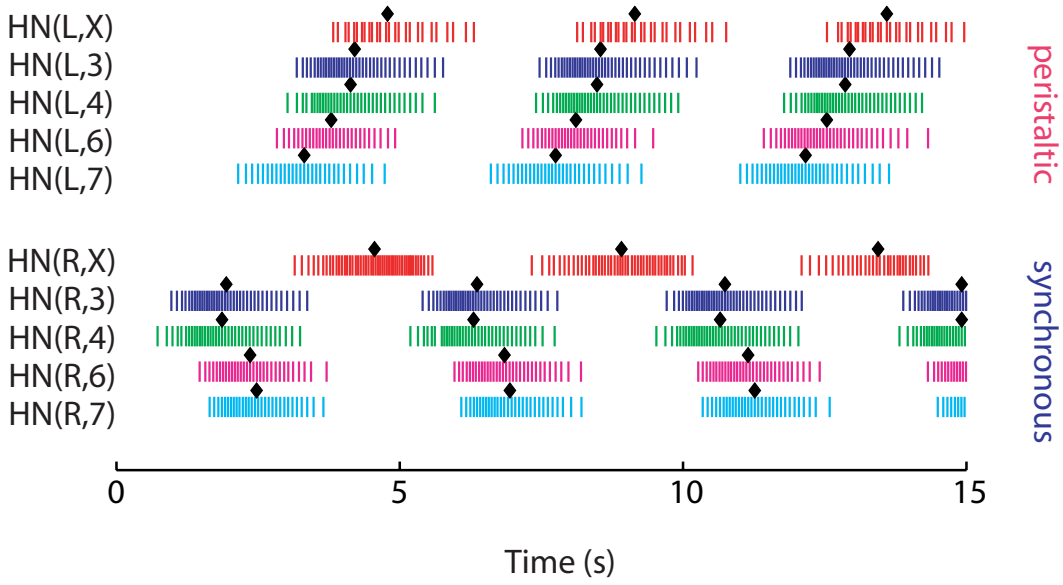

Figure 9: Raster of premotor spike-time inputs to the model of intersegmental coordination of heart motor neurons in the leech. Spike events of both peristaltic (upper 5 traces) and synchronous (lower 5 traces) inputs are represented as vertical lines. Median spike of the bursts are designated with black diamonds. Red designates the HN(X) interneuron; blue, the G3 interneuron; green, the G4 interneuron; magenta, the G6 interneuron; and cyan, the G7 interneuron. These color designations are consistent throughout. The traces shown are only the first 15 s of the data files used as inputs; the entire data file applied to the model was 60 s in length. The period of these inputs (4.3 s) set the period of the motor neuron bursts.

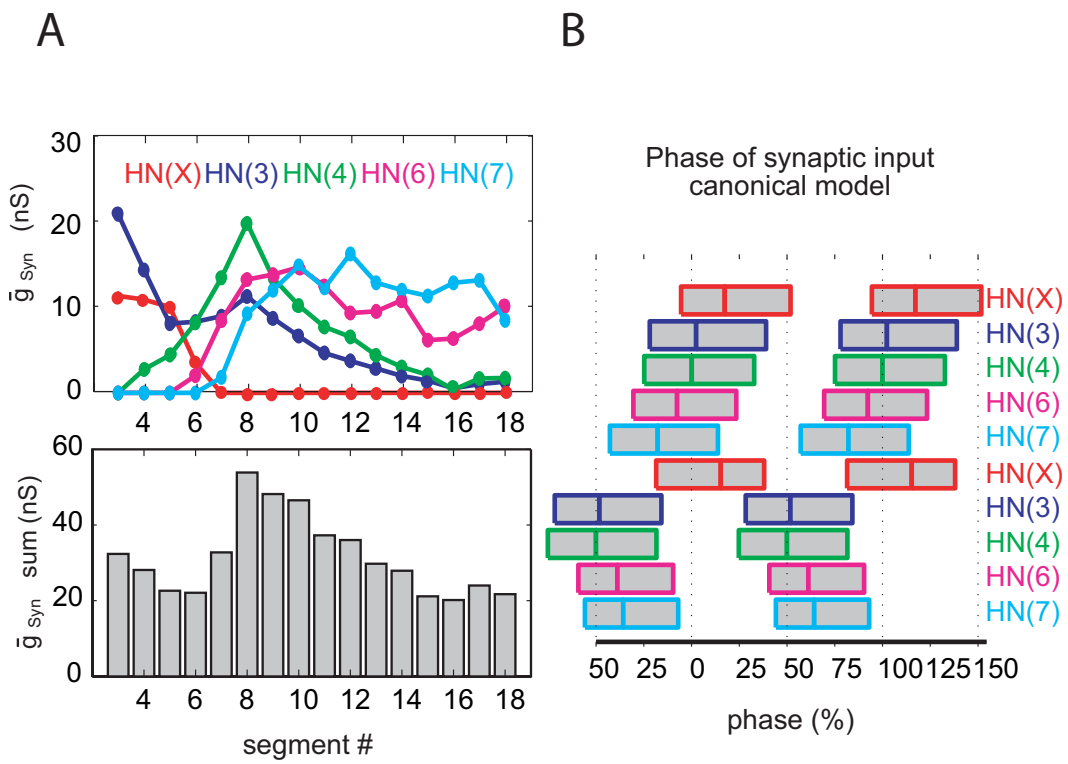

Figure 10: Details of the premotor inputs into the canonical model. A. The spatial pattern of synaptic weights used in the canonical model is presented with the sums of their maximal synaptic conductances for each model motor neuron. See text for an explanation of the deviations of this figure from the experimentally-derived weights shown in Figure 7B. The temporal pattern of premotor inputs used in the canonical model is presented as phase diagrams. These phase diagrams are derived from the spike time files presented in Figure 9.

the motor neurons in each segment as used in the model.

2.5 Estimating the Temporal and Spatial Patterns of the HN(X) Interneurons

For the estimation of the synchronous premotor input from the HN(X) interneuron, an extracellular record obtained in the living system from the switch interneuron, HN(5), was substituted for its temporal pattern of spikes. Experimental evidence [6] suggests a strong correlation between the firing of HN(X) and the firing of the switch interneuron HN(5). However the switch interneuron is silent on the peristaltic side, while the peristaltic HN(X) interneuron continues to inhibit the G3 – G6 motor

neurons [6]. Therefore, the spike train data for the peristaltic input from the HN(X) interneuron had to be constructed *de novo*. The input spike pattern for the peristaltic HN(X) interneuron was derived from modifying the peristaltic HN(3) input file. Post-synaptic currents recorded intracellularly from the G3 motor neuron suggest that the HN(X) interneuron fires slightly fewer spikes per burst and at a lower frequency than the HN(3) interneuron. The spike train data for the HN(X) interneuron was constructed with the same period and duty cycle of the HN(3) interneuron but with a lower average intra-burst frequency. The phase and frequency of the input from the HN(X) interneuron used in the model was a compromise between previous published estimations of the phase [6] and the phase estimated from intracellular recordings of the postsynaptic target cell, the G3 motor neuron (Ølsen and Calabrese). Figure 10B shows the phase diagram of all of the inputs used in the model.

Based on previous experiments on the premotor inputs [6, 53, 54, 55], it is known that the HN(X) interneuron has two spike-initiation zones. And that the conduction delays of the HN(X) interneuronal input travel in different directions across the two sides of the organism. Intracellular recordings of the G3 – G6 motor neurons reveal that the synchronous input from the HN(X) interneuron originates in a ganglion posterior to ganglion 6, because the post-synaptic potentials can be observed to occur first in the synchronously coordinated G6 motor neuron, then in the synchronous G5, synchronous G4, and finally the synchronous G3 motor neuron [6]. The conduction delays of the peristaltic HN(X) interneuronal input travel from front-to-rear like the conduction delays of the identified premotor cells. Figure 11 designates these two spike-initiation zones with colored boxes. All conduction delays in the model including those from the HN(X) interneurons were set to 20 ms per segment.

Examining our estimation of the temporal pattern of the input from the HN(X) interneurons reveals a difference not only in the conduction delays from this input but also burst structure. Figure 9 illustrates that although the duty cycle of the HN(X)

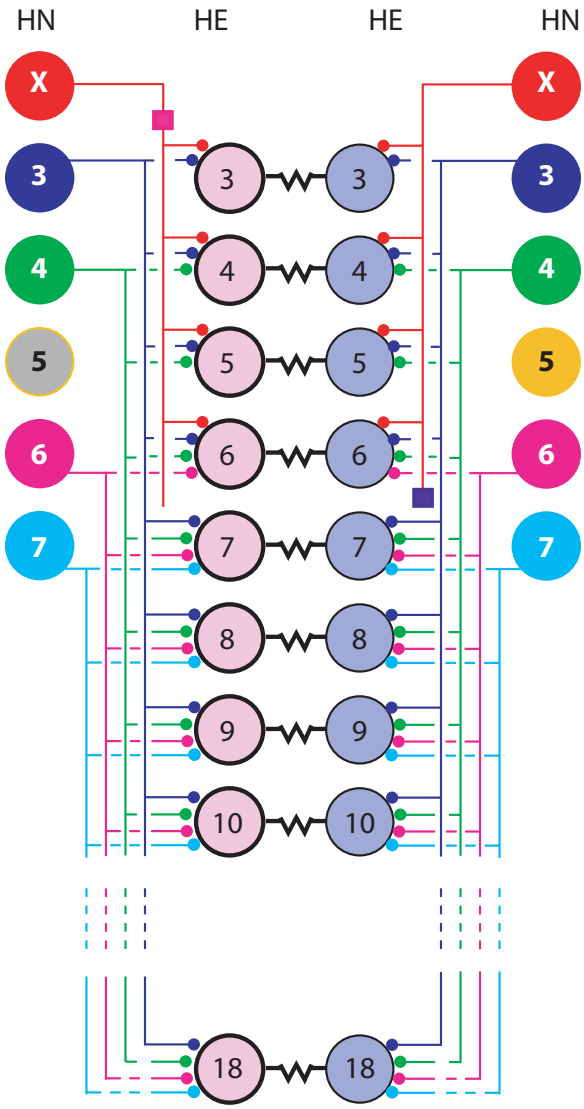

Figure 11: Wiring diagram for the heart motor neuron model with the inclusion of the HN(X) interneurons. All non-zero synaptic conductances used in the model are shown as connections in the wiring diagram. Coupling via electrical junctions is represented as resistor symbols between the motor neurons (HE). As evident by the synaptic weight diagram (Figure 10) G3 and G4 interneurons have little influence on the rearmost motor neurons. The G4, G6, and G7 interneuronal input onto the motor neurons in their corresponding ganglion is also very small in comparison to the other inputs.

inputs are similar across the two sides (and comparable to that of the other inputs), the peristaltic and synchronous spike files for the HN(X) interneuron had different maximal firing frequencies. And, the modulation of the spike frequency during the burst is different. The median spike of each burst is closer to the middle or rear of the burst in synchronous mode as opposed to the front or middle for the peristaltic mode. These side-to-side differences in conduction delays and burst structure are unique to the input from the HN(X) interneuron in our model.

Although the burst structure and conduction delays of the HN(X) inputs was different between the two sides, the value for maximal conductance remained the same. Like the derivation of the temporal pattern for the peristaltic HN(X) interneuron the spatial pattern of synaptic weight was estimated by comparing the post-synaptic current attributed to the HN(X) interneuron to that attributed to the HN(3) interneuron. The size of the postsynaptic currents attributed to the HN(X) interneuron are lower in comparison to those attributed to the HN(3) interneuron. Figure 10 compares the maximal conductances for all of the inputs to the model.

2.6 Mathematical Description of Inhibitory Synapses and Properties

The relative timing of the ipsilateral synaptic input varied slightly in each segment due to the inclusion of axonal conduction delays. As mentioned earlier, with the exception of the G17 and G18 motor neurons, the relative synaptic weights of premotor inputs were assigned based on experimental data [41]. In the model this was accomplished by setting the maximal synaptic conductance from each premotor input to each motor neuron to a conductance value calculated from the post-synaptic current records obtained by [41]. The equation used for this calculation was:

$$\overline{g}_{Syn} = \frac{I_{Syn}}{(V_h - E_{rev})} \tag{2}$$

where $\overline{g}_{Syn}$, is the calculated maximal conductance of the specific premotor input; I_{Syn}, is the amplitude of the measured post-synaptic current; V_h, is the holding potential, -40 mV; and E_{rev}, is the reversal potential, assumed to be -52.5 mV.

The $I_{SynTotal}$ in the current-balance equation (Equation 1) is the sum of all synaptic input onto each premotor cell:

$$I_{SynTotal} = \sum_{G\#=X,3,4,6,7} I_{Syn(G\#)} \tag{3}$$

where $I_{Syn(X)}$ is the specific synaptic current onto that motor neuron from the HN(X) heart interneuron, $I_{Syn(3)}$ is the specific synaptic current onto that motor neuron from the G3 heart interneuron, and so on.

Short-term, intra-burst, synaptic plasticity was incorporated into the model as modeled by Hill *et al* [22].

$$I_{Syn(G\#)}(t,V) = (V(t) - E_{rev}) \times \sum_{s=1}^{\infty} M\overline{g}_{Syn(G\#)} f_{Syn(G\#)}(t - t_s) \tag{4}$$

Where $\overline{g}_{Syn(G\#)}$ is the maximal synaptic conductance from the premotor input originating from ganglion ($G\#$), t_s is the time of the spike event, and M is the modulation variable of the synapse (see Equation 8). The synaptic function f_{Syn} is determined by

$$f_{Syn}(t) = a(e^{-t/\tau_1} - e^{-t/\tau_2}) \tag{5}$$

Where a is a normalization constant chosen so that the maximal value of $f_{Syn} = 1$. Thus,

$$a = \frac{1}{e^{-t_{peak}/\tau_1} - e^{-t_{peak}/\tau_2}} \tag{6}$$

where

$$t_{peak} = \frac{\tau_1 \tau_2 \ln\left(\frac{\tau_1}{\tau_2}\right)}{\tau_1 - \tau_2} \tag{7}$$

The time constants determine, respectively, the decay and rise times of the synaptic conductance ($\tau_1 > \tau_2$). A comparison of synaptic plasticity for the model and the living system is shown in Figure 12. In the model, the synaptic time constants for the

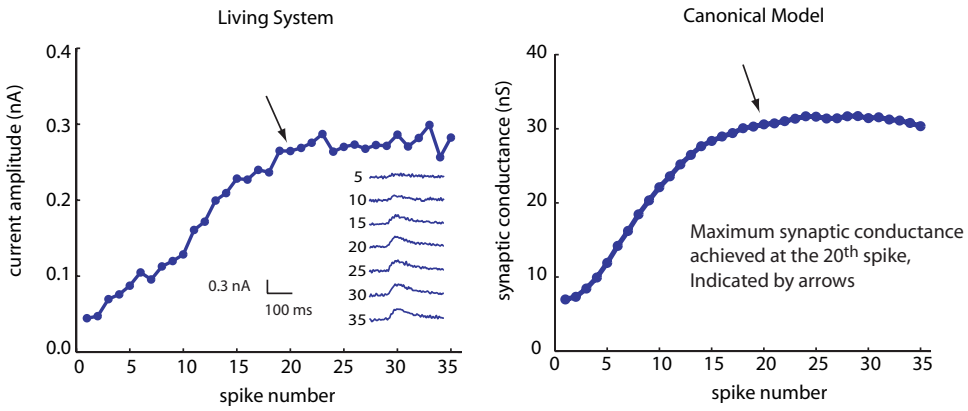

Figure 12: Synaptic modulation comparison between the canonical model and the living system. In the living system, the average postsynaptic current of each spike increases to a maximum at approximately the spike number 20. This trend is emulated in the model where synaptic conductance increases to a maximum value during the first 20 spikes of the train. Both graphs represent data obtained from the HN(3) to HE(3) synapse. Data from the living system was collected by Brian Norris. [41]

premotor input originating in G3, G4, G6, and G7 were set based on measurements from typical voltage clamp records: $\tau_1 = 0.050$ and $\tau_2 = 0.004$. Greater summation in the synaptic input from the inputs from the HN(X) interneurons has been observed experimentally, so τ_1 was increased to 0.1 for these synapses. The modulation factor M is determined by

$$\frac{dM}{dt} = \frac{M_\infty(V_{pre}) - M}{\tau_{plast}} \tag{8}$$

$$M_\infty = 0.1 + \frac{0.9}{1 + e^{-1000(V_{pre}+0.04)}} \tag{9}$$

where V_{pre} is the presynaptic voltage and τ_{plast} is the time constant of the synaptic plasticity. The time constant for synaptic plasticity used in the model was 1.250 s and this value was measured from typical simultaneous recordings involving both the presynaptic interneurons and its postsynaptic target the motor neuron provided by B. Norris (unpublished). This value corroborates the finding of Nicholls and Wallace [39]. A notable modification of the implementation of the plasticity was necessary for our model. Because only the spike events of the premotor cells are played back, the voltage

of the presynaptic cell (V_{pre}) cannot be directly incorporated into the modulation equation. This was remedied by simultaneously playing back a voltage waveform that simulated the presynaptic membrane potential for each premotor input. This waveform linearly increased from -50 mV to -30 mV during the first 500 ms of each burst and abruptly returned to -50 mV at the termination of the burst. Figure 12 illustrates the good approximation of the post-synaptic response amplitude for both model and experiment.

2.7 Modeling Electrical Coupling

The electrical junctions between the bilateral heart motor neuron pairs were modeled to reflect the measured results for coupling coefficient and low-pass filtering gathered on experiments in the living system in isolated ganglia [44]. The cutoff frequency for the low pass filter was 50 Hz and the maximal conductance of the junctions was adjusted to so that the coupling coefficient matched that of the living system, 0.34 [44]. This match was achieved by setting the maximal conductance of the electrical coupling, $\overline{g}_{coup}$, to 6 nS . The equations for the model electrical synapse were

$$I_{coup} = I_a = \overline{g}_{coup}(V_a(t) - V_b(t)) \tag{10}$$

$$I_{coup} = I_b = -I_a \tag{11}$$

where I_a is the current into motor neuron a and I_b is the current into motor neuron b. V_a and V_b are the membrane voltages of motor neurons a and b, respectively; and $\overline{g}_{coup}$ is the maximal conductance of the electrical junction.

Coupling coefficient can be measured by the ratio between the voltage responses of a pair of neurons connected with electrical junctions in response to current injection into one of the cells. It is a number that varies between 0 and 1. Figure 13 demonstrates how the coupling coefficient was measured in the model and the relationship between coupling conductance and coupling coefficient. Injecting hyperpolarizing

current into one of the model heart motor neurons causes a hyperpolarization of the contralateral cell. By increasing the maximal conductance of the coupling term, $\overline{g}_{coup}$, an equivalent amount of hyperpolarization increases the amount of hyperpolarization experienced by the contralateral cell. Because more injected current is shared with the contralateral cell with higher values of maximal coupling conductance, synaptic input can become less effective with increases in electrical coupling. The relationship between maximal coupling conductance and coupling coefficient is shown in Figure 13.

2.8 Physiological Methods

Leeches(*Hirudo medicinalis*) were obtained from Leeches USA (Westbury, NY) and maintained in artificial pond water at 15° C. After anesthetization in cold saline, the ganglia were removed from the animals and pinned ventral side up in dishes filled with Sylgard ™(Dow Corning, Midland, MI). The preparation was superfused continuously with normal leech saline containing (in mM): 115 NaCl, 4 KCl, 1.8 $CaCl_2$, 10 glucose, 10 HEPES buffer, adjusted to pH 7.4. Preparations consisted of chains of ganglia from G3 – G9. For intracellular recordings of heart motor neuron activity, we used sharp, intracellular electrodes (20 – 25 $M\Omega$) filled with 4 M KAc, 20 mM KCl. For extracellular recordings from heart motor neurons, we used suction electrodes filled with normal saline. Extracellular signals were monitored with a differential AC amplifier (model 1700, A-M Systems, Carlsborg, WA) at a gain of 1000 with the low and high frequency cut-off set at 100 and 1000 Hz, respectively. Noise was reduced with a 60 Hz notch filter. Electrophysiological data were digitized using an Axon Instruments, Digi-Data 1200 A/D board (Foster City, CA) and acquired using pCLAMP software (same company) on a personal computer. Inhibitory synapses were blocked by bath application of 0.5 mM bicuculline methiodide (Sigma, St. Louis, MO). These effects were reversed with bath application of normal saline

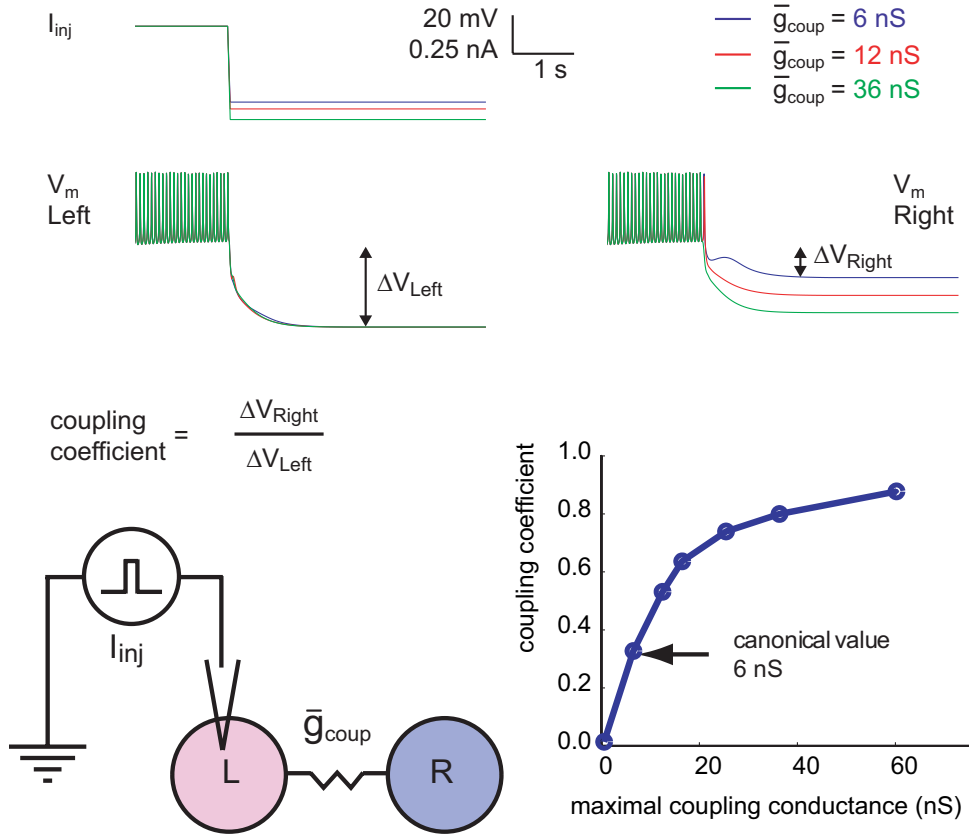

Figure 13: Electrical coupling in the heart motor neuron model. The upper traces illustrate the results of injecting 0.5 nA of hyperpolarizing current into one model motor neuron (left motor neuron) in 3 different experimental levels of maximal conductance of the electrical coupling. The contralateral motor neuron receives more hyperpolarizing current when the current stimulation is constant and the maximal conductance of the electrical coupling is increased. The lower right panel shows the relationship of coupling coefficient with maximal coupling conductance. The value of maximal conductance of the electrical coupling used in the canonical model is demarcated with an arrow.

via the superfusion system.

2.9 Data Analysis

Our burst marker for measuring period is the median spike of each burst. In nearly all bursts, the median spike of each motor neuron burst corresponded to the highest density of spikes in a burst and to the time of minimal synaptic inhibition. For discussions of longitudinal phase relationships during intersegmental coordination, the phase reference is the median spike of the G10 motor neuron in both synchronous and peristaltic coordination modes. This reference point has 0% phase and no standard deviation. The reference point from both the living system and the model will always share the same value. In side-to-side phase comparisons we use the median spike phase of the peristaltic G10 motor neuron as our phase marker. Custom analysis programs were written in MATLAB to find the average timing of the median spike for all of the model motor neuron voltage records. Maximal and minimal values of this result were used to determine maximal phase differences for each coordination mode. Our burst detection paradigm recognized a burst as groups of at least 4 spikes separated from other spikes by a minimum inter-burst interval of 300 ms. The minimum number of spikes per burst was waived for bursts of the G3 and G4 model motor neurons which occasionally had only 2 or 3 spikes in each burst. All error bars shown in the figures represent standard deviations not standard error. Values for standard error for model results are approximately one-tenth the value of standard deviation.

CHAPTER III

MODEL STRATEGY

The previous chapter described the techniques used in modeling the motor neurons and their synapses with mathematical equations. This chapter focuses on describing how rhythmic activity is produced by our model. The heart motor neurons were modeled as tonically active neurons that are driven into rhythmic bursting as a consequence of receiving rhythmic inhibitory input. The motor neuron activity pattern is "sculpted out" by the extinguishing of tonic spike activity at regular intervals by the premotor inputs. This chapter describes how the coordinated burst activity by the motor neurons is shaped by the interaction of inhibitory synaptic input and electrical coupling with intrinsic properties in this model. These results can then be used to identify future experimental approaches to the production of rhythmic burst activity by motor neurons in the living system.

3.1 Blocking Inhibitory Synaptic Input Onto Heart Motor Neurons With Bicuculline

Although reproducing the intersegmental coordination not the physiology of the heart motor neurons with mathematical equations was the primary goal of the model, their intrinsic activity was examined by conventional extracellular and intracellular recording techniques to ensure the physiology of our model motor neuron was relevant to that of the living system (see Chapter 2). Bicuculline methiodide (Sigma, St. Louis, MO), was used to block the effects of the inhibitory synapses from premotor heart interneurons onto heart motor neurons, so the intrinsic activity of the motor neurons could be observed without synaptic input [49]. The activity of motor neurons

bathed in 0.5 mM bicuculline is different in extracellular and intracellular recordings (Figure 14). Intracellular recordings reveal that heart motor neurons are tonically active when inhibitory synaptic input is blocked with bath-applied bicuculline (see expanded time scale, Figure 14B). Simultaneous extracellular recordings resulted in silencing of action potentials in preparations with inhibitory synapses blocked by bicuculline. The effects of bicuculline on silencing activity in extracellular recordings was reversible upon wash with normal saline (data not shown). These results with the motor neurons are in contrast to the results from similar experiments performed on the premotor heart interneurons, which continue to burst in the presence of inhibitory synaptic blockade with bicuculline, when recorded extracellularly [13]. Non-specific leak due to impalement by sharp microelectrode was implicated in discrepancies between intracellular and extracellular recordings in premotor interneurons. It may be that this same mechanism can account for the observed differences between extracellular and intracellular recordings in motor neurons, as well.

On first examination of the bicuculline experiments, it is tempting to presume that heart motor neurons are intrinsically silent and their observed bursting activity is dominated not by cessation of spiking by inhibitory synaptic input but instead by intrinsic currents that provide significant post-inhibitory rebound. However, the waxing and waning of spike frequency during bursts [60] is not compatible with this hypothesis. An alternative hypothesis is that bicuculline may depress excitability of the motor neurons and this effect is somewhat alleviated by intracellular recording technique. Coordinating heart interneurons are likewise silenced by bicuculline [13]. And, this second hypothesis is further supported by personal observations of depression of motor neuron firing frequency after bathing the preparation for several minutes in saline containing high enough concentrations of bicuculline (0.5 mM or above) necessary to block the inhibitory synaptic influence of the premotor interneurons. The decrease in motor neuron excitability in the presence of high concentrations

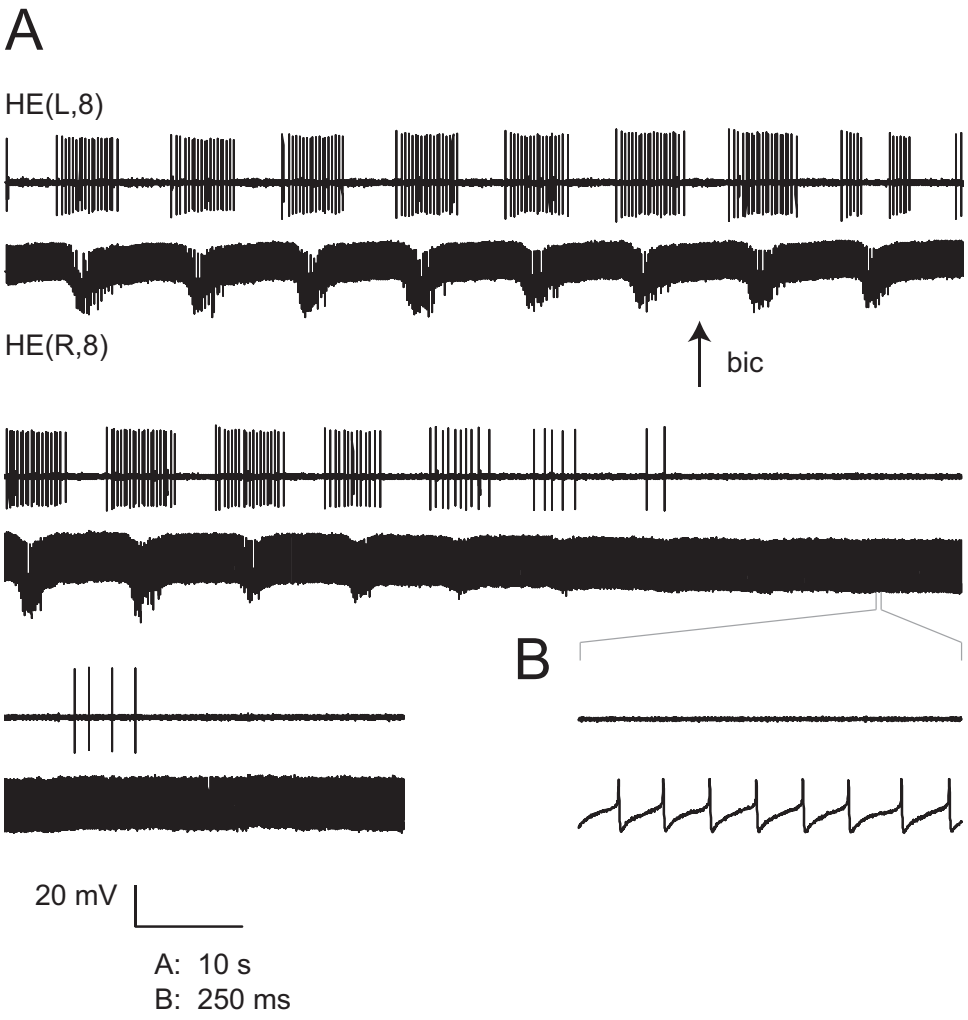

Figure 14: The effect of blocking inhibitory synaptic input onto heart motor neurons with bicuculline with different recording methods. A. Continuous extracellular (top) and intracellular (bottom) recordings of the bilateral pair of G8 heart motor neurons in a preparation that also contained segments 3 through 9 removed form the organism in an intact chain. Soon after the preparation was superfused with saline containing 0.5 mM bicuculline methiodide, the inhibitory synaptic input to the motor neurons was blocked and tonic firing could be observed in the intracellular record. The extracellular record became quiescent. B. shows a time expansion of the same two traces taken from the marked position. In these traces the intracellular record (bottom) exhibited stable firing at a regular frequency and the extracellular record (top) was silent. Motor neuron spike activity ceased in (9/9) extracellular recordings of heart motor neurons bathed in this concentration of bicuculline.

of bicuculline made it difficult to determine the relationship between observed firing frequency and injected current for motor neurons in the living system isolated from their chemical synaptic input. The motor neurons were modeled as tonically active in the absence of inputs and the set of intrinsic currents used for the model did not include inward currents activated with hyperpolarization. For this first generation model, our approach was to model the coordinated activity of motor neurons as simply as possible while retaining relevancy to the living system. The effects of bicuculline on excitability in extracellular recordings should be further characterized with experiments in the living system and then perhaps, incorporated into future generations of this model.

3.2 Excitability in the Model Heart Motor Neurons

The relationship between firing frequency and maximal conductance of the persistent sodium channel ($\overline{g}_P$) is shown in Figure 15 for the model motor neurons. The linear portion of the curve was used to determine the canonical value of the conductance of this channel in the model by matching the intrinsic firing frequency to the maximal firing frequencies observed in extracellular records [60]. The canonical value for the maximal conductance of the persistent sodium channel ($\overline{g}_P$) was set at 8.5 nS. At this value the intrinsic firing frequency of the model motor neurons in the absence of synaptic input and electrical coupling was 18 Hz. Typically average maximum intra-burst firing frequency for experimental recordings of heart motor neurons in the middle segments varied between 12 – 23 Hz (A. Wenning, unpublished data).

The relationship between firing frequency and injected current into the model motor neuron also demonstrates a quasi-linear region over a portion of the physiologically relevant range (Figure 15B). Because of the constant depolarization of the cell through the actions of the persistent sodium channel, the model motor neurons

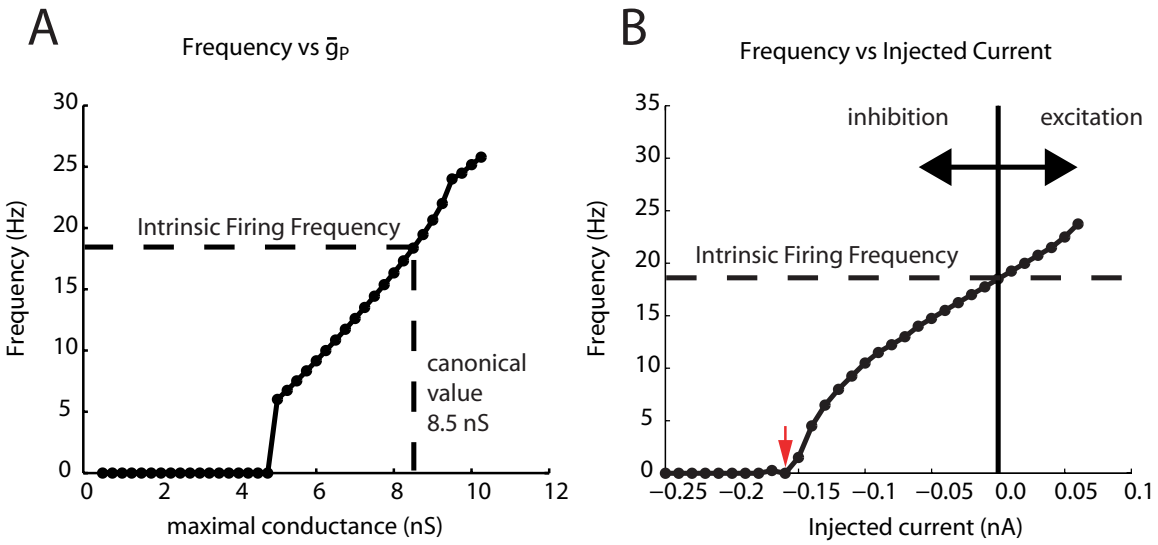

Figure 15: Excitability of Model Heart Motor Neurons. A. In model motor neurons the average firing frequency over 10 s was measured for different values of the maximal conductance of the persistent sodium channel ($\overline{g}_P$) in the absence of their synaptic inputs and electrical coupling. The relationship was essentially linear over the range from 4.75 – 10.25 nS. The canonical value (8.5 nS) used for the model of intersegmental coordination in heart motor neurons was chosen by matching the intrinsic firing frequency to the measured maximal firing frequency observed in extracellular recordings [60]. At this conductance level, this non-inactivating depolarizing current resulted in tonic activity of the model motor neuron in the absence of applied current. B. Frequency vs Injected current curve for a model motor neuron disconnected from inhibitory synaptic input. The intrinsic firing frequency was 18 Hz. Applying -0.16 nA of current silenced the tonic spike activity. When synaptic input was present, the motor neuron firing frequency varied from zero (0 Hz) to at or near the intrinsic firing frequency according to the amount of inhibition received by the model motor neuron (see text).

are tonically active when no current is injected into the cell. Injecting $-0.16\ nA$ of current was sufficient to silence spike activity entirely. The activity of the model motor neurons is essentially modulated along this curve by the inhibition received from the inhibitory synaptic input of the premotor interneurons and outward current from the inhibited contralateral partner due to electrical coupling. Although depolarizing and hyperpolarizing current was shared between segmental pairs of motor neurons via the electrical coupling, the activity of the model motor neurons rarely attained the intrinsic firing frequency due to the integration of input from the inhibitory synapses and the electrical coupling resulting in a net outward current received by the cell for the majority of each heartbeat cycle (described further in Section 3.3). Because the amount of total current received by the motor neuron from its synaptic input and electrical coupling typically remained in the range net outward current range of 0.0 to 0.5 nA , the firing frequency of the motor neuron was usually restricted to values between zero (0 Hz) and the intrinsic firing frequency according to the pattern of premotor inputs. Brief instances of inward current were observed in the current traces of the model motor neurons, and were usually associated in time with contralateral spikes. In the living system, coupling potentials are not observed among segmental pairs of motor neurons, therefore, we consider the inward current in the model as artifactual.

3.3 Synaptic Activity and Electrical Coupling Sculpts Motor Neuron Activity In the Canonical Model

Each model heart motor neuron received a specific pattern of synaptic inputs; because no two motor neurons received the exact same spatiotemporal pattern every voltage trace output from the motor neuron model was unique. To investigate how these different firing patterns in the motor neurons are produced by the differences in patterns of the premotor cell input, we examined the individual inhbitory synaptic

contributions of each of the premotor inputs and their combined effect. We examine these specific contributions by graphing synaptic conductance in Figure 16. Figure 17 examines the integration of all of the synaptic current with the electrical coupling current.

Voltage records of two pairs of model motor neurons from the 3rd and 10th ganglia are shown with concurrent traces of the synaptic conductances in Figure 16 . The G3 model motor neuron receives two inhibitory synaptic inputs: one is from the premotor heart interneuron in the same ganglion, HN(3), and the other from the HN(X) interneuron. There is no synaptic connection from the HN(X) interneuron to the G10 motor neuron or to any other motor neuron posterior to ganglion 6. The G3 interneuron does make synaptic contact with both the G3 and the G10 motor neurons. The synaptic conductance traces caused by the activity of this interneuron illustrate the differences in the spatial and temporal patterns between these two motor neurons. The amplitude of the synaptic conductance of the G3 heart interneuron is considerably reduced in the G10 motor neuron as compared to the G3 motor neuron. The different amplitudes reflect the differences in maximal synaptic conductance set in the model from experimentally-determined values. The temporal pattern of inhibitory synaptic inputs to the two motor neurons is identical in the sequence of spike times except that the G10 motor neuron receives its information from the G3 interneuron delayed by 140 ms to account for the conduction time between ganglia 3 and 10.

The G3 motor neuron is representative of the other front motor neurons that received synaptic input from the HN(X) interneuron. These front motor neurons were inhibited throughout the entire heartbeat cycle in synchronous coordination because the input from the HN(X) interneuron is anti-phasic to the input from the other premotor interneurons in the synchronous coordination mode. In the middle and rear segments, gaps of inhibitory input occurred, as demonstrated by the G10 motor neuron. These gaps in synaptic inhibition also occurred during peristaltic

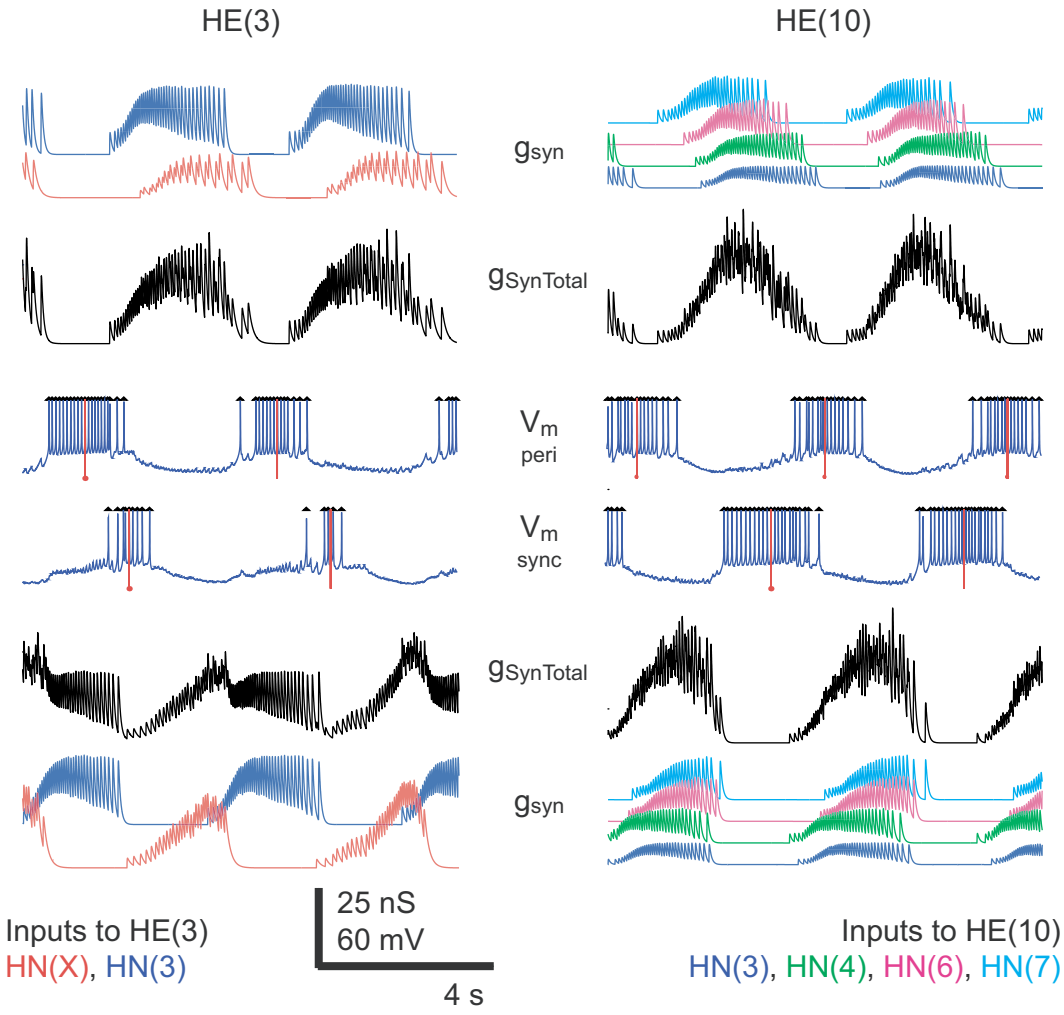

Figure 16: Bilateral simultaneous voltage and synaptic conductance records for simulated G3 and G10 motor neurons. Ten-second traces of membrane voltage are shown for both peristaltic and synchronous inputs in motor neurons that receive different synaptic input (median spike is marked with a red line). The G3 motor neuron receives synaptic input from two sources as shown by the 10 s of overlaid conductance (g_{syn}) traces and by the sum traces ($g_{SynTotal}$). Unique to the G3 motor neurons is the strong contribution from the heart interneuron in its own ganglia (HN(3) shown in blue). The G10 motor neurons receive input from 4 of the 5 pairs of premotor heart interneurons (HN(3), blue; HN(4), green; HN(6), magenta; and HN(7), cyan). Note the difference between the peristaltic traces (above from middle) and the synchronous traces (below from middle) of $g_{SynTotal}$ for these two motor neurons. The third heart motor neuron receives synaptic inhibition for the entire duration of its period and fires action potentials only when the inhibition is low. Whereas the G10 heart motor neuron has substantial epochs where the presynaptic inputs are quiescent allowing for longer bursts of action potentials in the synchronous mode.

coordination mode in front, middle and rear motor neurons, but were shorter than the gaps seen in synchronous coordination in the middle and rear motor neurons. Because the motor neurons were modeled as being tonically active (see Chapter 2), small amounts of synaptic inhibition decreased the firing rate and large amounts stopped the firing. Therefore motor neurons often fired action potentials during periods of weak inhibition; and motor neuron bursts often overlapped with the premotor inhibitory input, although with decreased firing rates. Our burst marker, the median spike of each burst, is designated in Figure 16 by a vertical red line. In nearly all bursts, the median spike of each burst corresponded to the highest density of spikes in a burst and to the time of minimal synaptic inhibition. For discussions of phase relationships during intersegmental coordination, the phase reference is the median spike of the G10 motor neuron in both synchronous and peristaltic coordination modes.

Small amounts of hyperpolarizing current did not suppress action potential firing in the model motor neuron - more hyperpolarizing current was required to silence the cell (Figure 15). Despite pauses in synaptic inhibition during the heartbeat cycle, the intrinsic maximal steady-state frequency was rarely achieved by the motor neurons in the model. Because the synaptic current was shared among the coupled pair of motor neurons via the electrical coupling, each cell remained subjected to net outward current during the entire heartbeat cycle, except on rare occasions where a spike-mediated coupling potential made the current net inward very transiently. Through the electrical coupling, the contralateral cell also acted as a current sink; diminishing strong ipsilateral inhibitory input by transmitting some synaptic current to the contralateral cell. Figure 17 shows the coupling current through the electrical junctions and the total synaptic current received by the G3 and G10 motor neurons from the premotor cells that inhibit them. The sum of these two currents is also shown. The driving force behind the coupling current was the difference in voltage between the coupled pair of motor neurons. Each motor neuron received outward

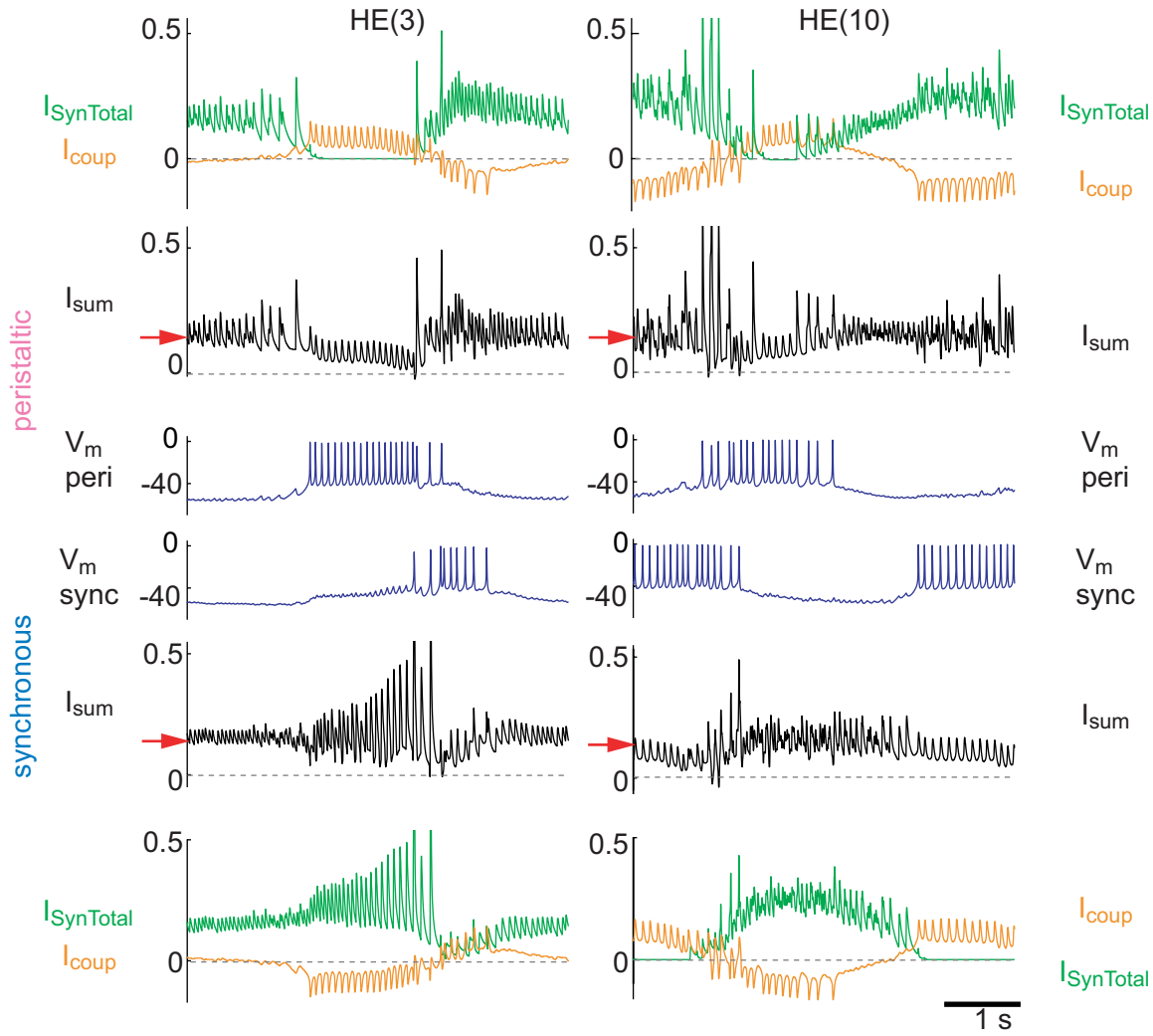

Figure 17: Bilateral simultaneous voltage and current records for simulated G3 and G10 motor neurons. Five-second traces of total synaptic current from premotor inputs (I_{syn}), coupling current from the electrical junctions (I_{coup}), and the sum of these input currents (I_{sum}) are shown for the G3 (left) and G10 (right) pairs of model motor neurons. The activity of the motor neurons in both coordination modes are shown in the middle voltage (V_m) traces. The peristaltically coordinated model motor neurons are shown above the contralateral synchronously coordinated motor neuron; and the current applied to those cells spread away from the voltage traces (above for the peristaltic motor neurons and below for the synchronous). Approximately one heartbeat cycle is shown in these traces. The electrical junctions tend to synchronize the burst activity of the motor neurons and this effect is strongest when the synaptic inhibition from the premotor cells overlaps (see text for further explanation).

coupling current when its contralateral homolog was being inhibited; and some inward current due to spike activity of that opposite motor neuron. In the living system, the electrical junctions between heart motor neurons pass hyperpolarizing current better than depolarizing current; moreover, the frequency response of the coupling is very low presumably due to the cable properties of the neurites that lead to the actual gap junctions [44]. The electrical junctions are modeled with low pass filter characteristics (see Chapter 2) which reduced the depolarizing current through the junctions associated with spikes, but did not abolish it.

The effects of the electrical coupling resulted in a synchronization of burst activity of the segmental motor neuron pairs (for this effect on motor neuron phasing see Figure 21). When there is side-to-side overlap in inhibitory input the coupling makes this input more effective. See, for example, the decrease in spike frequency at the end of the peristaltic bursts especially in the G10 motor neuron (Figure 17). Correspondingly, action potential firing can be synchronized across a pair of motor neurons that receive weak inhibitory input because the contralateral cell can act like a current sink mitigating the inhibitory synaptic current. These effects are revisited in Chapter 4 which describes the results of the experiments with the canonical model of intersegmental coordination in heart motor neurons.

3.4 Tuning the Canonical Model

The synaptic weights were measured in the living system as described by Norris *et al* [41]. These measured weights had to be scaled by a constant factor to render them effective at controlling the spiking activity in our model of intersegmental coordination among heart motor neurons; and with the exception of the two most posterior model motor neurons they are all scaled by the same scale factor (see Section 2.4). Figure 18 shows activity for 3 representative motor neuron pairs with different scale factors of maximal synaptic conductance. With a low scale factor (0.6) the bursts of the G6

and G14 model motor neurons have ill-defined beginnings and ends. The duty cycle in these cases was 95% or greater. However, the average duty cycles for the pair of G10 model motor neurons are well-matched to the duty cycles observed in the living system. Table 1 compares the duty cycles in the living system and in the canonical model. Increasing the scale factor for the synaptic weights decreased the duty cycle in all of the segmental pairs of model motor neurons. Unity scale factor, resulted in duty cycles of the G10 model motor neuron below those observed in the living system in both coordination states; yet matched the duty cycle in both coordination states for the G14 model motor neuron. The G6 model motor neuron was well matched in the synchronous mode but differed from the living system in the peristaltic mode (50% duty cycle in the model compared to 37% duty cycle in the living system). To match the duty cycles in the peristaltic mode for the G6 motor neurons the scale factor would need to be increased to at least 1.4. At this level, the duty cycles for most motor neurons compared poorly with the values measured from the living system and the G3 and G4 model motor neurons rarely fire action potentials (not shown). The duty cycles of the middle and rear motor neurons (those not receiving input from the HN(X) interneuron) were more robust to changes in the synaptic weight scaling. Scale factor had no significant effect on the phase relationship between the motor neurons (see parameter variation in Section 4.5).

3.5 Summary of Model Strategy

The burst firing of action potentials in our heart motor neuron model was achieved by extinguishing the intrinsic tonic spike activity at regular intervals by the synaptic input from inhibitory premotor heart interneurons. Although the rhythm of the motor neurons is dictated by the rhythm of the premotor inputs, the duty cycle, the modulation of intra-burst firing frequency, and most importantly, the coordination of longitudinal phase differences is shaped by the integration of the premotor input

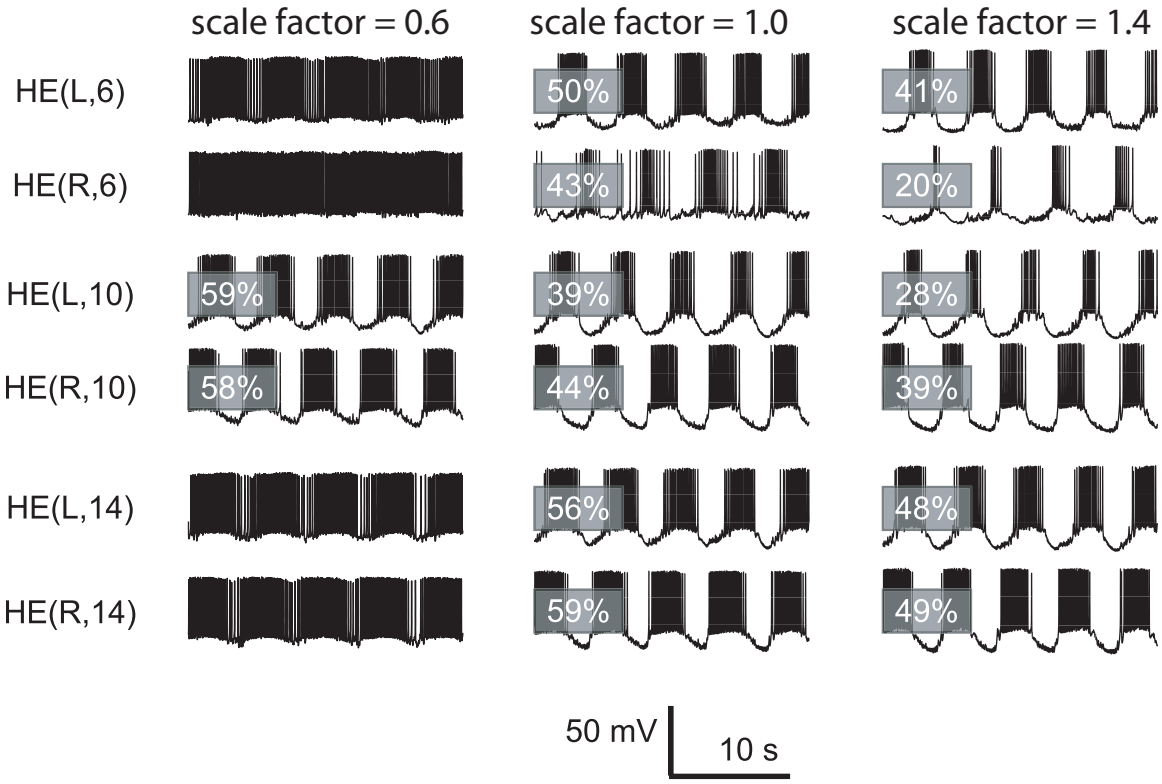

Figure 18: Tuning the weight of synaptic input in the canonical model by examining the duty cycle. Results from these three pairs of motor neurons are representative of the front, middle, and rear motor neurons. Each premotor cell affects heart motor neurons in each segment with a specific maximal synaptic conductance (or weight). These weights were derived from experimental data recorded in voltage-clamp mode. The global excitability of the model can be tuned by changing values of the scale factor, a constant that is multiplied by all of the synaptic weights. At a low scale factor (0.6) the model heart motor neurons in the middle segments (7 – 13) approximate experimental values for duty cycle (represented in the figure by HE(L,10) and HE(R,10)); while, front and rear segments do not receive enough inhibition (represented by the G6 and G14 motor neurons). The unity scale factor used in the canonical model results in good matching between living system and model of the dutycycles in the pair of G14 motor neurons and in the G6 motor neuron receiving synchronous input (HE(R,6)). Unfortunately this value for scale factor also results in smaller duty cycles for the middle segments. In order for the dutycycle of the model heart motor neuron which receives persitaltic inputs to match experimental data requires an increase in the scale factor (scale factor = 1.4). This value resulted in poor matching of the duty cycles of the majority of the motor neurons in the simulation including the contralateral G6 motor neuron. Table 1 lists the duty cycles for the living system and the canonical model.

with intrinsic membrane properties and the electrical coupling among segmental pairs of motor neurons. As the intersegmental coordination of heart motor neurons is the focus of our modeling efforts, Chapter 4 examines the phasing of the model motor neurons and the contribution of intrinsic membrane properties, synaptic properties and the spatiotemporal pattern of inputs to the peristaltic and synchronous phase relationships.

CHAPTER IV

CANONICAL MODEL OF INTERSEGMENTAL COORDINATION OF HEART MOTOR NEURONS

The previous two chapters concentrated on the construction of the motor neuron model and an exploration of the mechanisms involved in determining motor neuron activity in this model. This chapter examines the intersegmental coordination produced by the model motor neurons and presents results of experiments performed with the model. In this chapter, these results are compared to those from the living system. Discrepancies between the living system and the model are presented not to highlight the failures of the model but instead to guide further experiments on the living system. Like most models, this model is limited by its assumptions and the current knowledge about the living system; and it is also an efficient way to concentrate experimental efforts in the living system and to potentially develop new hypotheses on the mechanisms involved in the production of this rhythmic behavior.

4.1 Intersegmental Coordination of the Canonical Model

Voltage traces for all 16 bilateral pairs of heart motor neurons in the model are shown in Figure 19. The general trend of the intersegmental phase relationships seen in the living system were observed in the results obtained with the canonical model. In the peristaltic coordination mode, burst activity in the rear segments occurred sooner than the burst activity in the more anterior segments in phase, i.e., the rear bursts

led the more anterior bursts in phase. Conversely, in the synchronous coordination mode, front bursts led the rear in phase. A characteristic spike pattern in each motor neuron burst was observed in the middle and rear segments; the inter-spike interval is longer at the ends of the burst and shortest in the center. This waxing and waning of spike frequency is clear in the front motor neurons in peristaltic coordination but in synchronous coordination the burst structure varies.

The phase relations of these bursts are shown in Figure 20; the phase diagrams for the living system are overlaid as shadows for comparison. By examination of the phase diagrams, a pattern of duty cycles along the leech body axis was apparent. From front to rear, the duty cycles of the model motor neurons decreased through the middle segments and increased in the posterior segments. This is in contrast to the pattern observed in the living system where duty cycle is longest in the middle segments. The duty cycles of the G3 – G6 model motor neurons vary considerably from burst-to-burst. This is reflected in the phase diagrams by larger error bars which represent standard deviation. Table 1 shows the average and standard deviation of the duty cycles for every motor neuron in the canonical model and includes the results from the living system for comparison. The two most anterior model motor neurons in synchronous mode have noticeably shorter duty cycles compared to the rest. In the model, the shortest average duty cycle observed on the synchronous side is not in the middle segments like the peristaltically coordinated side, where the G8 motor neuron is shortest, but instead at the G3 motor neuron. As mentioned in Chapter 3, these cells receive synaptic inhibition throughout the heartbeat cycle during synchronous coordination due to the influence of the HN(X) interneuron.

The rear-to-front phase progression of the peristaltic coordination mode and the near synchrony of the synchronous coordination mode were observed in the model, but the magnitude of phase progressions was much smaller in the peristaltic mode and there is a distinct jump in the synchronous mode at the G6 – G7 border when

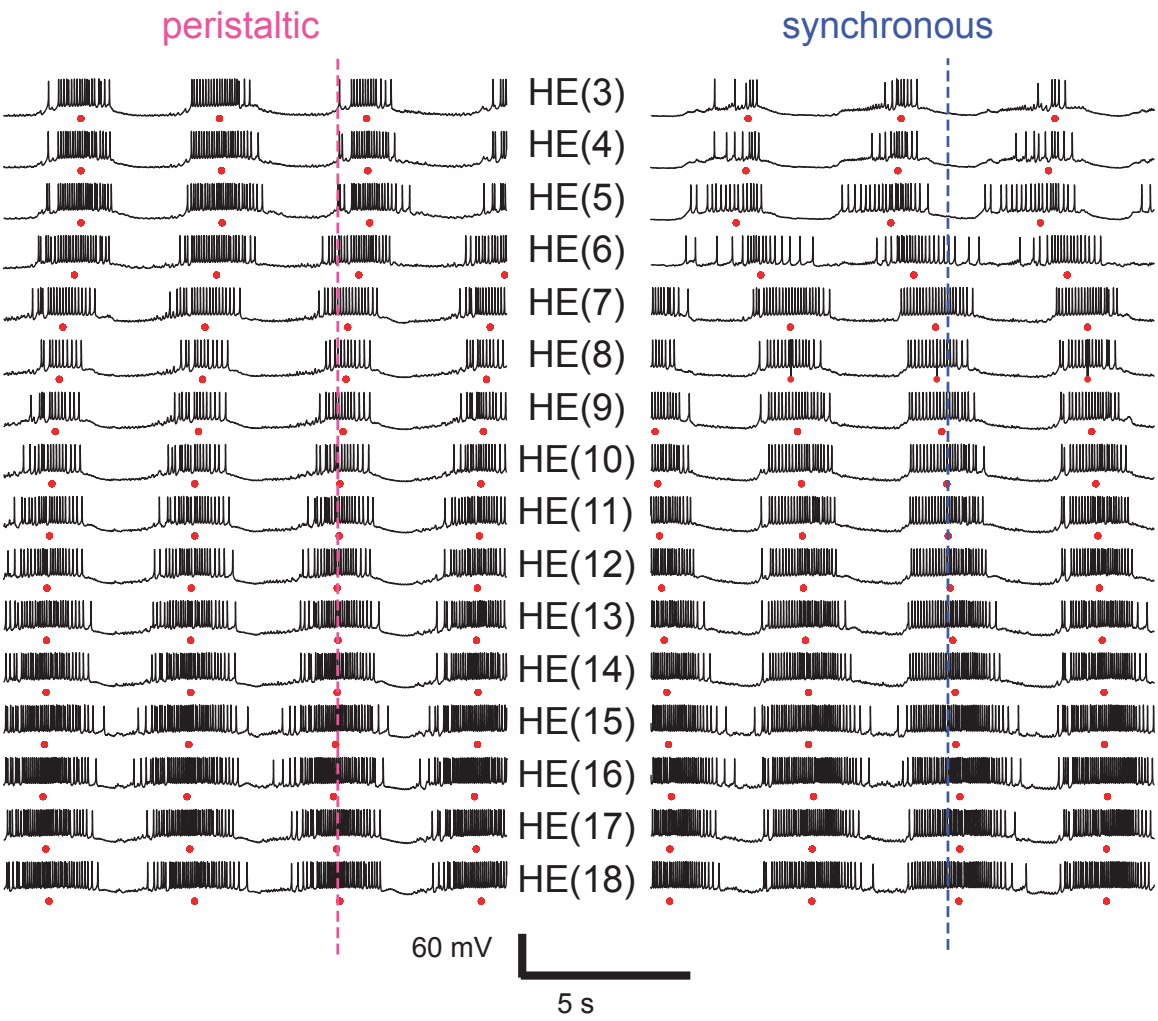

Figure 19: Voltage records for all 16 bilateral pairs of heart motor neurons for the canonical model of intersegmental coordination. The model neurons received simulated inhibitory post-synaptic potentials derived from previously recorded data from experiments with the living system (see Chapter 2). Both peristaltic (left) and synchronous (right) coordination states were modeled in each segment. Vertical dotted lines designate the median spike in one of the bursts from the phase reference cells, the G10 motor neurons. A slight rear-to-front progression was evident in the peristaltically coordinated bursts. The bursts in the rear segments precede those in anterior segments both in onset and in median spike (circle). The synchronously coordinated bursts exhibit a slight front-to-rear progression in the middle (G7 – G13) and rear (G14 – G18) motor neurons. An abrupt change in phase difference occurs between the front (G3 – G6) and middle motor neurons. This phase "jump" is evidence of the dominance of the inputs from the HN(X) interneuron in the front motor neurons.

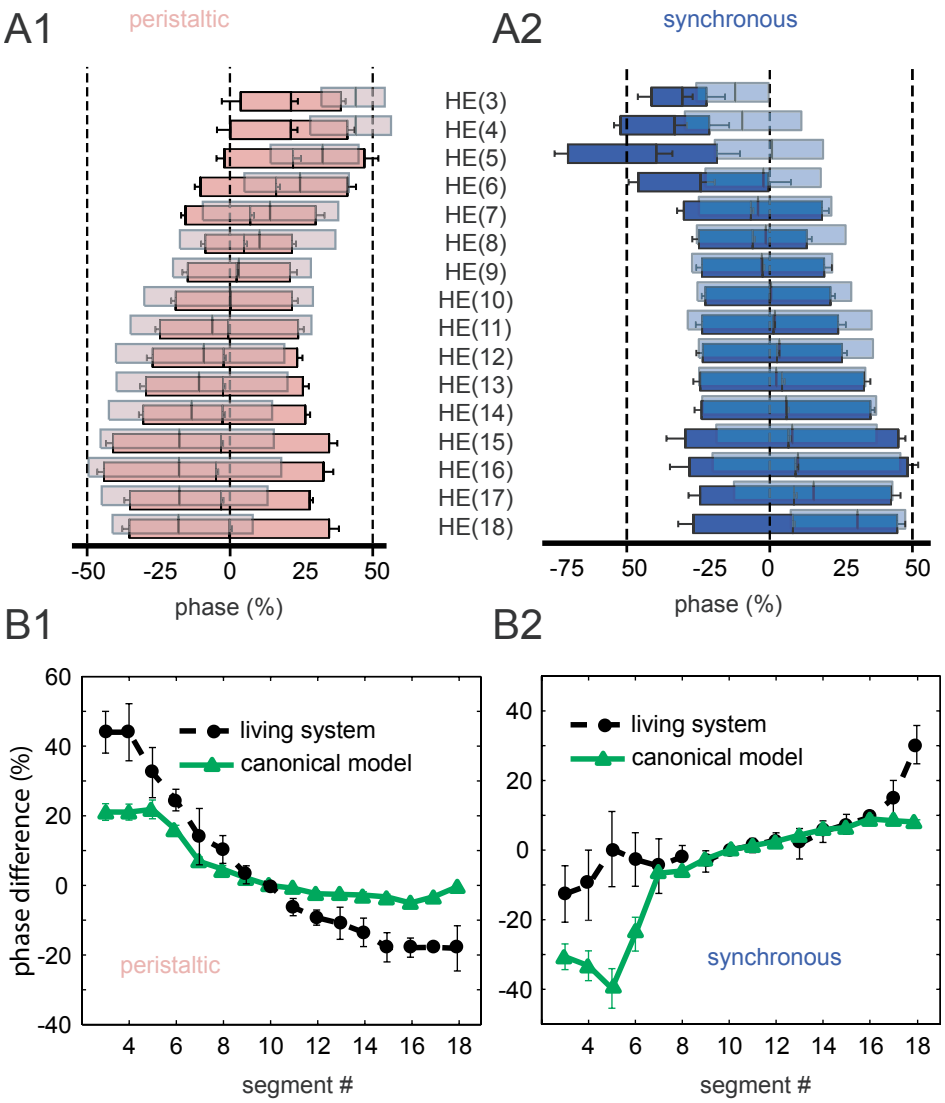

Figure 20: Phase relationships for the model heart motor neurons and comparison to the living system. A. Average phase timing of the burst firing of the heart motor neurons in peristaltic (A1) and synchronous (A2) modes. The leftmost boundary of the rectangle represents the average timing of the first spike in the burst, the right most boundary of the rectangle represents the average timing of the last spike and the median spike is represented by a vertical line near the middle of each rectangle. The phase reference for each coordination mode (in parts A and B) is the G10 motor neuron on that side. The phasing of the living system [60] is shown for comparison by the semi-transparent rectangles. Standard deviation is shown by errors for the model and was omitted for the living system for clarity. B. Horizontal plots of average phase differences for the model (green) and the living system (black) in the two coordination states (peristaltic B1 and synchronous B2). Median spike of the burst is used as our phase marker.

compared to the living system. In model motor neurons receiving peristaltically coordinated inhibitory input, the motor neurons traverse 27% of phase in a rear-to-front progression between all of the segments. However, as observed in the living system these segmental changes in phase are not uniform (Figure 3). The rear-to-front progression starts at segment 16 and proceeds anteriorly with gradually increasing segmental phase steps to its maximum, 7%, between segments 6 and 7. The largest phase difference between adjacent segments in the living system also occurs between segments 6 and 7. The G3 through G5 model heart motor neurons fire in near synchrony; and a slight front-to-rear progression can be observed in the G16 – G18 motor neurons. This deviation from the general trend in peristaltic phase progression for the most posterior model motor neurons matches the phase relationships measured in the living system for the peristaltically coordinated motor neurons in these same segments. However, the magnitudes of the phase differences in that section and along the entire peristaltically coordinated side are much more modest in our model.

In the synchronous coordination mode, model heart motor neurons traverse 48% of phase from front-to-rear. Like the peristaltic coordination mode there is not a uniform phase progression. The majority of the synchronous phase difference occurs between the model motor neurons in segments 5 – 7. The two largest segmental phase steps are between the G5 and G6 motor neurons, 14% and the G6 and G7 motor neurons, 15%. The largest phase difference between motor neurons in adjacent segments in the living system occurs between the G17 and G18 motor neurons in synchronous coordination. In contrast to the peristaltic side, the model exhibited a larger phase difference than observed in the living system for the synchronous coordination mode, mainly due to the phasing of the most anterior motor neurons. The near synchronous phasing of the middle segments and most of the rear segments in synchronous coordination matches closely that seen in the living system.

The maximal phase difference in each coordination mode or, longitudinal phase

Table 1: Duty cycle for canonical model and for the living system in two different coordination modes. All numbers are in percentages. Standard deviations are included in parentheses. Data for the living system is from A. Wenning [60].

duty cycles peristaltic coordination

segment #	canonical model	living system
3	36.3 (5.9)	22 (4.4)
4	40.6 (4.7)	28 (3.0)
5	48.3 (2.9)	31 (5.7)
6	50.3 (3.3)	37 (4.1)
7	45.4 (4.3)	47 (5.0)
8	30.2 (2.3)	55 (13)
9	34.8 (2.1)	48 (13)
10	39.1 (2.2)	59 (14)
11	48.2 (2.2)	63 (17)
12	50.2 (3.1)	59 (9.5)
13	54.6 (3.0)	60 (16)
14	56.3 (2.8)	57 (11)
15	73.6 (4.9)	61 (8.5)
16	74.8 (4.6)	68 (6.0)
17	62.5 (2.8)	58 (9.1)
18	69.5 (4.3)	49 (9.5)

duty cycles synchronous coordination

segment #	canonical model	living system
3	21.6 (5.6)	25 (9.3)
4	32.0 (5.6)	41 (8.0)
5	48.7 (9.4)	38 (5.0)
6	43.0 (8.5)	40 (5.9)
7	47.6 (4.1)	46 (7.6)
8	37.7 (3.1)	52 (9.0)
9	42.0 (3.8)	58 (22)
10	43.7 (2.7)	61 (11)
11	47.6 (3.7)	56 (13)
12	48.8 (2.9)	61 (12)
13	57.4 (2.4)	56 (13)
14	59.1 (2.7)	61 (12)
15	71.7 (5.0)	56 (13)
16	75.8 (6.9)	66 (6.6)
17	65.5 (5.2)	56 (8.8)
18	67.6 (4.0)	40 (16)

difference, is measured as the largest phase difference between any two ipsilateral segments along the body axis of the leech. The phase differences in the middle and rear segments were essentially the same magnitude but progressed in different directions for both peristaltic and synchronous coordination modes in the intersegmental model. In both coordination modes, the maximum longitudinal phase difference of the motor neurons is less than the maximal longitudinal phase difference of the premotor inputs. Table 2 shows the maximal longitudinal phase differences of the inputs and the outputs of the model compared to the living system.

The two figures below the phase diagrams in Figure 20 compare only the phase of each burst, between the living system and the canonical model. The rear-to-front progression characteristic of the peristaltic coordination mode is represented by a negative slope in the two curves representing peristaltic coordination. The discrepancy of the magnitude of maximal phase difference in the peristaltic mode of the model motor neurons with the living system is particularly evident. The discrepancy of the phasing of the model motor neurons on the synchronous side is also evident. However, relatively good matching along segments 7 – 16 exists between the model and the living system.

4.2 Experiments with the Canonical Model

4.2.1 Effects of electrical coupling on motor neuron phasing

The effect of removing the electrical coupling in our model on the intersegmental phase relationship in our canonical model is shown in Figure 21. The characteristic rear-to-front progression in the peristaltic coordination mode and the synchronous coordination were not changed with the removal of the electrical coupling. The maximal phase difference in peristaltic coordination mode decreased from 27% (canonical) to 21%. And, the range of synchronous phase jump changed from 48% (canonical) to 36%. This is most evident in the G3 – G6 model motor neurons.

The electrical coupling had a side-to-side synchronizing effect on burst activity in the canonical model; its effects were to bring the bursts closer together in phase by sharing the inhibitory input from each coordination mode (see Chapter 3). By examining the bilateral phase diagrams, we see that the synchronizing effect of the electrical coupling on burst activity was greater on those motor neuron pairs whose inputs were most synchronous and thus whose bursts were most synchronous in the absence of coupling (see Figures 26 and 27). The longitudinal phase differences were decreased and the side-to-side phase differences were increased with the removal of the electrical coupling.

Side-to-side phase differences of the G6 – G9 model motor neurons were changed only slightly with the removal of the coupling. These model motor neurons received the most anti-phasic inhibitory input with respect to their contralateral homolog. The G10 – G18 model motor neurons exhibited significant increases in side-to-side phase differences with the removal of the electrical coupling as they also receive synaptic inhibition in-phase across the two sides. The effect of this shift on phase progression is somewhat masked because the phase reference (G10 motor neuron) also increased its side-to-side phase difference with the removal of the coupling. The average firing frequency and duty cycles of the bursts from the G7 – G13 motor neurons was increased with the removal of coupling due to the decrease in the sharing of inhibition among these motor neurons. Similar phasing results were obtained with the model when the maximal conductance of the persistent sodium channel ($\overline{g}_P$) was modified (changed from 8.5 nS to 7.5 nS) to control for this effect (not shown).

In the canonical model, the electrical coupling effectively caused the peristaltic bursts of motor neurons anterior to the G6 – G9 motor neurons to fire later in phase and those posterior to the G6 – G9 motor neurons to fire earlier. The result was an enhancement of rear-to-front phase progression. This enhancement came at the expense of enhancing the front phase jump in the synchronous coordination mode,

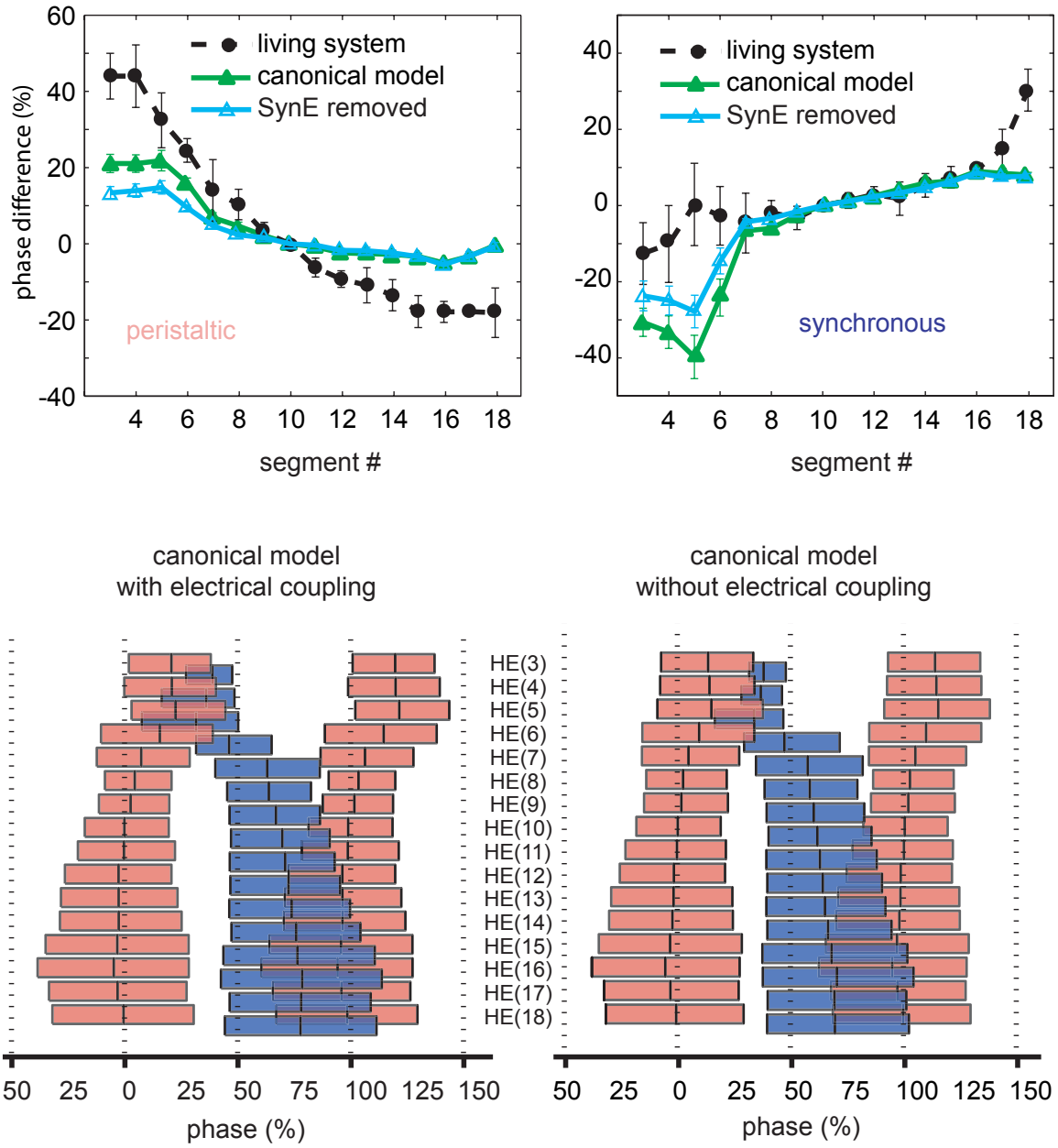

Figure 21: Synchronizing effect of electrical coupling on heart motor neuron phase relations. The phase difference curves (above) compare the canonical model (green) to the same model with the electrical coupling removed (blue). The curves for the living system are included in black. The bilateral phase diagrams (below) show the side-to-side phase relationships of the canonical model with and without the electrical coupling. The average bursts in the front motor neurons move towards each other and increase in overlap. The side-to-side phase difference also changes in the rear motor neurons, its effect on the intersegmental phase relationship is somewhat masked in the phase difference curves because the side-to-side phase relationship of the bursts of the phase reference (G10 motor neurons) also changes (see also Figure 26).

because the effect of the electrical coupling was to influence earlier firing of the motor neurons anterior to the G6 – G9 motor neurons and later firing in those posterior to these motor neuron pairs. In general, electrical coupling caused the model motor neurons to fire bursts of action potentials more in phase with their contralateral homolog. This effect is examined more completely in Section 4.4.

4.2.2 Effects of synaptic properties on motor neuron phasing

We examined the contribution of intersegmental conduction delays and synaptic modulation in producing the intersegmental phase relationship by analyzing the output of the canonical model with each of these synaptic properties removed. By changing the conduction delays from 20 ms per segment to 0 ms, the timing of the synaptic input was modified while preserving the temporal phase relationship among the premotor inputs. Similarly, by changing the time constant of the intra-burst, short-term synaptic plasticity from its canonical value, 1.250 s, to 0 s (see Chapter 2 for a thorough description of this synaptic modulation) the experimentally-derived spatial pattern of relative synaptic weights was preserved while the amplitude of the synaptic input was changed.

Figure 22 shows the effects of removing the conduction delays and the synaptic modulation from the canonical model on phase progression. The general structure of the peristaltic and synchronous median spike phase curves did not change much with the removal of the segmental delays (Figure 22A1 and 22A2). The maximal longitudinal phase difference in the synchronous mode changed from 48% front-to-rear (canonical model) to 37% without the conduction delays (Figure 22A2). As the vast majority of the conduction delays are in the front-to-rear direction (see Chapter 2) their removal resulted in a decrease in the front-to-rear phase difference during synchronous coordination. Interestingly, the maximal phase difference in peristaltic coordination was also decreased when the conduction delays were removed. The

canonical model exhibited a 27% longitudinal phase difference with the conduction delays set to their canonical values and the longitudinal phase difference decreased to 24% when the conduction delays are set to 0 ms (Figure 22A1). This seems unexpected because the conduction delays increase in the posterior direction and that would be expected to decrease the rear-to-front phase differences in peristaltic coordination mode and therefore, removal of the conduction delays should increase the longitudinal phase difference in peristaltically coordinated model motor neurons. Indeed, this paradigm holds true for the maximal phase differences in the middle and rear segments (see Section 4.5). Yet, the phase differences from the G3 – G6 motor neurons to the phase reference, the G10 motor neuron, were slightly decreased upon removal of the conduction delays. This result occurs because the relative-timing of the input from the HN(X) interneurons were changed with removal of the delays.

A decrease in maximal phase difference in both synchronous and peristaltic mode was also observed when the synaptic modulation is removed. With this experimental perturbation, the maximal amplitude of each synaptic event is constant throughout the premotor burst. Figure 22B1 shows the decrease in maximal phase difference in the peristaltic coordination mode from 27% (canonical) to 22% with the removal of the synaptic modulation. The effect of removing the synaptic modulation is less apparent in the synchronous coordination mode. The maximal phase difference in synchronous coordination changed from 48% (canonical) to 42% with the removal of intra-burst synaptic plasticity (Figure 22B2). The phase for the G3 and G4 model motor neurons are not shown for synchronous coordination because they were silent throughout several heartbeat cycles. In the canonical model, the G3 and G4 motor neurons fired bursts in the synchronous mode at low intraburst spike frequencies and only when synaptic inhibition was at a minimum (see Figure 16), increasing synaptic inhibition through the removal of the synaptic modulation abolished several of these bursts. The removal of synaptic modulation caused an increase in the inhibitory

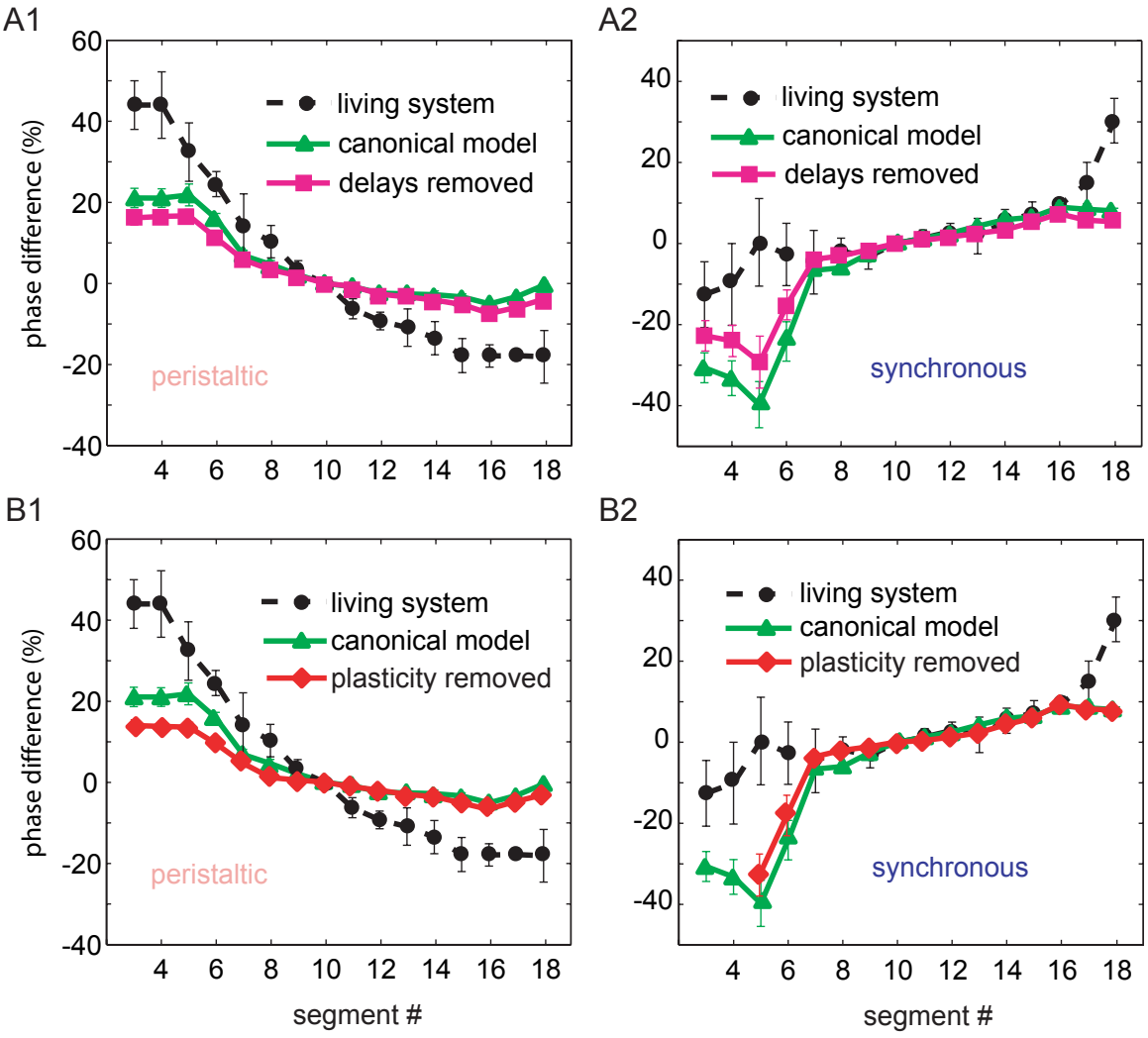

Figure 22: A. Removing the conduction delays between segments had a small effect on the phasing in the peristaltic (A1) and synchronous (A2) coordination modes. The effect of removing the conduction delays decreased the maximal phase differences in both coordination modes (see also Table 2). B. When the intra-burst synaptic plasticity was removed decreases in the maximal phase difference of the model were also observed. The effect on phasing by removing the synaptic plasticity is larger than the effect of removing coupling but still mild. B1 shows the phase relations in peristaltic coordination and synchronous coordination is featured in B2. The G3 and G4 model motor neurons in the synchronous mode without plasticity were subjected to large hyperpolarizing current throughout the heartbeat cycle (see Figures 16 and 17) and this resulted in bursts of action potentials occasionally being skipped by these cells. These segments were not included in the calculation of phase.

synaptic current at the beginning of the premotor burst, resulting in more abrupt endings to bursts in model motor neurons. This premature ending of motor neuron bursts affected the phase of the motor neurons in the front segments more than those motor neurons in the middle and rear segments. The inhibitory synaptic input from the HN(X) interneuron was modeled with longer synaptic time constants than the other premotor inputs (see Chapter 2). Therefore, removing the synaptic modulation led to greater increases in the inhibition on these motor neurons from the G3 – G6 motor neurons in both coordination modes.

4.2.3 Comparison of different temporal patterns of synaptic input

Although, the removal of different synaptic properties had small effects on the phasing of the canonical model, these effects did not fully explain the discrepancy between motor neuron phasing of the living system and the canonical model. In order to control for unintended effects of the specific input pattern used in the canonical model, two other premotor spike input patterns were "played back" into the canonical model (see Chapter 2). The results of these simulations are shown in Figure 23. The results of the model with a new pattern of inputs is shown in Figures 23A1 and 23A2. This new pattern of inputs was also derived from extracellular records of the 4 identified premotor interneurons. The period of the new pattern (5.3 s) was longer than that in the canonical model (4.3 s). This new set of inputs also differed slightly in the phase relationship among the identified premotor cells. The spike-time input and phasing of the HN(X) interneurons were modeled similarly to that for the canonical inputs (as described in Chapter 2). Although, we did not expect any model results to depend on period checking for stable phase progressions in different periods is criticial as it is considered a hallmark of intersegmental coordination. The general peristaltic and synchronous trends are preserved with these different inputs. Table 2 compares the longitudinal phase differences of these inputs with results presented earlier. Both the

canonical and the novel input patterns were representative of typical recordings of the premotor inputs in the living system [41].

Figure 23B1 and Figure 23B2 show the phase relationship among the model motor neurons when the canonical inputs are phase adjusted to reflect the averages for the identified premotor cells. As no average phase exists for the HN(X) interneurons the synchronous HN(X) input was phased according to the HN(5) switch interneuron and the phase of the peristaltic HN(X) interneuron was set to the same phase as HN(3). The general peristaltic and synchronous trends were again preserved when the canonical inputs were phased according to the averages. Table 2 compares the magnitude of these longitudinal phase differences with the results shown earlier.

Taken as a whole, the similarity of the general phase relationships observed in peristaltic and synchronous coordination mode suggests that a range of inputs can produce similar outputs of the model and that the discrepancies between the results of the model and that of the living system are not input specific. Therefore, we conclude that our canonical model of intersegmental coordination of leech heart motor neurons is an incomplete model of the heartbeat system of the leech. We do not intend to provide the model as a substitution for the living system but instead shift our focus of the model on using it as a tool to guide new experiments designed to increase our knowledge of the heartbeat system of the leech.

4.3 Side-to-side Phase Differences and the Patterned Coupling Model

Figure 24 plots the absolute value of the phase differences between motor neurons in the same ganglion for the canonical model. The phase differences of the living system and the canonical model with the coupling removed are also plotted. The side-to-side phase differences of the living system are better matched by the canonical model in the G7 and G11 – G15 model motor neurons. Upon the removal of electrical coupling,

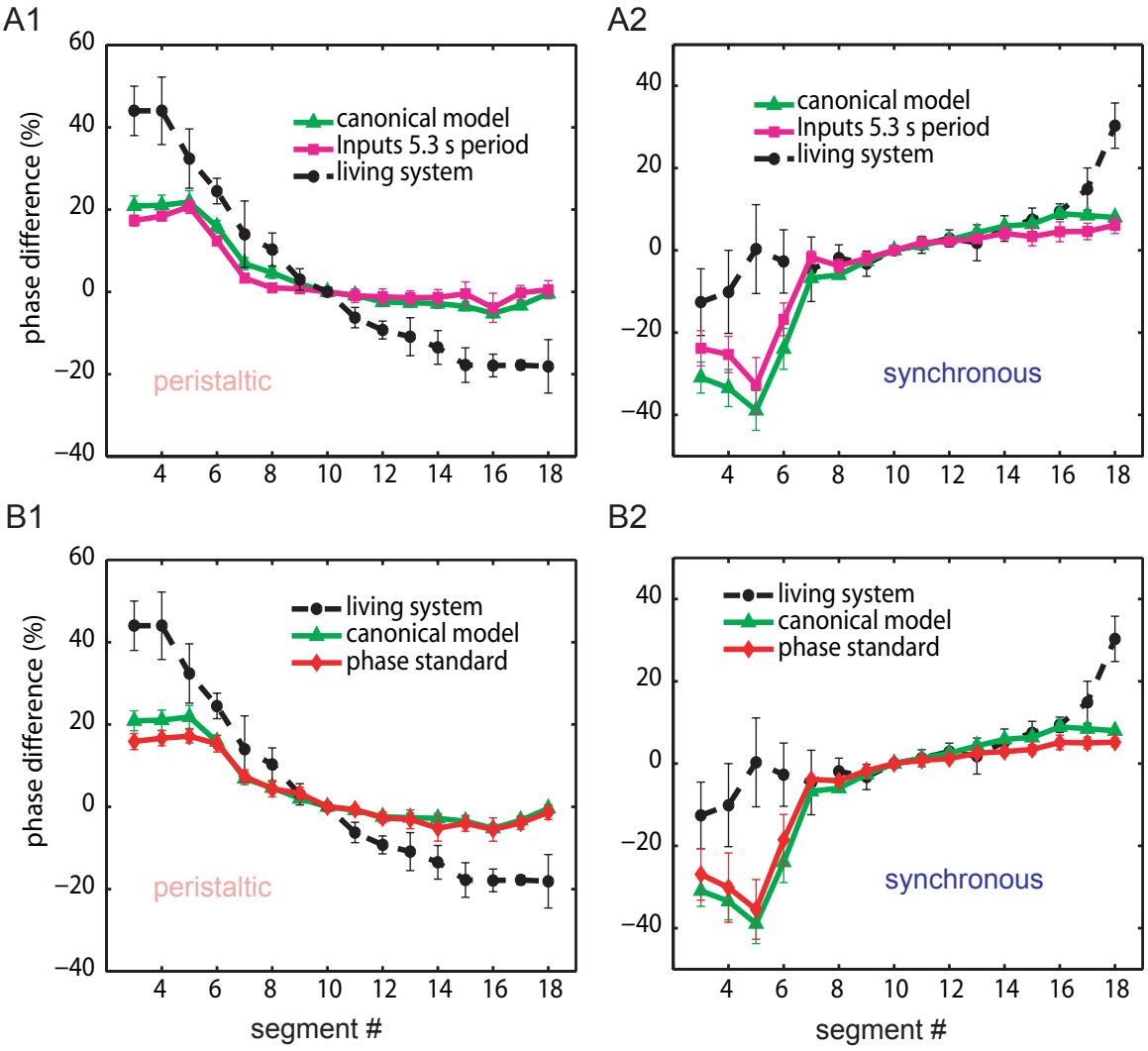

Figure 23: A. Similar results are obtained when the temporal pattern of premotor spike bursts is determined by a different set of extracellular records (see Chapter 2). The period of this different temporal pattern (shown in magenta) was 1 second longer than that of the records used in the canonical model (shown in green). Peristaltic (A1) phase progression and synchronous (A2) phase progression are compared to the living system (black). B. When the temporal pattern of the inputs used in the canonical model are adjusted to reflect the average phase timing taken from many recordings of premotor activity (shown in red), the intersegmental phase relationship changes slightly in the peristaltic (B1) and synchronous (B2) coordination modes.

Table 2: Comparing maximal phase differences for the results of the experiments with the heart motor neuron model. All values are percentages. Standard deviations are included in parentheses. Data for the living system is from A. Wenning [60].

maximum phase differences

living system

	peristaltic	synchronous
phase differences	62.1 (8.8)	42.9 (9.8)

canonical model

	peristaltic	synchronous
inputs	35.1 (3.8)	65.3 (6.3)
phase differences	27.1 (2.8)	47.8 (5.8)
remove coupling	20.8 (2.7)	35.8 (4.2)
remove delays	24.1 (1.9)	36.6 (6.5)
remove plasticity	21.5 (1.9)	42.2 (5.3)

different input pattern (period = 5.3 s)

	peristaltic	synchronous
inputs	32.7 (4.5)	67.9 (6.1)
phase differences	24.6 (3.9)	38.9 (7.0)

canonical model:
inputs with standard phasing

	peristaltic	synchronous
inputs	21.5 (2.4)	68.1 (6.4)
phase differences	22.6 (3.5)	40.6 (7.3)

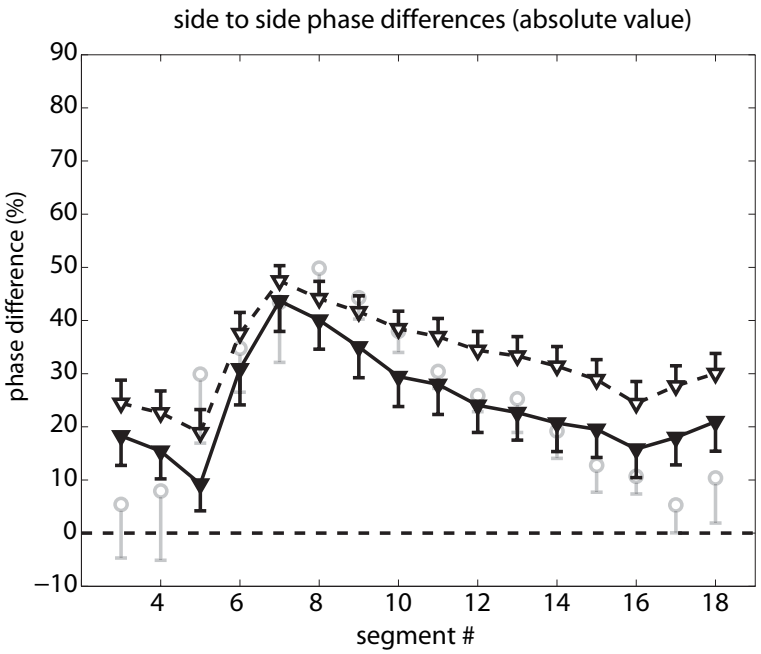

Figure 24: Comparing side-to-side phase differences between each pair of heart motor neurons. Side-to-side phase differences for the canonical model (filled triangles) and for the canonical model without electrical coupling (open triangles) are shown in comparison with the living system (gray transparent circles). Error bars are standard deviations

the G5 – G6 and the G8 – G10 model motor neurons are better approximations of the living system. Neither implementation of the model matched the side-to-side phase differences of the G3 – G4 and G17 – G18 motor neurons. In these regions, marked overlap of the bursts between motor neuron pairs of the same segment is known to occur in the living system. By increasing the electrical coupling in these segments it is clear that an increase in the synchronization of their bursts should follow and perhaps an increase in phase progression on the peristaltic side and an improvement in synchronous coordination among the front motor neurons as well.

In order to determine if a better matching of the side-to-side phase differences of the G3 – G4 motor neurons and the G17 – G18 motor neurons would result in better matching of the phase progressions we constructed the "patterned coupling model". Figure 25A shows the patterns of electrical coupling used in these simulations. An exponentially decreasing function describes the pattern in the front and exponentially

increasing function describes the function in the rear. Different values for the exponent factor (tau) can then be used to describe how steeply the values for coupling changes segment-by-segment. At tau = 0.6, the G3 and G18 motor neurons are nearly perfectly in phase side-to-side. The coupling coefficient in the motor neuron pairs of these segments is over 0.8.

Although, an improvement in the matching of side-to-side phase differences with the living system was accomplished with the patterned coupling model (Figure 25B) this improvement did not extend to the phase progressions. The matching of the longitudinal phase difference to the living system did not improve remarkably in this version of the model. Figure 25C shows the phase progression in the peristaltic mode for the canonical model and the patterned coupling model. Although an increase in phase progression can be observed it still fails to be of the appropriate magnitude. The synchronous phase progression (Figure 25D) does not improve with these manipulations but actually worsens on the whole; although, it should be noted that the G18 motor neuron shows good matching with the living system.

4.4 Phase Differences Between Motor Neurons and Premotor Interneurons

Thus far, all experiments on the canonical model which affected the phase progression of the peristaltic side in our model have been accompanied by reciprocal changes on the synchronous side. Because our phase reference, the G10 motor neuron, was not immune to these changes, it is difficult to assess whether the magnitude of these changes in phase progression were different across the two sides. In order to determine if our experimental manipulations caused changes in the phasing of the motor neurons with respect to their inputs, the phase relationship among the model heart motor neurons needed to be determined with a phase anchor that was not affected by the experiment. These phase relationships in the living system have not yet been

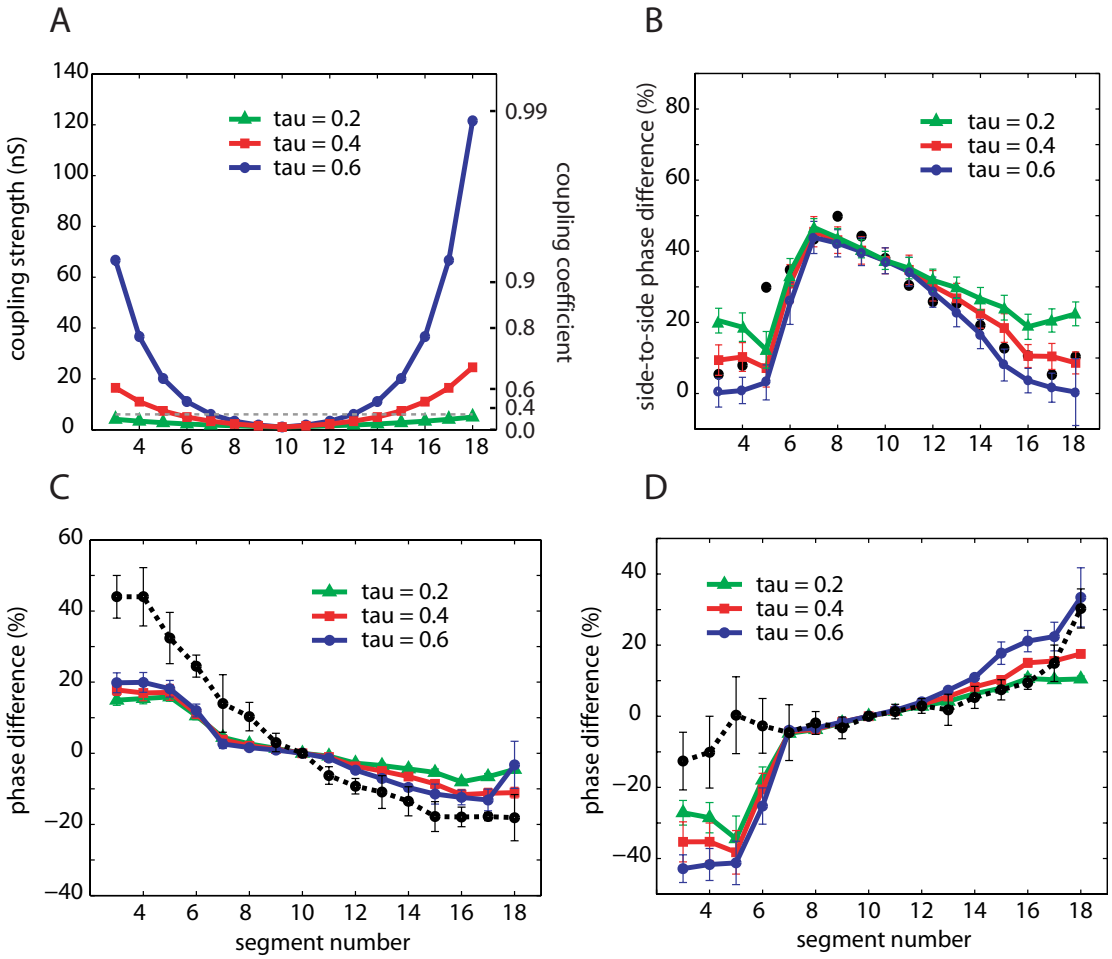

Figure 25: Effects of segmental differences in electrical coupling on motor neuron phasing in the patterned coupling model. A. The different segmental patterns of electrical coupling were based on combining an exponentially decaying function from segment 3 to 10 with an exponentially rising function from 10 to 18. Three different factors of the exponent resulted in 3 different segmental patterns of electrical coupling. In A, B, C, and D these are represented by 0.2 in green, 0.4 in red, and 0.6 in blue. The value for the maximal conductance of the electrical coupling used in the canonical model (6 nS) is shown in A as a gray dotted line. The vertical scale on the right is coupling coefficient. B. The comparison of side-to-side phase differences among the different coupling patterns is shown with the side-to-side phase differences of the living system (black circles; error bars removed for clarity). C. The peristaltic phasing in the 3 different patterned-coupling models reveals a mild increase in phase differences with an increase in exponent factor. D. The synchronous phasing in the 3 different patterned-coupling models also reveals an increase in phase progression with an increase in exponent factor.

determined experimentally. The phase relationship among the identified premotor interneurons has been determined in the living system [41] [58] and the phase relationships of the motor neurons has been determined in the living system [60]. However the relationship of the phase of each premotor input to each premotor output has not been examined in the living system.

Figure 26 illustrates the phase relationships between all of the motor neuron bursts and all of the synaptic input in the canonical model. It is intended to be compared with the same graph for the canonical model with the electrical coupling removed shown in Figure 27. The phase anchor for these two phase diagrams is the peristaltically coordinated G4 interneuron; as its phase timing (and that of the rest of the premotor inputs) was unchanged with removal of the electrical coupling .

The phase diagrams in Figure 26 and Figure 27 show that the inputs from the HN(X) interneuron are relatively in phase across the two sides. Therefore, mutual inhibition was shared amongst the segmental pairs during these premotor bursts in the canonical model with electrical coupling. Because the bursts of the G3 and G4 interneurons are in anti-phase, their inhibitory influence is slightly diminished through the electrical coupling because approximately one-third of the inhibitory synaptic current was effectively leaked to the contralateral cell via the electrical coupling. The artifactual sharing of depolarizing current via the electrical coupling (discussed in Section 3.2) may also contribute to this effect because the contralateral motor neuron was active while receiving the contralateral inhibitory current. Interestingly, the phase of the peristaltically coordinated G3 – G5 motor neurons had little change in their phase relationship with respect to their premotor inputs when the electrical coupling is removed, although, their phase differences with the G10 motor neuron did change. The synchronously coordinated G3 – G5 motor neurons had a noticeable shift in their phasing with respect to their synaptic input when the coupling was removed.

These changes in phase are more apparent in the summary phase diagram, Figure

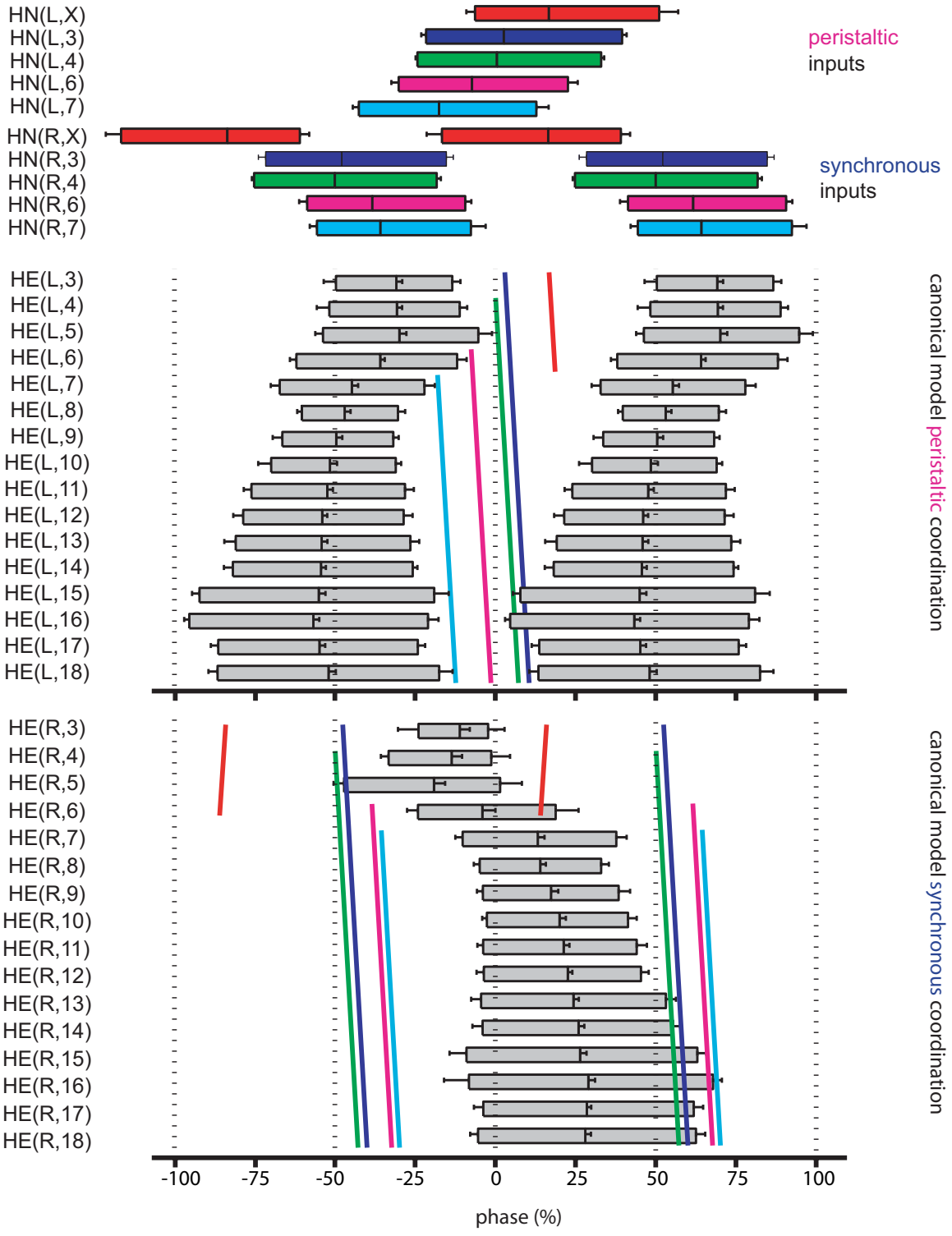

Figure 26: Phase diagrams of the canonical model timed with respect to the phase reference of the premotor inputs. The G4 interneuron on the peristaltic side is used as the reference for the activity of all motor neurons in the model. Vertical lines represent the phase of each of the premotor inputs in peristaltic coordination (above) and synchronous coordination (below). The slope of the vertical line indicates the conduction delays in each segment. Color legend is the same as Figure 9.

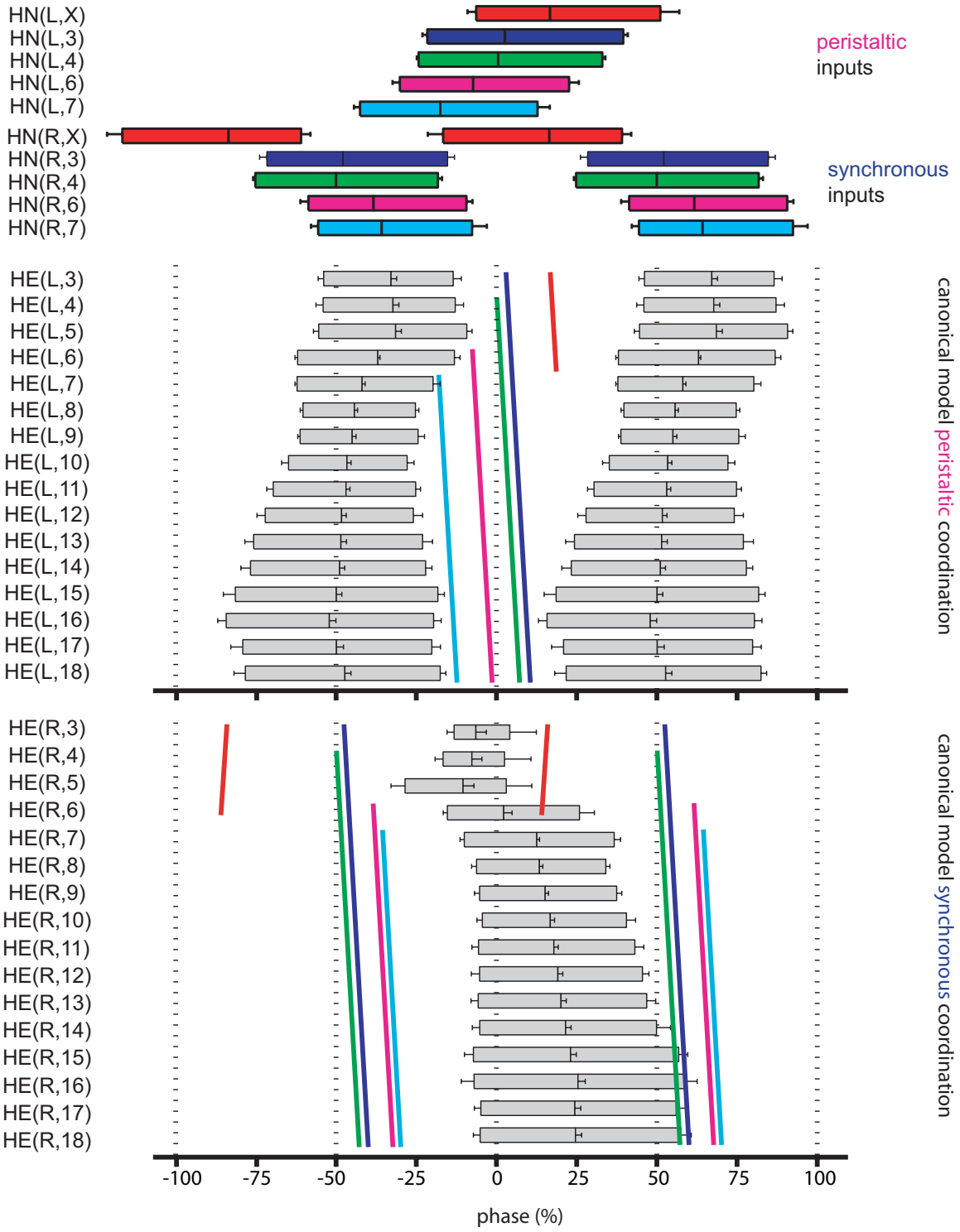

Figure 27: Phase diagrams of the canonical model without electrical coupling timed with respect to the phase reference of the premotor inputs. The G4 interneuron on the peristaltic side is used as the reference for the activity of all motor neurons in the model. Vertical lines represent the phase of each of the premotor inputs in peristaltic coordination (above) and synchronous coordination (below). The slope of the vertical line indicates the conduction delays in each segment. Color legend is the same as Figure 9.

28, where the phasing of the canonical model is compared to the phasing without electrical coupling and the G4 peristaltically coordinated interneuron is used as the phase anchor. This effect on phasing is unnoticeable by examining phase diagrams like those shown in Figure 21 because in those phase diagrams the phase of the anchor cell (G10 motor neurons) was changed with the experimental manipulation. This effect is also undetectable in Figure 24 which examined the absolute value of the phase differences from side-to-side.

Although small, the changes in motor neuron phasing with respect to the phase of the premotor inputs upon removal of the electrical coupling inspire us to determine these phase relationships in the living system. Further examination of the changes in input/output phasing resulting from manipulation of intrinsic membrane currents and synaptic properties, like synaptic modulation and the conduction delays, should be performed in this model and in perhaps other more abstract models, like that presented in Chapter 5.

4.5 Parameter Variation

We have examined the effects of the synaptic properties: electrical coupling, conduction delays, and intra-burst synaptic plasticity by removing them in the model. These and other parameters were systematically varied over a range of values to get a more complete picture of their role in the canonical model. We illustrate our results of parameter variations by examining three coupled pairs of motor neurons from the middle segments 7, 10, and 13 that receive inhibitory input from the same premotor interneurons. The parameter variation manipulated key factors in synaptic function, excitability, and outward K^+ currents. The synaptic parameters varied were: the time constant of plasticity, the maximal conductance of the electrical coupling, and the length of the conduction delays. The excitability factors were: maximal conductance of the persistent sodium current, membrane resistance, and the scale factor of

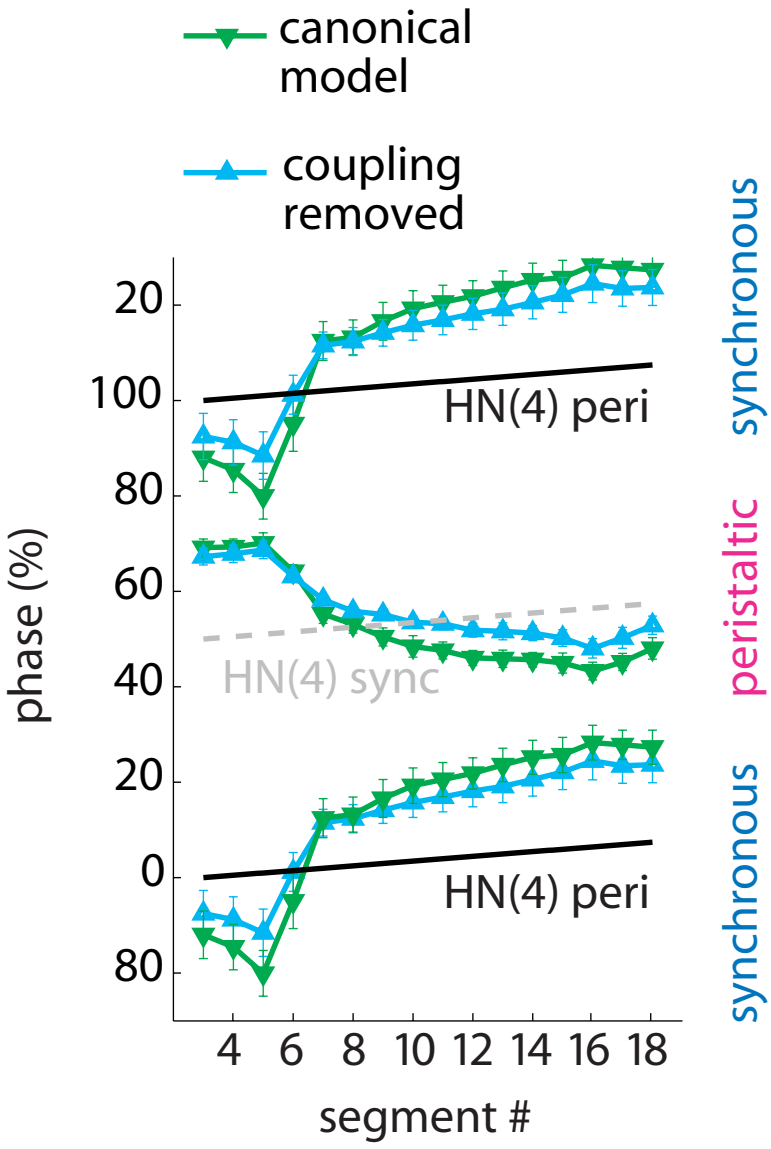

Figure 28: The bilateral phase relationship of the canonical model with and without electrical coupling timed with the peristaltic G4 interneuron as phase reference. The green triangles represent the canonical model and the cyan triangles represent the canonical model without electrical coupling. Two synchronous (above and below) and one peristaltic (middle) phase curves are shown for the results of each model. The phase reference, the G4 peristaltic interneuron is shown as a solid black horizontal line, and the phase of its contralateral homolog, the G4 interneuron on the synchronous side is shown as a dotted gray line. The slopes of these lines indicate the conduction delays from segment to segment.

the inhibitory synaptic input (see Figure 18). The maximal conductance of the inactivating potassium current (K1), the non-inactivating K^+ current (K2), and the fast transient K^+ channel (KA) were also manipulated in the parameter variation. Each of these parameters was systematically varied between 0 and 200% of the canonical value.

Figure 29 shows the results of the parameter variation on the duty cycle of the G10 motor neuron in synchronous coordination. The results in peristaltic coordination were similar. The results for the G7 and G13 motor neurons were also similar. Duty cycle decreases with lower values of the synaptic plasticity but does not increase with higher values. Electrical coupling and conduction delays had little effect on duty cycle. Duty cycle was greatly affected by variations of the excitability factors. Increases in persistent sodium current and in membrane resistance correspond to increases in duty cycle. As the synaptic scale factor increased the duty cycle decreased. Only small changes in duty cycle are observed with manipulation of the conductance of the potassium channel. Although, a slight downward trend to the curves can be seen (especially in the non-inactivating K^+ current, K2) this is to be expected as increasing these conductances leads to an increase in outward current to the motor neuron.

Figure 30 shows the phase difference between the G7 and G13 motor neurons in each coordination state and the side-to-side phase differences of these motor neurons for variations in the critical parameters for the synaptic properties. Variations of the parameters involved in the production of K^+ currents and the excitability factors had little to no effects on phase progression in these motor neurons. The phase difference between the G7 and G13 motor neurons is decreased with decreasing the conductance of the electrical coupling in both coordination modes. This phase difference is decreased with a decrease in the synaptic plasticity time constant and the conduction delays for the synchronous mode but a decrease in these parameters causes an increase in phase difference between G7 and G13 in the peristaltic mode. In both the

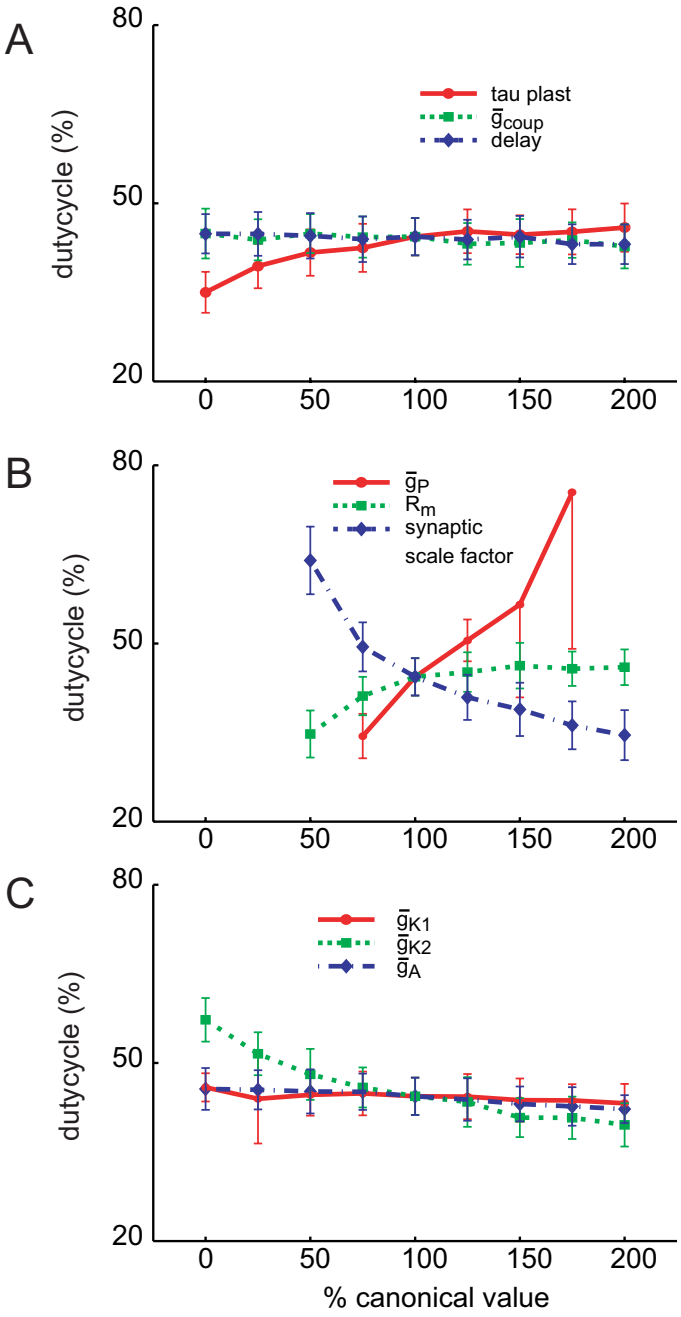

Figure 29: The effect of varying synaptic factors, excitability factors, and maximal conductance of outward currents on the duty cycle of the synchronous G10 motor neuron in the canonical model. A. The rise-time of the synaptic plasticity (tau plast), the maximal conductance of the electrical coupling (gcoup), and the value of the conduction delays (delay) were varied from 0% to 200% of canonical values. B. The maximal conductance of the P-current (gP), the membrane resistance (Rm), and the scale factor for the inhibitory synaptic input (scalefactor) were varied. C. The maximal conductance of the delayed rectifier K+ current (gK1), the persistent K+ current (gK2), and the A-current (gA) were varied.

peristaltic and synchronous modes the manipulation of the time constant of synaptic plasticity appears to have a bi-phasic effect. The side-to-side phase differences are changed very little with manipulations of the delays or the plasticity but the coupling term tends to collapse these differences especially in the G13 motor neuron; as its inhibitory synaptic input was more in phase.

4.6 Summary of Canonical Model Results

In this first-generation model of the production of the heartbeat by motor neurons in the medicinal leech, we did not expect an exact reproduction of the phase timing involved in the intersegmental coordination present in the living system. The canonical model mainly deviated from the living system in the magnitude of the phase progression in the two coordination states. Rather surprisingly was the relatively small effects of synaptic phenomena on phasing. Experimentally determining the phase of the motor neurons with respect to the premotor interneurons would help identify which motor neuron segments are not modeled appropriately. Our model also identifies new avenues for theoretical modeling in order to fully characterize the effects of synaptic phenomena and electrical coupling on phase progression.

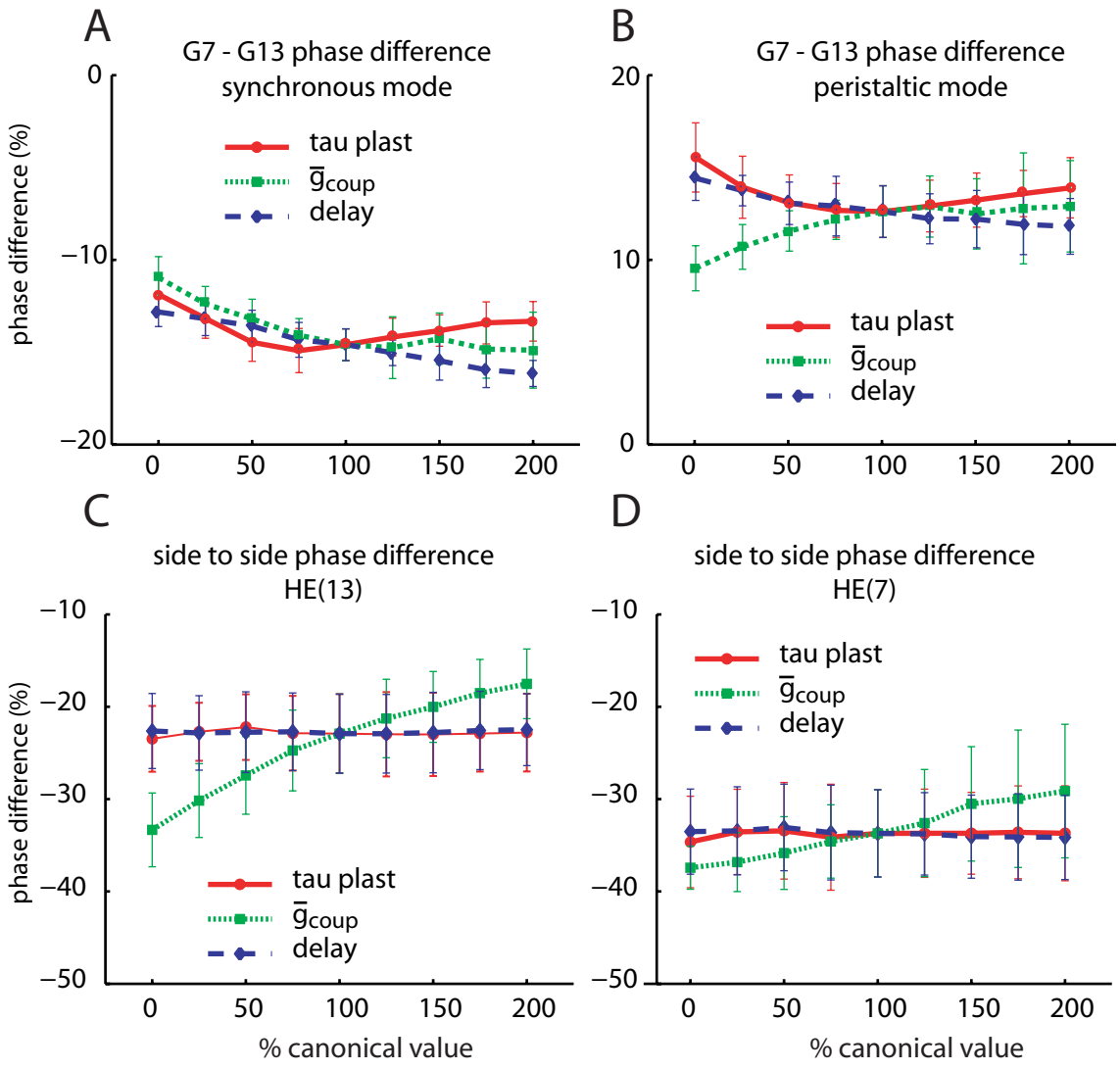

Figure 30: The effect of varying synaptic factors on phasing and side-to-side phase-timing in G7 and G13 motor neurons. The legend labels are identical to those in Figure 29A. A. The effect of varying the synaptic factors on the phase difference between the G7 and G13 peristaltic motor neurons in the canonical model. B. The effect of varying the synaptic factors on the phase difference between the G7 and G13 synchronous motor neurons in the canonical model. C. The effect of varying the synaptic factors on the side-to-side phase difference between the pair of G13 motor neurons in the canonical model. D. The effect of varying the synaptic factors on the side-to-side phase difference between the pair of G7 motor neurons in the canonical model.

CHAPTER V

INTERSEGMENTAL COORDINATION IN AN ABSTRACT MODEL OF MOTOR NEURONS

The canonical model does a reasonable job at describing the behavior of the system and certainly further understanding of the heartbeat system of the leech will involve revisions to that model. However, the results of our experiments with the canonical model, also encouraged us to examine general theories of the involvement of electrical coupling, synaptic plasticity and conduction delays on phasing. These would be difficult to address in the canonical model because the magnitude of the phase differences was mild. Therefore, we undertook the construction of an abstract model not constrained by the temporal and spatial input patterns based on results from the living system. We aimed to produce a more general model of intersegmental coordination of motor neurons that achieved larger phase differences with which to begin the investigation of synaptic properties on motor neuron phasing. By developing general theories about phasing of motor neurons by rhythmic inputs, we hope to impact future versions of our experimentally-constrained canonical model and models of other intersegmentally coordinated systems.

5.1 Temporal and Spatial Patterns of Synaptic Input of the Abstract Model

In the canonical model, both the synchronous and peristaltic maximal phase differences were smaller than the maximal phase differences of their respective premotor inputs (Table 2). To determine how the phasing of the inputs combined with electrical coupling to influence maximal phase difference of the motor neurons, we constructed

an abstract model with artificially constructed temporal and spatial input patterns. The spatial pattern was intended to maximize the phase difference of the inputs among the phase differences of the outputs. Figure 31 compares the spatial pattern of synaptic weights and the temporal phase pattern between the inputs to the canonical model and those of the abstract model. Our abstract model had four inputs instead of five with an increase in the phase differences among these four premotor cells. But, the maximal phase differences of the peristaltic and synchronous inputs to the abstract model did not exceed that of the inputs used in the canonical model (see Table 3).

The spatial pattern of synaptic weights used in the abstract model was inspired by the natural pattern of the heartbeat system, but it was modified so that each motor neuron received a combination of only two synaptic inputs; and that the curves of these weights varied segmentally as a cosine relationship with each premotor input offset by 90 degrees. Although, the individual conductances for each synapse were higher in the abstract model, the total synaptic inhibition received was similar between the model motor neurons in the abstract model and those that received the maximum in the canonical model. The temporal pattern for each premotor input in the abstract model are not derived from extracellular recordings but are simulated spike-time data arranged in bursts. Raster plots of these inputs are shown in Figure 32. The characteristic waxing and waning of intra-burst spike frequency seen in the inputs to the motor neurons was reproduced in the inputs to the abstract model (compare Figure 32 to Figure 9), the period was the same between the abstract model and the canonical model. Like, the canonical model, each segment in the abstract model contained an electrically-coupled pair of motor neurons. The parameters for the electrical coupling, the intrinsic membrane properties, the plasticity, and the conduction delays were all identical between the abstract and canonical model. The intrinsic properties of each output motor neuron of the abstract model were exactly like that

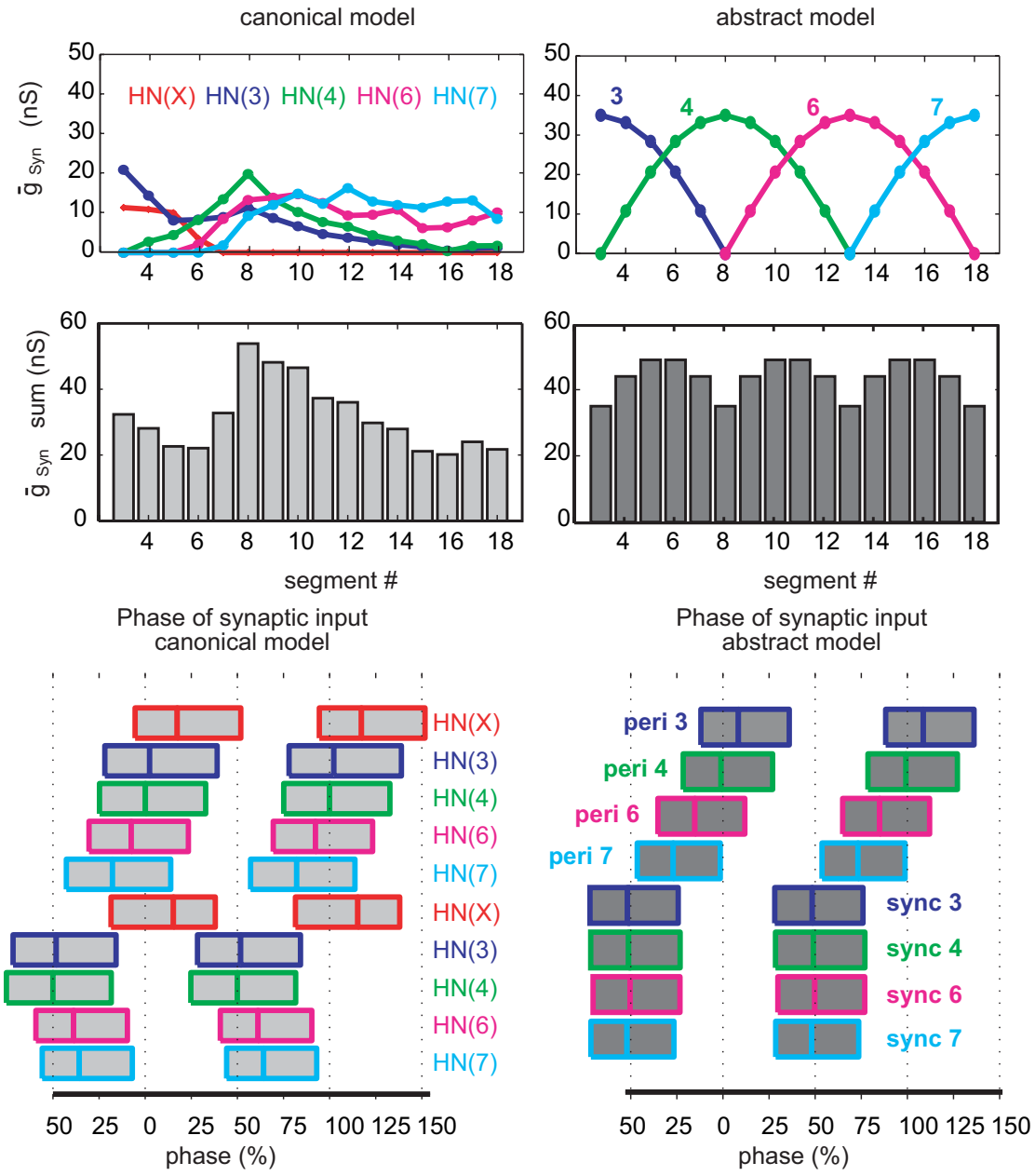

Figure 31: A comparison of inputs to the canonical model with inputs to the abstract model. For the abstract model, both the spatial (upper four panels) and the temporal (lower two panels) were modified from the canonical model. Each motor neuron in the abstract model received synaptic inhibition 2 of a possible four premotor cells. The spatial pattern was distributed in a regular pattern. The synchronous inputs to the abstract model were in near synchrony (see Table 3). A rear-to-front progression occurs in the peristaltic inputs. Peri 7 (cyan) leads peri 6 (magenta) by 10% of phase. Peri 6 leads peri 4 (green) by 15%. And, peri 4 leads peri 3 (blue) by 10%.

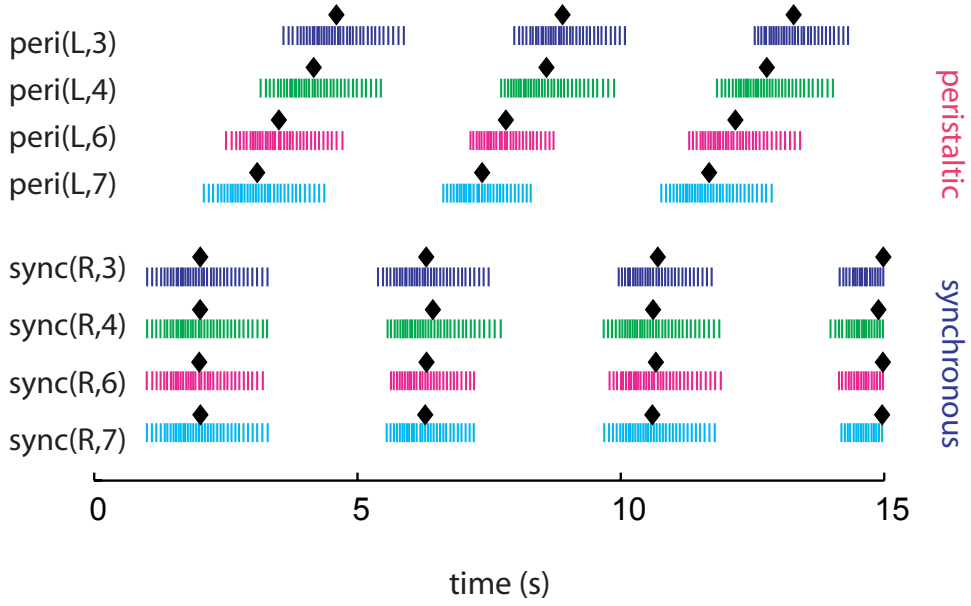

Figure 32: Raster plots of premotor spike-time inputs to the abstract model of intersegmental coordination. Spike events of both peristaltic (upper 4 traces) and synchronous (lower 4 traces) inputs are represented as vertical lines. Median spike of the bursts are designated with black diamonds. Color legend is the same as Figure 31. The traces shown are only the first 15 s; the model was run for 60 s. The period of the inputs to the abstract model was the same as the inputs to the canonical model, 4.3 s.

for the canonical model, as described in Sections 2.3 and 3.2.

5.2 Voltage and Phasing Results of the Abstract Model

The voltage records and longitudinal phase difference curves for the abstract model are shown in Figure 33. The trends of peristaltic and synchronous coordination were easily recognizable in the abstract model of intersegmental coordination. A subtle pattern of duty cycles was present on the peristaltic side; where the middle segments were slightly shorter in duration than the front and rear segments. Interestingly, a subtle pattern of intra-burst spike frequency in the motor neuron bursts can be

observed in the rear segments. The highest spike frequencies in each peristaltic burst appear more often at the beginning of each burst and at the end of each burst in synchronous coordination. These regions correspond to a sharing of depolarizing current via the electrical coupling as the pair of motor neurons are active at the same point in time. The bilateral phase diagram in Figure 21 shows this overlap in phase.

The phase difference curves of the abstract model are compared with the canonical model to contrast the results of two different sets of input patterns. Table 3 compares these values of phase differences. A greater maximal phase difference was observed on the peristaltic side than on the synchronous side in the abstract model. The front-to-rear maximal phase difference among the peristaltic segments (39%) exceeded maximal phase difference of its inputs (35%) in magnitude. On the synchronous side, the phase difference among the inputs (2%) was also smaller than maximal phase difference among the outputs (15%). The phase differences of the peristaltic G3 – G11 motor neurons were similar between the abstract and canonical models. The G12 – G18 motor neurons show greater phase differences in the abstract model because a greater difference among the G6 and G7 premotor inputs was realized with the changes in the spatial pattern. The temporal phase difference among these premotor inputs was actually greater in the canonical model. The longitudinal phase differences in synchronous coordination were similar in most motor neurons of the canonical and abstract models, except among the G3 – G6 motor neurons. The HN(X) interneuron dominates the phasing of these inputs in the canonical model and its input was excluded in the abstract model.

5.3 Experiments with the Abstract Model

5.3.1 Effects of electrical coupling on motor neuron phasing in the abstract model

The results of the abstract model with the coupling removed are presented in Figure 34 in order to examine its contribution to maximal phase difference in this abstract

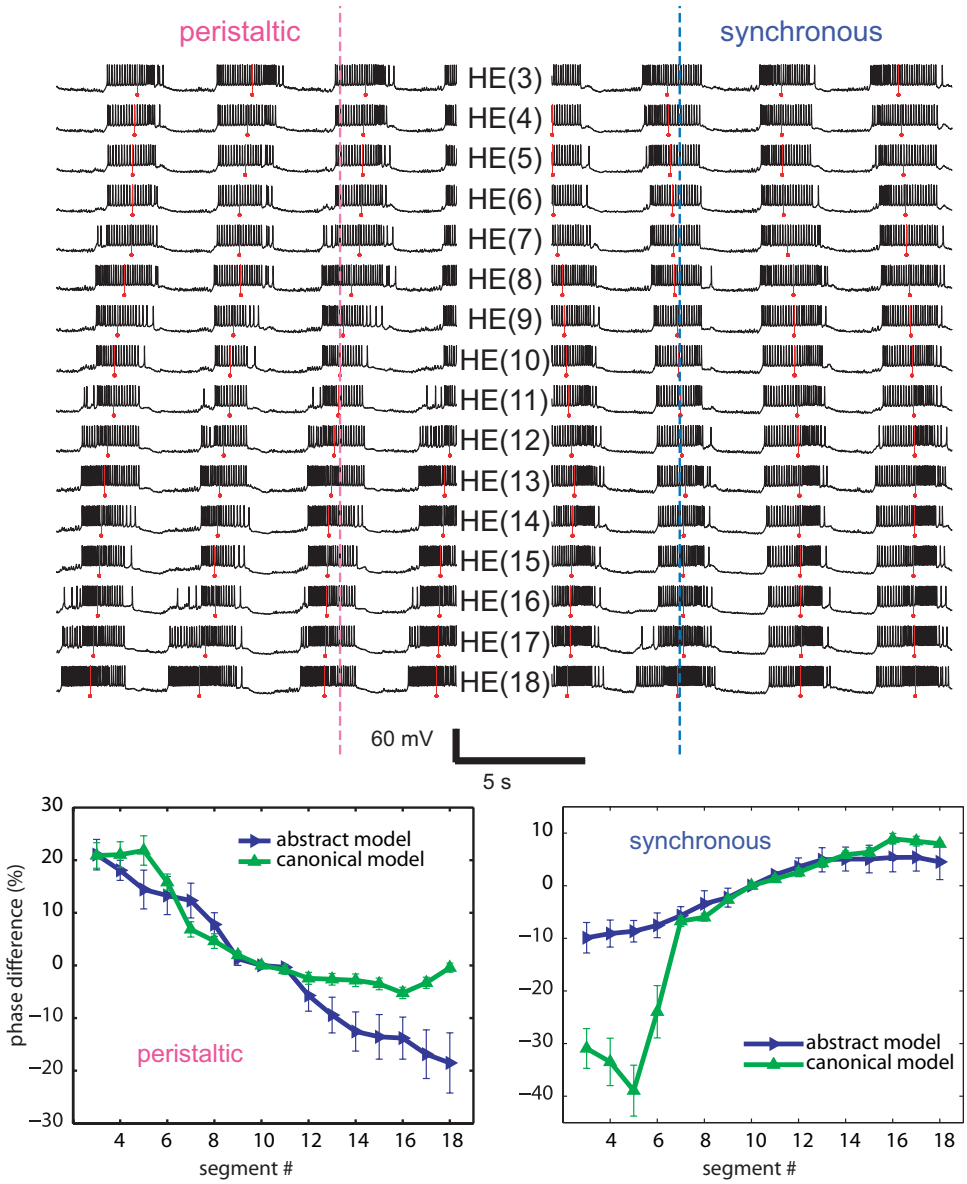

Figure 33: Voltage records and longitudinal phase difference curves for all neurons in the abstract model. Like the canonical model (Chapter 4), both peristaltic (left) and synchronous (right) coordination states were modeled in each segment. Our phase markers are represented as a red circle below the voltage trace. The G10 motor neuron of the abstract model is used as the phase reference. The rear-to-front phasing in peristaltic coordination is evident as is the near synchronous firing of bursts in synchronous coordination. The effect of the input patterns presented in Figure 31 on the magnitude of the segmental phase differences is shown in the longitudinal phase difference curves (below).

model. The longitudinal phase relationships were similar with and without the electrical coupling in the abstract model but the magnitude of the maximal phase difference decreased to values similar to the maximal phase differences of the inputs: 31% for peristaltic coordination mode and 5% for synchronous coordination (see Table 3). As shown by the bilateral phase diagrams (Figure 34), the activity of the front and rear motor neurons was synchronized by the electrical coupling in the abstract model; and its removal decreased the overlap of their spike activity. In the abstract model, the rear motor neurons received more similar input across the two-sides and the effect of the electrical coupling was greater on these motor neurons. Like the phase results presented in Chapter 4, this effect is somewhat masked in the longitudinal phase difference curves because our phase reference the G10 motor neuron changes its phase.

5.3.2 Effects of removing synaptic plasticity and conduction delays on motor neuron phasing in the abstract model

The rear-to-front phase progression in the peristaltic mode is hampered by the front-to-rear conduction delays in the abstract model and their removal increases maximal phase difference in the peristaltic mode increased as might be expected (Figure 35). The contribution of the HN(X) interneuron to the G3 – G6 motor neurons in the canonical model resulted in a mild decrease in maximal phase difference with removal of the conduction delays (Figure 22). The phase differences with respect to the G10 motor neuron decrease in the synchronous mode. The effect of removing the intra-burst synaptic plasticity in the abstract model was also opposite the effect of removing this synaptic property in the peristaltic mode of the canonical model. In the abstract model, the G3 – G8 motor neuron pairs, who received synaptic input from the premotor cells that were most anti-phasic in their firing across the two sides, increased their average phase difference with respect to the G10 motor neuron with a removal of the plasticity. Only little changes in the phase difference occurred in

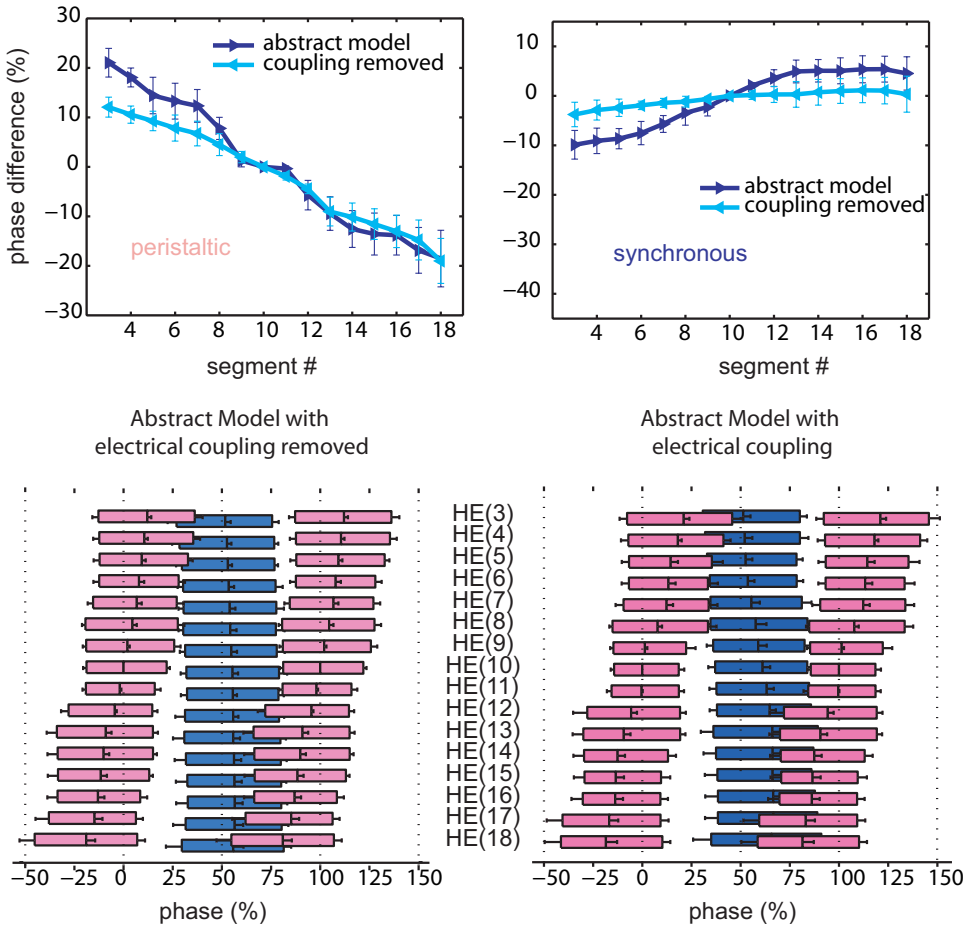

Figure 34: Removing electrical coupling decreases longitudinal phase differences in the abstract model. Similar to the canonical model (Chapter 4), removal of the electrical coupling decreases the maximal phase differences in each coordination mode (see also Table 3). This occurs because the electrical coupling has a synchronizing effect on the motor neuron bursts that is greatest in the front and rear segments.

Table 3: Comparing maximal phase differences for the results of the experiments with the abstract model. All values are percentages. Standard deviations are included in parentheses.

maximum phase differences

abstract model

	peristaltic	synchronous
inputs	35.3 (2.2)	1.7 (4.0)
phase differences	39.6 (6.4)	15.3 (3.9)
remove coupling	31.1 (5.0)	4.9 (3.5)
remove delays	44.1 (6.0)	10.9 (4.1)
remove plasticity	48.7 (6.8)	17.6 (4.6)

the other motor neurons. The synchronous coordination mode shows a small increase in maximal phase difference due to the change in phase difference seen in the front motor neurons.

5.4 Chapter Summary

The inputs of the abstract model are more efficient at preserving the longitudinal maximal phase differences of each coordination mode. The differences in the temporal and spatial patterns between the canonical and abstract model results in the maximal phase difference actually exceeding that of the inputs in each coordination state. Unlike the parameter variations of the canonical model that resulted in mild changes in phase difference among the G7 - G13 motor neurons that were often mirror images across the two sides, the abstract model produced different maximal phase differences in each coordination mode among these middle segments. Further experimentation with the abstract model could be used to address more general questions regarding the effects of input patterns and synaptic properties on phasing. For example, this model can be used to measure the output phasing from many different temporal and spatial input patterns in order to determine the critical features necessary to maximize intersegmental phase differences. The abstract model also gives us insight

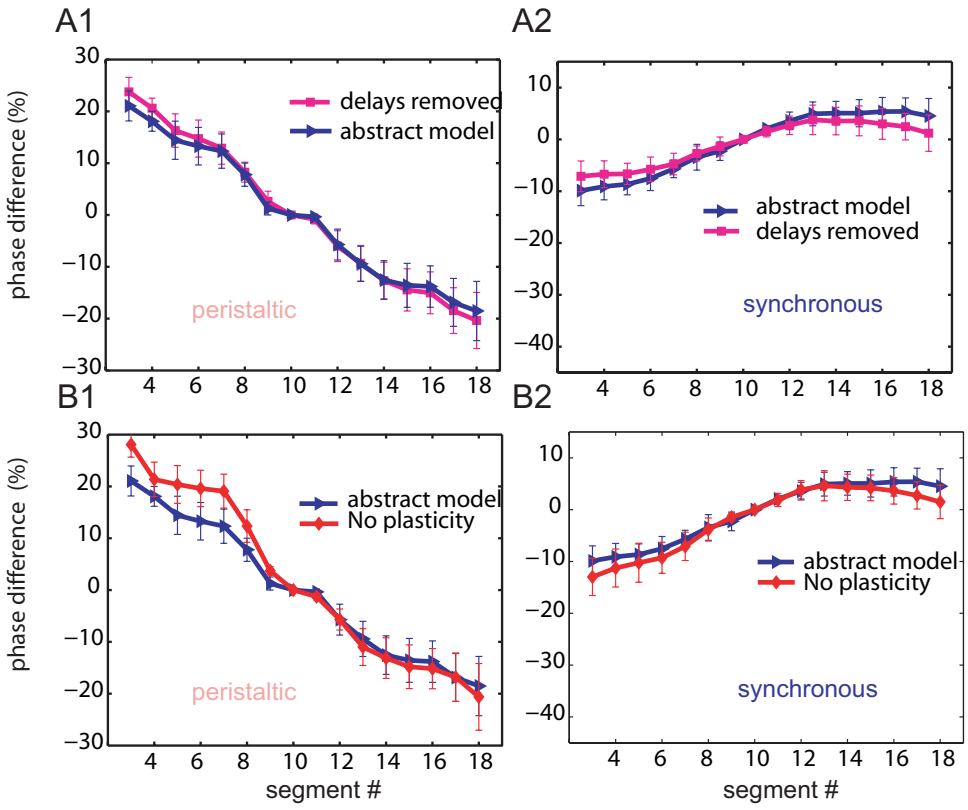

Figure 35: Effects of removing conduction delays and intra-burst synaptic plasticity on longitudinal phase differences in the abstract model. A. In the peristaltic coordination mode (A1) the removal of the conduction delays resulted in a mild increase in the phase difference curve for the canonical model. This is an opposite effect than what is seen in the canonical model (Figure 22A1). In the synchronous mode (A2) the delays appear to enhance phase differences in the abstract model. This is a similar effect to that shown in Figure 22A2. B. The removal of the intra-burst synaptic plasticity also increases the maximal phase difference in the peristaltic mode (B1). In synchronous coordination (B2), the removal of plasticity in the abstract model increases the phase difference between the front motor neurons and the phase reference but decreases the phase difference between the rear segments and the phase reference.

into the intersegmental coordination of motor neurons in the leech heartbeat system. For example, we can be fairly certain that the living system makes use of an inefficient pattern of synaptic weights for its temporal pattern of premotor inputs. Determining how the heartbeat system uses its pattern to achieve motor neuron coordination or perhaps, discovering its maximization of a different variable besides longitudinal phase difference (e.g. energy) will be enormously helpful in understanding the system.

CHAPTER VI

DISCUSSION

The purpose of this thesis research was to study how the output of a central pattern generating (CPG) network coordinates segmental motor neurons into bilaterally asymmetric patterns of rhythmic activity. The construction of the model of intersegmental coordination of heart motor neurons rigorously examined our current knowledge of the leech heartbeat system. The reproduction of the general characteristics of both the peristaltic and synchronous coordination mode is a satisfying result. However, greater appreciation of the specific features of the heartbeat system was achieved through the experimentation with the model and by investigating the portions of the model that are most inconsistent with the living system.

6.1 Conclusions on the Model of Intersegmental Coordination

6.1.1 General Conclusions on Phasing Results

In our model of intersegmental coordination the most important determinant of the phase relationship among the motor neurons was the spatial and temporal pattern of synaptic inputs. The bursts of action potential firing in each motor neuron was generated from the cessation of inhibitory synaptic input (see Figure 16). Although it was expected that motor neuron phasing would reflect the input pattern, it was not expected that the electrical coupling, the intra-burst synaptic plasticity, and the conduction delays would have such little influence on motor neuron phasing in the canonical model. Taken in its entirety, our model is essentially driven by its synaptic inputs and for this reason its phasing results do not match perfectly those of the

living system (Figure 3). We propose that future work concentrate on characterizing how these inputs are integrated by the heart motor neurons in the living system and then update this model to quantitatively describe the intersegmental coordination of motor neuron phasing in the leech heartbeat.

Our results show that the plasticity, delays, and coupling have only a mild contribution to phase differences of motor neurons in the model. The removal of each of these factors from the canonical model resulted in decreases in maximal unilateral phase difference (Figures 22 and 21). Decreasing maximal phase differences in peristaltic coordination decreased the matching to the living system and decreasing maximal phase differences in synchronous coordination increased the matching to the living system (summarized in Table 2). Manipulation of parameters involved in the electrical coupling, conduction delays and intra-burst synaptic plasticity beyond physiologically measured ranges did show mild effects on phase differences between motor neurons. These more specific effects on phase differences are discussed in the next sub-section.

The canonical model produced only the general characteristics of the peristaltic and synchronous coordination modes and did not reproduce the proper amplitudes of the characteristic unilateral phase differences. Because this model incorporates our best available experimental data, we must consider which assumptions made during the model construction might be limiting the ability of our model to describe the phasing of the living system. The intersegmental coordination of heart motor neurons was modeled as a system driven by both its synaptic input and the integration of nonlinear properties of these synaptic inputs, such as synaptic plasticity. We have concluded that these properties have little effect on the phase difference curves characteristic of peristaltic and synchronous coordination. Therefore, we must examine how we modeled the integration of synaptic inputs by the motor neuron in order to determine how our model failed to reproduce the phasing of the living system.

The motor neurons responded predictably to their synaptic inputs as described by the Frequency vs Injected Current (F-I) curve in Figure 15B. The shape of the F-I curve will depend on the values chosen for the maximal conductances of the ion channels. The values for these conductances were not based on values measured from the living system but instead tuned by hand to resemble intracellular recordings of the motor neurons. Most notably, the canonical value of the maximal conductance of the persistent sodium channel, $\overline{g}_{NaP}$, was used to tune the intrinsic firing frequency of the model motor neurons (Figure 15A) to resemble the maximum frequency within a burst observed in extracellular nerve recordings of the heart motor neuron [60]. The results of systematic variation of the conductance of this channel illustrated how sensitive the motor neuron activity (duty cycle) is to this channel (Figure 29B). The motor neuron activity is less sensitive to similar variations of the maximal conductances of the outward currents over this range (Figure 29C). Combined with the results from the extracellular recordings of motor neurons in the presence of bicuculline (Figure 14) this latter result suggests that better characterization of the currents that determine the firing threshold (inward currents) will be most critical in determining which excitability characteristics should be adjusted or added in future generations of the model. In summary, the model motor neurons were modeled very simply in this first-generation model. It will be important to better characterize the actual ion channels in the heart motor neurons through experiments in the living system. Examining differences among current densities between motor neurons of different segments or between different compartments of the same motor neuron (as in a multi-compartment model) could also be important for reproducing the phase relationships of these cells.

6.1.2 Specific Conclusions and Experimental Recommendations

The time due to axonal propagation was modeled by delaying synaptic input to the model motor neurons according to the segmental ganglion of origin. A constant 20 ms per segment was used to determine the conduction delays. We don't recommend evaluating the delays due to axonal conduction in the living system as their relative contribution is minimal (Figure 22). The effect of delays on phasing is decreased with increases in period and their effect was already comparatively small in our canonical model which was based on premotor inputs with period on the lower end of the range measured in the living system (Section 2.4). The results of manipulating the 20 ms delays on peristaltic phase differences in the G7 – G13 motor neurons and the abstract model illustrate that conduction delays oriented in the rearward direction will in general slightly decrease rear-to-front phase differences and slightly enhance front-to-rear phase differences (Figures 30 and 35). The reason why removal of conduction delays decreased phase differences in peristaltic coordination along all segments in the canonical model illustrates how effective the HN(X) inhibitory input is on determining the phase of these cells.

The inhibitory synaptic input from the HN(X) interneurons dominates the phasing of the front motor neurons in the model (see Figures 19 and 20). This input is the least understood of all of the inputs used in the model (see Section 2.5). The spatial and temporal pattern for the HN(X) interneuronal inputs should be more accurately estimated through experimentation in the living system and then incorporated into the model of intersegmental coordination of motor neurons. Additionally, the failure of the two rearmost motor neuron segments to produce clear bursts when their synaptic weights are set to the values measured from the living system supports the hypothesis that additional synaptic input to these motor neurons may exist. If these inputs are identified and characterized in the living system than their spatial and temporal pattern of synaptic input should also be included in future generations of

this model.

Not only should the relative phasing of these unidentified rear inputs and HN(X) interneurons with respect to the other premotor inputs be determined but also the phasing of all premotor inputs with respect to the motor neurons should be quantified. Our model shows a specific phase relationship between motor neurons and their premotor input (Figure 28). But these phase relationships cannot be evaluated for correctness as they have not been determined in the living system. Because bursting in our model motor neurons primarily depends on the inhibitory synaptic input (see above), comparing these input/output phase relationships is critical to evaluating which motor neuron segments are properly phased in the model.

Although, the spatial and temporal input patterns are of primary importance in determining motor neuron phasing in our model, the peristaltic and synchronous phase progressions are inter-dependent because of the electrical junctions (Figure 21). Electrical coupling decreases side-to-side phasing between each segmental pair of motor neurons. This effect is greatest in the front (G3 – G6) and rear (G15 – G18) motor neuron pairs because their peristaltic and synchronous inputs overlap in phase bilaterally (Figure 24). Increasing the conductance through the electrical junctions to unphysiological values improved the matching of the side-to-side phase diagrams but did not improve longitudinal phase differences (Section 4.3). The results from the parameter variation show that the decrease in side-to-side phasing that occurs with increases in electrical coupling is greater in those segmental pairs which receive inhibitory input that is more in phase bilaterally (Compare Figure 30C to 30D). The overall effect on phase differences is still comparatively small with the input pattern of the canonical model. However, should experiments reveal different input patterns for the HN(X) interneuron or additional rear inputs, the electrical coupling effects on unilateral phase differences could change. Therefore, we propose that experiments addressing segmental differences in electrical coupling be evaluated

in the living system.

We recommend that researchers interested in determining the quantitative phase relationship of the intersegmentally coordinated heart motor neurons in the leech improve upon this model by tuning the parameters for ion channels and electrical coupling among a specific segmental pair. The tuning could be done by hand or with some optimization routine that uses ranges for the parameter variation based on intuition gained from this model and the experiments aforementioned on characterizing intrinsic membrane properties of the motor neurons. The parameters to be varied would include: the maximal conductances of the newly characterized ion channels and the conductance of the electrical coupling. This tuning should be done in both single-compartment and multi-compartment motor neuron models because motor neuron cell geometry is known to effect the filtering and rectification of the electrical junctions in the living system [44]. Success of the tuning would be evaluated by comparing the matching of the maximum and minimum firing frequencies within a burst, the side-to-side phase differences of the motor neuron pair, and the phasing of these motor neurons with respect to their inputs. This tuning could then be done for each motor neuron segment and compared to segmental differences as observed in the living system. If the results of the tuning of these parameters within ranges established from experiments in the living system still result in poor matching between the model and the living system, the time constant of synaptic plasticity, and the maximal synaptic conductance values for the premotor cells be incorporated into the tuning. Our intuition gained from this thesis suggests that the spatial pattern of inputs is less specific in the living system than the temporal pattern of inputs. This intuition is based on the manipulation of these two patterns in the abstract model. However, the characterization of the different contributions of these two patterns to motor neuron phasing is still incomplete in the abstract model.

6.2 Predictions for the Living System

Influencing experimental design is a positive contribution of many models towards understanding a neuronal network [9]. Here we propose several new avenues for exploration in the living system that will enhance our understanding of the leech heartbeat and intersegmental coordination in general. Briefly, we propose that experimenters examine (1) the excitability and production of bursting activity in heart motor neurons (2) the effects of electrical coupling on side-to-side and longitudinal phase differences, and (3) the differences in the temporal pattern of the HN(X) input in the two coordination modes and the effects of these differences on phasing.

6.2.1 Generation of burst activity by heart motor neurons

The burst firing of action potentials in our heart motor neuron model was achieved by extinguishing the intrinsic tonic spike activity at regular intervals by the synaptic input from inhibitory premotor heart interneurons (see Chapter 3). This is supported by data from intracellular recordings of heart motor neurons (see Figure 14). Our model proposes that in addition to the coordination of longitudinal phase differences of the motor neurons, the duty cycle, and the modulation of intra-burst firing frequency are also shaped by the integration of the premotor input with intrinsic membrane properties and the electrical coupling. Despite, much of our discussion thus far being on phase relationship among the motor neurons, it is not known if the waxing and waning of spike frequency during motor neuron bursts occur according to the mechanisms proposed by our model. Intracellular recordings of segmental pairs of motor neurons in isolated nerve cords could help determine if the structure of a burst in one motor neuron is influenced by the synaptic input in its contralateral homolog.

Clearly, the duty cycles of the model motor neurons were not well-matched with the duty cycles of the living system (see Table 1). Several parameters that can affect duty cycle were not determined from measured values obtained from the living system

but were set empirically. Perhaps most critical was the maximal conductance of the persistent sodium current; as it was shown in the parameter variation (Figure 29) to have profound impact on excitability and therefore phasing in our model. Future revisions of our model could include values for this inward current based on voltage-clamp data from the living system.

Not only was the scale factor set empirically in our model, but the relative synaptic weight of the G6 and G7 interneurons to the G17 and 18 motor neurons was increased in order to observe bursting activity with duty cycles less than 95% in these motor neurons (see Section 2.4). We predict that additional premotor cells in the rear of the organism could exist in the living system. Based on the poor matching of phase differences of the G18 motor neuron we might predict that these additional premotor cells could be anti-phasic with respect to the G6 and G7 premotor inputs.

6.2.2 Electrical coupling effects on motor neuron phasing

A characteristic feature of electrical coupling of neurons is synchronization of neural activity [2]. This feature is evident in our results from experimentation with the canonical and abstract model. The synchronization of burst firing observed in our models has an effect on longitudinal phase differences (Figures 21 and 34). The effects of electrical coupling on phasing as demonstrated by our model occur as a result of the temporal pattern of the premotor inputs, specifically because some of the inputs to the front motor neurons and the rear motor neurons overlap in time. Side-to-side phase differences are decreased by sharing current via the electrical junctions and because some of the front inputs overlap with one burst of premotor activity and the rear inputs overlap with the next burst of premotor activity, the peristaltic and synchronous maximal phase differences are larger in the presence of the electrical coupling than in the absence. Although the phase differences observed in the model were not perfect matches with the phase differences observed in the living system, we

hypothesize that electrical coupling plays a role in determining the specific longitudinal phase differences in the intersegmental coordination of the leech heartbeat motor pattern. This result could be tested with a blocker of gap junctions between leech neurons. These experiments may depend upon the discovery of a new gap junctional blocker, as the protein responsible for forming gap junctions between leech neurons (*Hm-inx1*) is a member of the innexin gene family not the connexin gene family commonly studied in vertebrate nervous systems [15].

Although enhancement of longitudinal phase differences by electrical coupling results in better matching between model and living system in peristaltic coordination and poorer matching in synchronous coordination, studies of neurons coupled with gap junctions suggest that electrical transmission depend not only on conductance but also on cell morphology and membrane properties [1, 2, 29]. It is conceivable that the activity of the electrical synapse in synchronous coordination can be reversibly modulated by factors not included in our model. For example, the membrane potential of non-spiking neurons have been shown to regulate coupling and uncoupling of motor neurons involved in the network that controls swimming in the leech [47]. Different effects of electrical coupling in each coordination mode could be further examined through experimentation in the living system and in further theoretical work with the model.

The motor pattern of the living system demonstrates near synchrony in the front and rear motor neurons (Figure 3) and the overlap in phase of burst activity in these pairs of motor neurons could be reproduced with the patterned-coupling model (Figure 25). Although, the longitudinal phase differences in the synchronous coordination mode deviated further from phase differences observed in synchronous coordination in the living system, we propose that segmental differences in electrical coupling may exist in the living system and be important to synchronizing the burst activity in the front and rear motor neurons.

6.2.3 Effects of the HN(X) interneuron on phasing in each coordination mode.

Despite the poor matching of longitudinal phase differences in the motor neuron pairs that receive input from the HN(X) interneuron, we can use the results of the model to help us understand how the HN(X) interneuron contributes to the proper phase relationships among these motor neurons. Although identifying the cell body of the HN(X) interneuron would simplify the determination of its temporal pattern of spikes and its spatial pattern of synaptic weights to the G3 – G6 motor neurons, it is not our opinion that identification of the HN(X) interneuron is essential to understanding the intersegmental coordination of the heartbeat system in the leech. However, the characterization of the postsynaptic effects of the HN(X) input is essential to furthering our understanding of the system. Most critical to the intersegmental coordination of phase differences in the front motor neurons will be the determination of the phase of the burst of the HN(X) interneuron with respect to the other premotor inputs and with respect to the burst activity of the G3 – G6 motor neuron pairs. Once these phase relationships are determined from physiological recordings in the living system, we can determine which motor neuron pairs are most discordant in terms of phase with respect to the HN(X) interneurons in the model. Currently, only the phasing data from the model compares the phasing of the motor neurons with respect to the inputs (Figures 26, 27, and 28).

In our model, the majority of the synaptic input to the G3 – G6 motor neurons comes from the G3, G4 interneurons and the HN(X) interneurons [54, 55, 6]. The G6 and G7 interneurons have very small synaptic contributions to the front premotor cells (see Figure 10). The G6 and G7 interneuronal input is more in-phase as you move rearward and this effect was enhanced by the spatial pattern. The front motor neurons received overlapping input from the HN(X) interneuron. Yet, it differed from the other premotor inputs in that its conduction delay, burst structure, and maximal firing

frequency were different in each coordination mode. Effects of removing plasticity and delays were qualitatively and quantitatively different in these motor neurons between the canonical and abstract model due to these differences in peristaltic and synchronous HN(X) input. Confirming these findings in the living system may prove to be difficult without the identification of the HN(X) cell. However, investigating the effects of different temporal spike patterns with and without intra-burst synaptic plasticity in a general model of intersegmental coordination might give some insight into the effects of intra-burst synaptic plasticity from the HN(X) interneuron in each coordination mode.

6.3 Limitations of the Heart Motor Neuron Model

Our model of intersegmental coordination is far from complete. The activity of individual heart motor neurons was only characterized generally for this first generation model. Voltage-clamp experiments that characterize all of the intrinsic membrane currents in heart motor neurons would likely give a more accurate representation of the heart motor neuron physiology. Also, the use of a single compartment model is an oversimplification of the motor neuron geometry.

Although segmental differences between the conductances of outward currents in heart motor neurons exist [43], these differences were excluded in our model. The effects of varying the maximal conductance for several of the K^+ currents was examined in Figure 29. Future versions of our canonical model could include these segmental differences if better matching of heart motor neuron physiology is deemed necessary for the model. Calcium activated K^+ channels were not included in the model although, they have been shown to exist in the living system. The inward currents have not been characterized for the heart motor neurons of the leech. Only fast sodium and persistent sodium currents were included in the model (see Chapter

2). The effects of Ca^{2+} dependent post-inhibitory rebound [3] or hyperpolarization-activated inward currents [30] have been shown to influence phasing in other rhythm generating neuronal networks (for a review see [8]). Although, evidence for these membrane effects is not strong, the presence or absence of these effects should be determined definitively in the living system.

Cell morphology can have large effects on excitability and processing of dendritic information in neurons, and a single isopotential compartment was assumed in our model for two reasons (1) our aim was not reproducing activity in single heart motor neurons but rather the intersegmental coordination of heart motor neurons, and (2) for the computational simplicity of a single compartment. This assumption seemed appropriate for our model as it has been shown that heart motor neurons are electrotonically compact (by Rall's definition [46]), with an average electrotonic length of < 2 [43]. Although, a multi-compartment model of the motor neuron could prevent the artifactual depolarizing coupling potential seen in one motor neuron in response to the spiking of its contralateral homolog [44].

Certainly, sensory feedback plays an important role and may reinforce and fine-tune the phase relationships in many CPG systems [10, 14]. However like models of lamprey swimming [61], the fictive motor pattern of the leech heartbeat resembles the constriction pattern in deafferented preparations [59, 60]. Therefore the ease of an open-loop model construction for a first-generation model sacrifices little in regard to the coordination that is attempting to be reproduced.

Other limitations have been highlighted in Section 6.2, such as setting values of maximal conductance in intrinsic and synaptic currents empirically, and the lack of data on the phasing of motor neurons with respect to premotor cells. Perhaps, future versions of the model will address these limitations.

6.4 General Summary

The peristaltic and synchronous coordination modes were evident in the results with the canonical model; although, the maximal phase differences of each coordination mode in the model was not a match with the living system (Figure 19). It is our intuition that improving the match of the side-to-side phase differences between model and living system in each segmental pair would be fruitful in order to better emulate the living system. Through experimentation with our canonical model it has been shown that determination of the phase of the motor neurons with respect to the premotor inputs in the living system will be critical to understanding the intersegmental coordination of the leech heartbeat system. Longitudinal phase differences in our model were influenced by the integration of electrical coupling, conduction delays, intra-burst synaptic plasticity, and intrinsic membrane currents at the motor neuron (Chapter 4). Attributing individual magnitudes of phase differences to each of these features can be misleading as their effects were often inter-dependent.

The most critical features of our model of the intersegmental coordination of heart motor neurons were the spatial and temporal patterns of synaptic input. Further experimentation with different spatial patterns of synaptic weights and different temporal patterns of spike-mediated synaptic input may reveal that some combinations of spatial and temporal input patterns are synergistic with respect to maximal phase differences of the outputs, the motor neurons. We suggest that systematic manipulation of spatial and temporal input patterns will help determine the properties of synaptic input that result in the most efficient distribution of maximal phase differences of the inputs among the outputs. These general qualities of phasing could hopefully be extended to other rhythmic intersegmentally coordinated systems and perhaps even applied to complicated networks such as those responsible for terrestial limbed locomotion.

REFERENCES

[1] Bennett, M. V. L., "Physiology of electrotonic junctions.," *Annals of the New York Academy of Sciences*, vol. 137, pp. 509–539, 1966.

[2] Bennett, M. V. L. in *Cellular Biology of Neurons, Volume 1, Handbook of Physiology. The Nervous System.* (Kandel, E. R., ed.), pp. 509–539, Baltimore, MD: Williams and Wilkins, 1977.

[3] Bertrand, S. and Cazalets, J. R., "Postinhibitory rebound during locomotor-like activity in neonatal rat motoneurons *in vitro*.," *Journal of Neurophysiology*, vol. 79, pp. 342–351, 1998.

[4] Bower, J. M. and Beeman, D., *The Book of Genesis: Exploring Realistic Neural Models With the General Neural Simulation System.* Springer Verlag, 2nd ed., 1998.

[5] Brodfuehrer, P. D., Debski, E. A., O'Gara, B. A., and Friesen, W. O., "Neuronal control of leech swimming.," *Journal of Neurobiology*, no. 27, pp. 403–18, 1995.

[6] Calabrese, R. L., "The neural control of alternate heartbeat coordination states in the leech, *Hirudo medicinalis*.," *Journal of Comparative Physiology*, vol. 122, pp. 11–143, 1977.

[7] Calabrese, R. L. and Maranto, A. R., "Neural control of the hearts in the leech, *Hirudo medicinalis*. III. regulation of myogenicity and muscle tension by heart accessory neurons.," *Journal of Comparative Physiology [A]*, vol. 154, pp. 393–406, 1984.

[8] Calabrese, R. L., "Cellular, synaptic, network, and modulatory mechanisms involved in rhythm generation," *Current Opinion in Neurobiology*, vol. 8, pp. 710–717, 1998.

[9] Calabrese, R. L., "Neural coordination: Taking the lead from a model," *Current Biology*, vol. 9, pp. R680–R683, Sep 1999.

[10] Cang, J. and Friesen, W. O., "Sensory modification of leech swimming: rhythmic activity of ventral stretch receptors can change intersegmental phase relationships.," *Journal of Neuroscience*, vol. 20, pp. 7822–7829, 2000.

[11] Cazalets, J. R., Borde, M., and Clarac, F., "Localization and organization of the central pattern generator for hindlimb locomotion in newborn rat," *Journal of Neuroscience*, vol. 15, no. 7, pp. 4943–4951, 1995.

[12] Cohen, A. H. and Kiemel, T., "Intersegmental coordination: Lessons from modeling systems of coupled nonlinear oscillators," *American Zooligist*, vol. 33, pp. 54–65, 1993.

[13] Cymbalyuk, G. S., Gaudry, Q., Masino, M. A., and Calabrese, R. L., "Bursting in leech heart interneurons: Cell-autonomous and network-based mechanisms," *Journal of Neuroscience*, vol. 22, no. 24, pp. 10580–10592, 2002.

[14] Di Prisco, G. V., Wallén, P., and Grillner, S., "Synaptic effects of intraspinal stretch receptor neurons mediating movement-related feedback during locomotion.," *Brain Research*, vol. 530, no. 1, pp. 161–6, 1990.

[15] Dykes, I. M., Freeman, F. M., Bacon, J. P., and Davies, J. A., "Molecular basis of gap junctional communication in the cns of the leech *Hirudo medicinalis*," *Journal of Neuroscience*, vol. 24, no. 4, pp. 886–894, 2004.

[16] Friesen, W. O. and Pearce, R. A., "Mechanisms of intersegmental coordination in leech locomotion," *Seminars in the Neurosciences*, vol. 5, pp. 41–47, 1993.

[17] Gramoll, S., Schmidt, J., and Calabrese, R. L., "Switching in the activity state of an interneuron that controls coordination of the hearts in the medicinal leech (*Hirudo medicinalis*).," *Journal of Experimental Biology*, vol. 186, pp. 157–171, 1994.

[18] Grillner, S., Matsushina, T., Wadden, T., Tegner, E., Manira, A., and Wallén, P., "The neurophysiological bases of undulatory locomotion in vertebrates," *Seminars in Neuroscience*, vol. 5, pp. 17–27, 1993.

[19] Grillner, S., Parker, D., and Manira, A. E., "Vertebrate locomotion: A lamprey perspective," *Annals of the New York Academy of Sciences*, vol. 860, pp. 377–392, 1998.

[20] Hill, A. A. V., Masino, M. A., and Calabrese, R. L., "Model of intersegmental coordination in the leech heartbeat neuronal network," *Journal of Neurophysiology*, vol. 87, pp. 1586–1602, 2002.

[21] Hill, A. A. V., Masino, M. A., and Calabrese, R. L., "Intersegmental coordination of rhtyhmic motor patterns," *Journal of Neurophysiology*, vol. 90, pp. 531–538, 2003.

[22] Hill, A. A. V., Lu, J., Masino, M. A., Ølsen, O., and Calabrese, R. L., "A model of a segmental oscillator in the leech heartbeat neuronal network," *Journal of Computational Neuroscience*, vol. 10, no. 3, pp. 281–302, 2001.

[23] Hodgkin, A. L. and Huxley, A. F., "A quantitative description of membrane current and its application to conduction and excitation in nerve," *Journal of Physiology (London)*, vol. 117, pp. 500–544, 1952.

[24] Huerta, R., Sanchez-Montanés, M. A., Corbacho, F., and Sigüenza, J. A., "A central pattern generator to control a pyloric-based system," *Biological Cybernetics*, vol. 82, pp. 85–92, 2000.

[25] Jezzini, S. H., Hill, A. A. V., Kuzyk, P., and Calabrese, R. L., "Detailed model of intersegmental coordination in the timing network of the leech heartbeat central pattern generator," *Journal of Neurophysiology*, vol. 91, no. 2, pp. 958–977, 2004.

[26] Kopell, N. and Ermentrout, G. B., "Coupled oscillators and the design of central pattern generators," *Mathematical Biosciences*, vol. 90, pp. 87–109, 1988.

[27] Kristan, W. B., Stent, G. S., and Ort, C. A., "Neuronal control of swimming in the medicinal leech. I. Dynamics of the swimming rhythm.," *Journal of Comparative Physiology*, vol. 94, pp. 97–119, 1974.

[28] Lansner, A., Hellgren-Kotaleski, J., and Grillner, S., "Modeling of the spinal neuronal circuitry underlying locomotion in a lower vertebrate," *Annals of the New York Academy of Sciences*, vol. 860, no. 1, pp. 239–249, 1998.

[29] Llinás, R., Baker, R., and Sotelo, C., "Electrotonic coupling between neurons in the cat inferior olive," *Journal of Neurophysiology*, vol. 37, pp. 560–571, 1974.

[30] Lüthi, A. and McCormick, D., "H-current: Properties of a neuronal and network pacemaker.," *Neuron*, vol. 21, pp. 9–12, 1998.

[31] Manor, Y., Nadim, F., Epstein, S., Ritt, J., Marder, E., and Kopell, N., "Network Oscillations Generated by Balancing Graded Asymmetric Reciprocal Inhibition in Passive Neurons," *Journal of Neuroscience*, vol. 19, no. 7, pp. 2765–2779, 1999.

[32] Maranto, A. R. and Calabrese, R. L., "Neural control of the hearts in the leech, *Hirudo medicinalis*. I. Anatomy, electrical coupling, and innervation of the hearts.," *Journal of Comparative Physiology [A]*, vol. 154, pp. 367–380, 1984.

[33] Maranto, A. R. and Calabrese, R. L., "Neural control of the hearts in the leech, *Hirudo medicinalis*. II. Myogenic activity and its control by heart motor neurons.," *Journal of Comparative Physiology [A]*, vol. 154, pp. 381–391, 1984.

[34] Marder, E. and Calabrese, R. L., "Principles of rhythmic motor pattern generation," *Physiological Reviews*, vol. 76, pp. 687–717, Jul 1996.

[35] Masino, M. A. and Calabrese, R. L., "Period differences between segmental oscillators produce intersegmental phase differences in the leech heartbeat timing network," *Journal of Neurophysiology*, vol. 87, no. 3, pp. 1603–1615, 2002.

[36] Masino, M. A. and Calabrese, R. L., "Phase relationships between segmentally organized oscillators in the leech heartbeat pattern generating network," *Journal of Neurophysiology*, vol. 87, no. 3, pp. 1572–1585, 2002.

[37] Mulloney, B., Skinner, F. K., Namba, H., and Hall, W. M., "Intersegmental coordination of swimmeret movements: Mathematical models and neural circuits," *Annals of the New York Academy of Sciences*, vol. 860, no. 1, pp. 266–280, 1998.

[38] Nadim, F., Ølsen, O., De Schutter, E., and Calabrese, R. L., "Modeling the leech heartbeat elemental oscillator: I. Interactions of intrinsic and synaptic currents," *Journal of Computational Neuroscience*, vol. 2, no. 3, pp. 215–235, 1992.

[39] Nicholls, J. and Wallace, B. G., "Modulation of transmission at an inhibitory synapse in the central nervous system of the leech.," *Journal of Physiology (London)*, vol. 281, no. 1, pp. 157–170, 1978.

[40] Nicholls, J. G., Martin, A. R., and Wallace, B. G., *From Neuron to Brain: A Cellular and Molecular Approach to the Function of the Nervous System.* Sinauer Associates, Inc., 3rd ed., 1992.

[41] Norris, B. J., Weaver, A. L., Morris, L., Garcia, P. S., and Calabrese, R. L., "Heart motor neuron activity is controlled by a spatiotemporal synaptic pattern of heart interneurons.," *(in preparation).*

[42] Ølsen, O., Nadim, F., and Calabrese, R. L., "Modeling the leech heartbeat elemental oscillator: II. Exploring the parameter space," *Journal of Computational Neuroscience*, vol. 2, no. 3, pp. 237–257, 1992.

[43] Opdyke, C. A. and Calabrese, R. L., "Outward currents in heart motor neurons of the medicinal leech.," *Journal of Neurophysiology*, vol. 74, pp. 2524–37, 1995.

[44] Peterson, E., "Frequency-dependent coupling between rhythmically active neurons in the leech.," *Biophysical Journal*, vol. 43, pp. 53–61, 1983.

[45] Prinz, A. A., Billimoria, C. P., and Marder, E., "Alternative to hand-tuning conductance-based models: Construction and analysis of databases of model neurons," *Journal of Neurophysiology*, vol. 90, no. 6, pp. 3998–4015, 2003.

[46] Rall, W., "Time constants and electrotonic length of membrane cylinders and neurons.," *Biophysical Journal*, vol. 9, pp. 1483–1508, 1969.

[47] Rela, L. and Szczupak, L., "Coactivation of motoneurons regulated by a network combining electrical and chemical synapses," *Journal of Neuroscience*, vol. 23, no. 2, pp. 682–692, 2003.

[48] Roberts, A., Soffe, S. R., Wolf, E. S., Yoshida, M., and Zhao, F. Y., "Central circuits controlling locomotion in young frog tadpoles," *Annals of the New York Academy of Sciences*, vol. 860, no. 1, pp. 19–34, 1998.

[49] Schmidt, J. and Calabrese, R. L., "Evidence that acetylcholine is an inhibitory transmitter of heart interneurons in the leech," *Journal of Experimental Biology*, vol. 171, pp. 329–347, 1992.

[50] Sigvardt, K., "Intersegmental coordination in the lamprey central pattern generator for locomotion," *Seminars in Neuroscience*, vol. 5, pp. 3–15, 1993.

[51] Skinner, F. K., Kopell, N., and Mulloney, B., "How does the crayfish swimmeret system work? Insights from nearest-neighbor coupled oscillator models.," *Journal of Computational Neuroscience*, vol. 2, pp. 151–60, 1997.

[52] Skinner, F. K. and Mulloney, B., "Intersegmental coordination in invertebrates and vertebrates.," *Current Opinion in Neurobiology*, vol. 6, pp. 725–32, 1998.

[53] Thompson, W. J. and Stent, G. S., "Neuronal control of heartbeat in the medicinal leech. I. Generation of the vascular constriction rhythm by heart motor neurons.," *Journal of Comparative Physiology*, vol. 111, pp. 261–279, 1976.

[54] Thompson, W. J. and Stent, G. S., "Neuronal control of heartbeat in the medicinal leech. II. Intersegmental coordination of heart motor neuron activity by heart interneurons.," *Journal of Comparative Physiology*, vol. 111, pp. 281–307, 1976.

[55] Thompson, W. J. and Stent, G. S., "Neuronal control of heartbeat in the medicinal leech. III. Synaptic relations of the heart interneurons.," *Journal of Comparative Physiology*, vol. 111, pp. 309–333, 1976.

[56] Turrigiano, G. G., LeMasson, G., and Marder, E., "Selective regulation of current densities underlies spontaneous changes in the activity of cultured neurons," *Journal of Neuroscience*, vol. 15, no. 5, pp. 3640–3652, 1995.

[57] Wallén, P. and Williams, T., "Fictive locomotion in the lamprey spinal cord *in vitro* compared with swimming in the intact and spinal animal.," *Journal of Physiology (London)*, vol. 347, pp. 225–39, 1984.

[58] Weaver, A. L. and Calabrese, R. L., "Effects of chemical and electrical synapses on phase relationshipsin a complete model of the heartbeat CPG in the medicinal leech," in *Abstract Viewer/Itinerary Planner. Online.*, p. 605.10, Society for Neuroscience, 2003.

[59] Wenning, A., Cymbalyuk, G., and Calabrese, R., "Heartbeat control in leeches: I. Constriction pattern and neural modulation of blood pressure in intact animals.," *Journal of Neurophysiology*, vol. 91, pp. 382–396, 2004.

[60] Wenning, A., Hill, A. A. V., and Calabrese, R. L., "Heartbeat control in leeches: II. fictive motor pattern.," *Journal of Neurophysiology*, vol. 91, pp. 397–409, 2004.

[61] Williams, T. L., Bowtell, G., Carling, J. C., Sigvardt, K. A., and Curtin, N. A., "Interactions between muscle activation, body curvature and the water in the swimming lamprey.," *Symposia of the Society of Experimental Biology*, vol. 49, pp. 49–59, 1995.

VITA

Paul García was born July 6, 1973. He lives in Decatur, Georgia with his loving wife, Meera Srinivasan García, MD. They have two daughters, Violet and Chloe. He is in the MD/PhD program at Emory University and is returning to complete his last two years of medical school in the Fall of 2004. He plans to pursue a career that involves both research and clinical work.